

Projet ANR-14-CE01-0018-01

I-GEM

Impact of Groundwater in Earth System Models

Programme Générique 2014

A	IDENTIFICATION	2
B	RESUME CONSOLIDÉ PUBLIC	2
B.1	Instructions pour les résumés consolidés publics	2
B.2	Résumé consolidé public en français	3
B.3	Résumé consolidé public en anglais	5
C	MEMOIRE SCIENTIFIQUE	6
C.1	Résumé du mémoire	7
C.2	Enjeux et problématique, état de l'art	7
C.3	Approche scientifique et technique	8
C.4	Résultats obtenus	9
C.5	Exploitation des résultats	9
C.6	Discussion	10
C.7	Conclusions	10
C.8	Références	11
D	LISTE DES LIVRABLES	12
E	IMPACT DU PROJET	13
E.1	Indicateurs d'impact	13
E.2	Liste des publications et communications	14
E.3	Liste des éléments de valorisation	17
E.4	Bilan et suivi des personnels recrutés en CDD (hors stagiaires)	19
F	ANNEXES	20
F.1	Comparison of the simulations with fixed WTD among the three climate models (D1.2)	20
F.2	Sensibilité aux constantes de temps des eaux souterraines (Nouveau livrable)	44
F.3	Paramétrisation des liens nappes/surface dans le modèle de l'IPSL (Nouveau livrable)	45
F.4	Influence of groundwater on present and past climate (D2.3 and D3.2)	47
F.5	Climate change impact on groundwater (D3.3)	65

Ce document est à remplir par le coordinateur en collaboration avec les partenaires du projet. L'ensemble des partenaires doit avoir une copie de la version transmise à l'ANR.

Ce modèle doit être utilisé uniquement pour le compte-rendu de fin de projet.

A IDENTIFICATION

Acronyme du projet	I-GEM
Titre du projet	Impact of Groundwater in Earth system Models
Coordinateur du projet (société/organisme)	Agnès Ducharne (UMR 7619 METIS, UPMC, Paris)
Période du projet (date de début – date de fin)	01/10/2014 30/09/2019
Site web du projet, le cas échéant	http://www.metis.upmc.fr/~ducharne/gem/anr.php

Rédacteur de ce rapport	
Civilité, prénom, nom	Mme Agnès DUCHARNE
Téléphone	01 44 27 51 27
Adresse électronique	agnes.ducharne@upmc.fr
Date de rédaction	30/11/2019

Liste des partenaires présents à la fin du projet (société/organisme et responsable scientifique)	Projet bilatéral franco-taiwanais): P1 METIS (UPMC/SU ; PI : A. Ducharne) P2 LMD (CNRS ; PI : F. Chéruy) P3 CNRM-GAME (CNRS ; PI : B. Decharme) P4 NTU (Taiwan ; PI : MH Lo, rapport direct au MoST)
---	--

B RESUME CONSOLIDE PUBLIC

Ce résumé est destiné à être diffusé auprès d'un large public pour promouvoir les résultats du projet, il ne fera donc pas mention de résultats confidentiels et utilisera un vocabulaire adapté mais n'excluant pas les termes techniques. Il en sera fourni une version française et une version en anglais. Il est nécessaire de respecter les instructions ci-dessous.

B.1 INSTRUCTIONS POUR LES RESUMES CONSOLIDES PUBLICS

Les résumés publics en français et en anglais doivent être structurés de la façon suivante.

Titre d'accroche du projet (environ 80 caractères espaces compris)

Titre d'accroche, si possible percutant et concis, qui résume et explicite votre projet selon une logique grand public : il n'est pas nécessaire de présenter exhaustivement le projet mais il faut plutôt s'appuyer sur son aspect le plus marquant.

Les deux premiers paragraphes sont précédés d'un titre spécifique au projet rédigé par vos soins.

Titre 1 : situe l'objectif général du projet et sa problématique (150 caractères max espaces compris)

Paragraphe 1 : (environ 1200 caractères espaces compris)

Le paragraphe 1 précise les enjeux et objectifs du projet : indiquez le contexte, l'objectif général, les problèmes traités, les solutions recherchées, les perspectives et les retombées au niveau technique ou/et sociétal

Titre 2 : précise les méthodes ou technologies utilisées (150 caractères max espaces compris)

Paragraphe 2 : (environ 1200 caractères espaces compris)

Le paragraphe 2 indique comment les résultats attendus sont obtenus grâce à certaines méthodes ou/et technologies. Les technologies utilisées ou/et les méthodes permettant de surmonter les verrous sont explicitées (il faut éviter le jargon scientifique, les acronymes ou les abréviations).

Résultats majeurs du projet (environ 600 caractères espaces compris)

Faits marquants diffusables en direction du grand public, expliciter les applications ou/et les usages rendus possibles, quelles sont les pistes de recherche ou/et de développement originales, éventuellement non prévues au départ.

Préciser aussi toute autre retombée= partenariats internationaux, nouveaux débouchés, nouveaux contrats, start-up, synergies de recherche, pôles de compétitivités, etc.

Production scientifique et brevets depuis le début du projet (environ 500 caractères espaces compris)

Ne pas mettre une simple liste mais faire quelques commentaires. Vous pouvez aussi indiquer les actions de normalisation

Illustration

Une illustration avec un schéma, graphique ou photo et une brève légende. L'illustration doit être clairement lisible à une taille d'environ 6cm de large et 5cm de hauteur. Prévoir une résolution suffisante pour l'impression. Envoyer seulement des illustrations dont vous détenez les droits.

Informations factuelles

Rédiger une phrase précisant le type de projet (recherche industrielle, recherche fondamentale, développement expérimental, exploratoire, innovation, etc.), le coordonnateur, les partenaires, la date de démarrage effectif, la durée du projet, l'aide ANR et le coût global du projet.

B.2 RESUME CONSOLIDE PUBLIC EN FRANÇAIS

Quel impact des eaux souterraines dans les modèles de climat ?

Des enjeux importants pour la simulation du climat et des ressources en eau

Les eaux souterraines constituent 30% des ressources en eau douce, et sont soumises à des prélèvements croissants. Leur effet tampon sur les débits est bien connu, et le projet IGEM s'intéresse à leur possible rôle tampon sur le climat : là où les nappes souterraines sont suffisamment proches de la surface du sol, elles peuvent alimenter l'humidité des sols et soutenir l'évapotranspiration, avec un impact possible sur le climat (températures, précipitation, persistance des événements extrêmes, amplitude du réchauffement régional), les ressources en eau et alimentaires (via l'irrigation). Notre objectif principal était donc d'explorer, par la modélisation numérique, les impacts des eaux souterraines sur le climat passé et futur. De plus, la plupart des modèles de climat négligent encore les pressions anthropiques sur l'eau, dont les prélèvements d'eaux souterraines pour l'irrigation et les usages domestiques. Un autre objectif du projet était donc d'améliorer la description des eaux souterraines dans les modèles de climat français, ce qui nous semble une étape clé avant de tenir compte les prélèvements humains et les transformer en vrais modèles du système Terre, permettant des études intégrées de l'impact des changements globaux sur les ressources en eau.

Un projet international basé sur la modélisation numérique

Notre consortium franco-taiwanais nous a permis de comparer la sensibilité du climat simulé à différentes représentations des eaux souterraines, dans 3 modèles climatiques différents, tous impliqués dans les programmes de simulations du climat futur analysées par le GIEC : les modèles français de l'IPSL et du CNRM, et le modèle américain CESM du NCAR, utilisé par l'équipe taiwanaise. L'intérêt de comparer trois modèles est de pouvoir isoler les impacts robustes parmi les caractéristiques spécifiques à chaque modèle, qui contribuent aux incertitudes des simulations du climat. Nous avons réalisé et analysé de nombreuses simulations : (S1) simulations idéalisées, non réalistes, car la profondeur de nappe est prescrite à des profondeurs fixes, allant de 1 à 10m, pour cartographier la profondeur de nappe « critique », sous laquelle le climat régional n'est pas sensible à la présence d'une nappe ; (S2) simulations réalistes, où la profondeur des nappes est dynamique et répond à la variabilité climatique. Elles couvrent le climat récent, pour évaluer nos modèles par rapport aux observations et comprendre les processus de

réponse impliqués, et le climat futur pour explorer l'impact des eaux souterraines sur les manifestations du changement climatique, et inversement l'impact du changement climatique sur les ressources en eau.

Résultats majeurs du projet

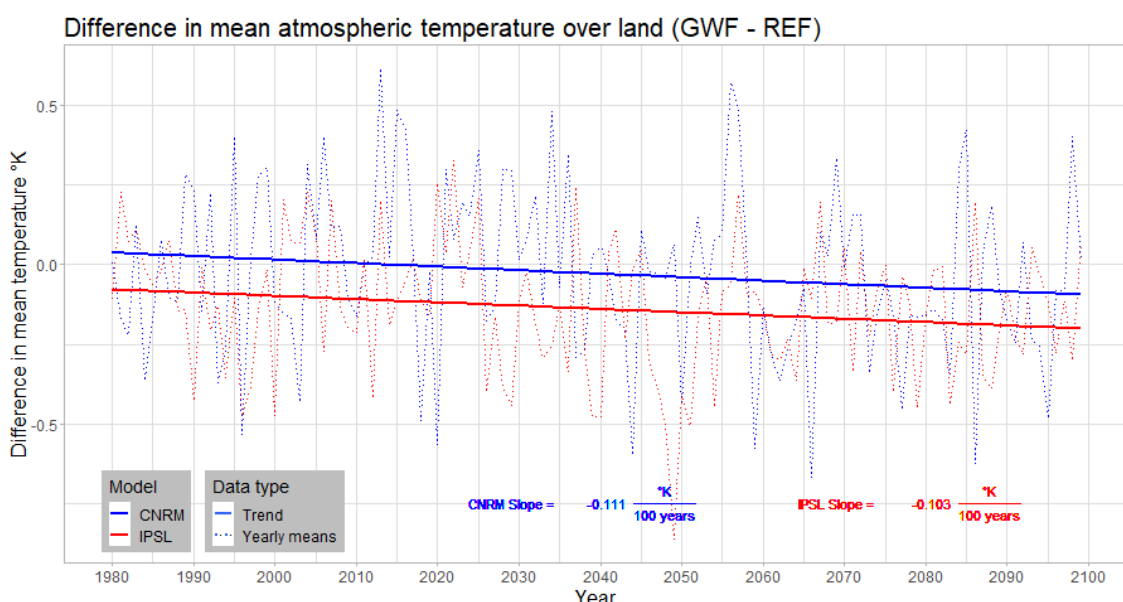
L'impact des eaux souterraines sur le climat simulé (précipitations accrues, températures réduites) s'est révélé assez faible quantitativement, mais significatif dans certaines régions, où l'humidité des sols est limitante, comme le pourtour méditerranéen ou le Sahel. Nous avons aussi montré que la présence d'eau souterraine est capable d'atténuer le réchauffement anthropique, i.e. ce réchauffement est (un peu) plus lent quand les modèles intègrent des eaux souterraines, dont le niveau est sensible au changement du climat. Notre projet a aussi permis de développer un partenariat fructueux avec Taiwan, d'organiser deux workshop internationaux qui ont massivement rassemblé la communauté travaillant sur les eaux souterraines à grande échelle, et d'améliorer les modèles de l'IPSL et du CNRM en vue de la 6^{ème} phase du programme international CMIP.

Production scientifique et brevets depuis le début du projet

Le projet IGEM a été valorisé par 12 articles scientifiques (5 parus dans les meilleures journaux de climatologie, 2 en révision dont un dans Nature Communications, 1 soumis et 4 en préparation). Nous avons présenté nos résultats par 25 communications internationales (dont 2 invitées) et 8 communications nationales (dont 3 invitées, y compris au Collège de France en juin 2019).

Illustration

Une illustration avec un schéma, graphique ou photo et une brève légende. L'illustration doit être clairement lisible à une taille d'environ 6cm de large et 5cm de hauteur. Prévoir une résolution suffisante pour l'impression. Envoyer seulement des illustrations dont vous détenez les droits.



Atténuation du réchauffement global sur les continents (-0.1°C/100 ans) entre des simulations du climat futur avec (GWF) et sans (REF) effet des nappes sur l'humidité des sols, sous forçage radiatif pessimiste (SSP5-8.5, avec un réchauffement de 6°C pendant la période). Simulations de 1980 à 2100 réalisées avec les modèles de climat du CNRM (en bleu) et de l'IPSL (en rouge).

Informations factuelles

Le projet IGEM (ANR-14-CE01-0018-01) est un projet de recherche fondamentale coordonné par Agnès Ducharne, du laboratoire METIS-IPSL à Sorbonne Université. Il associe aussi les laboratoires LMD-IPSL et CNRM du CNRS. Le projet a commencé en octobre 2014 et a duré 60 mois. Il a bénéficié d'une aide ANR de 300,000 € pour un coût global de l'ordre de 2,150,000 €.

B.3 RESUME CONSOLIDE PUBLIC EN ANGLAIS

Which impact of groundwater in climate models?

Important issues for the simulation of climate and water resources

Groundwater constitutes 30% of the fresh water resources, which are subjected to increasing withdrawals. Their buffering effect on stream flows is well known, and the IGEM project addresses their potential buffer effect on climate: when shallow enough, water tables can sustain soil moisture, thus increase evapotranspiration, with potential impact on the climate system (temperatures, precipitation, persistence of extreme events, magnitude of regional warming), water resources and food production. Our main goal was to explore, via numerical modeling, the impacts of groundwater on past and future climate. Besides, most current climate models still overlook anthropogenic pressures on water, as groundwater withdrawals for irrigation and domestic usages. Another goal of the project was thus to improve the description of groundwater in the French climate models, which is a key step before accounting for human withdrawals and to turn them to real Earth system models, allowing integrated studies of global change impacts on water resources.

An international project based on numerical modeling

Our international consortium allowed us to compare the sensitivity of simulated climate to different groundwater parameterizations within three different climate models, all involved in the programmes for future climate simulation analyzed by the IPCC: the French IPSL and CNRM climate models, and the American NCAR climate model CESM, used here by the Taiwanese team. The interest of comparing three models is to permit the isolation of robust impacts among the features specific to each model, which contribute to the uncertainties of climate simulations. We performed and analysed many simulations: (S1) idealized, nonrealistic simulations, as the water table is prescribed at fixed depths, ranging from 1 to 10 m, to identify the patterns of "critical" water table depth, below which groundwater do not impact regional climate; (S2) realistic simulations, where the water table depth dynamically responds to climate variability. They encompass recent climate, to evaluate the models against observations and understand the processes explaining the responses, and the future climate to explore the influence of groundwater on the climate change trajectory, and reversely, the impact of climate change on water resources.

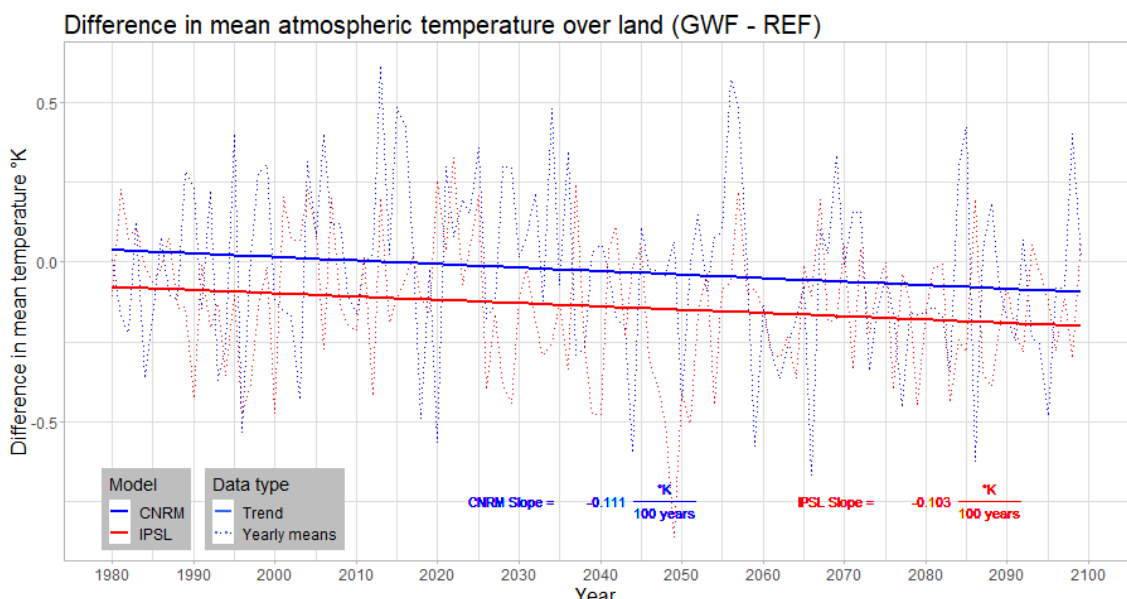
Main results of the project

The impact of groundwater on simulated climate (increased precipitation, decreased temperatures) is rather weak quantitatively, but significant in some regions, where soil moisture is a limiting factor, like the Mediterranean area and Sahel. We also showed that groundwater can attenuate anthropogenic warming, i.e. this warming is a (little) slower when models account for groundwater, the volume of which is sensitive to climate change. Our project also allowed us to develop a fruitful cooperation with Taiwan, to organize two international workshops which massively gathered the community working on groundwater at large scales, and to improve the models of IPSL and CNRM for the 6th phase of the international programme CMIP.

Scientific production since the beginning of the project

The IGEM project was valorized by 12 scientific papers (5 published in the best climatology journals, 2 in revision including one for Nature Communication, 1 submitted, and 4 in preparation). We also presented our results by 25 international communications (2 invited) and 8 national communications (3 invited, including at the Collège de France in June 2019).

Illustration



Attenuation of global warming over land ($-0.1^{\circ}\text{C}/100 \text{ years}$) between simulations of future climate with (GWF) and without (REF) groundwater impact on soil moisture, under a pessimistic radiative forcing scenario (SSP5-8.5, with a mean global warming of $+6^{\circ}\text{C}$ over the period). Simulations from 1980 to 2100 performed with the climate models of the CNRM (in blue) and IPSL (in red).

Factual information

The IGEM project (ANR-14-CE01-0018-01) is a fundamental research project coordinated by Agnès Ducharne, from laboratory METIS-IPSL at Sorbonne Université. It also associates laboratories LMD-IPSL and CNRM of CNRS. The project started in October 2014 and lasted 60 months. It benefited from an ANR support of 300,000 € for a global cost of about 2,150,000 €.

C MEMOIRE SCIENTIFIQUE

Maximum 5 pages. On donne ci-dessous des indications sur le contenu possible du mémoire. Ce mémoire peut être accompagné de rapports annexes plus détaillés.

Le mémoire scientifique couvre la totalité de la durée du projet. Il doit présenter une synthèse auto-suffisante rappelant les objectifs, le travail réalisé et les résultats obtenus mis en perspective avec les attentes initiales et l'état de l'art. C'est un document d'un format semblable à celui des articles scientifiques ou des monographies. Il doit refléter le caractère collectif de l'effort fait par les partenaires au cours du projet. Le coordinateur prépare ce rapport sur la base des contributions de tous les partenaires. Une version préliminaire en est soumise à l'ANR pour la revue de fin de projet.

Un mémoire scientifique signalé comme confidentiel ne sera pas diffusé. Justifier brièvement la raison de la confidentialité demandée. Les mémoires non confidentiels seront susceptibles d'être diffusés par l'ANR, notamment via les archives ouvertes <http://hal.archives-ouvertes.fr>.

Mémoire scientifique confidentiel : non

C.1 RESUME DU MEMOIRE

Les eaux souterraines constituent 30% des ressources en eau douce, et sont soumises à des prélèvements croissants. Leur effet tampon sur les débits est bien connu, et le projet IGEM s'intéresse à leur possible rôle tampon sur le climat : là où les nappes souterraines sont suffisamment proches de la surface du sol, elles peuvent alimenter l'humidité des sols et soutenir l'évapotranspiration, avec un impact possible sur le climat (températures, précipitation, persistance des événements extrêmes, amplitude du réchauffement régional), les ressources en eau et alimentaires (via l'irrigation). Notre objectif principal était donc d'explorer, par la modélisation numérique, les impacts des eaux souterraines sur le climat passé et futur. De plus, la plupart des modèles de climat négligent encore les pressions anthropiques sur l'eau, dont les prélèvements d'eaux souterraines pour l'irrigation et les usages domestiques. Un autre objectif du projet était donc d'améliorer la description des eaux souterraines dans les modèles de climat français, ce qui nous semble une étape clé avant de tenir compte les prélèvements humains et les transformer en vrais modèles du système Terre, permettant des études intégrées de l'impact des changements globaux sur les ressources en eau.

Notre consortium franco-taiwanais nous a permis de comparer la sensibilité du climat simulé à différentes représentations des eaux souterraines, dans 3 modèles climatiques différents, tous impliqués dans les programmes de simulations du climat futur analysées par le GIEC : les modèles français de l'IPSL et du CNRM, et le modèle américain CESM du NCAR, utilisé par l'équipe taiwanaise. L'intérêt de comparer trois modèles est de pouvoir isoler les impacts robustes parmi les caractéristiques spécifiques à chaque modèle, qui contribuent aux incertitudes des simulations du climat. Nous avons réalisé et analysé de nombreuses simulations : (S1) simulations non réalistes, car la profondeur de nappe est prescrite à des profondeurs fixes, allant de 1 à 10m, pour cartographier la profondeur de nappe « critique », sous laquelle le climat régional n'est pas sensible à la présence d'une nappe ; (S2) simulations réalistes, où la profondeur des nappes est dynamique et répond à la variabilité climatique. Elles couvrent le climat récent, pour évaluer nos modèles par rapport aux observations et comprendre les processus de réponse impliqués, et le climat futur pour explorer l'impact des eaux souterraines sur les manifestations du changement climatique, et inversement l'impact du changement climatique sur les ressources en eau.

L'impact des eaux souterraines sur le climat simulé (précipitations accrues, températures réduites) s'est révélé assez faible quantitativement, mais significatif dans certaines régions, où l'humidité des sols est limitante, comme le pourtour méditerranéen ou le Sahel. Nous avons aussi montré que la présence d'eau souterraine est capable d'atténuer le réchauffement anthropique, i.e. ce réchauffement est (un peu) plus lent quand les modèles intègrent des eaux souterraines, dont le niveau est sensible au changement du climat. Notre projet a aussi permis de développer un partenariat fructueux avec Taiwan, d'organiser deux workshop internationaux qui ont massivement rassemblé la communauté travaillant sur les eaux souterraines à grande échelle, et d'améliorer les modèles de l'IPSL et du CNRM en vue de la 6^{ème} phase du programme international CMIP.

C.2 ENJEUX ET PROBLEMATIQUE, ETAT DE L'ART

La question posée par ce projet est celle de l'influence possible des eaux souterraines (ES) sur le climat, qui reste peu abordée à l'échelle internationale. Pourtant, la modélisation des ES dans les modèles de surface continentale est une voie de recherche très active dans la communauté internationale depuis une vingtaine d'années [4], avec plusieurs types d'approche, récapitulées par [Gleeson et al., in prep] :

- a) L'approche la plus simple et la plus fréquente intègre explicitement le couplage entre la zone saturée (nappe) et le sol, mais néglige les flux horizontaux dans la zone saturée, ce qui peut donc être vu comme une extension en profondeur de l'approche 1D verticale utilisée pour décrire l'hydrologie des sols dans les modèles de surface [12]. Le couplage avec un modèle atmosphérique montre un impact sur la variabilité atmosphérique et les précipitations simulées, au moins dans certaines régions [1,10,11,13,18].

- b) Une autre approche vise à décrire les redistributions horizontales d'eau au sein de chaque maille, et leurs effets sur la distribution spatiale de la nappe et de l'humidité du sol. La redistribution de l'eau le long des versants est souvent basée sur modèle hydrogéologique simplifié TOPMODEL, comme développé dans le modèle de surface Catchment [8]. Ceci augmente la mémoire hydrologique dans un modèle atmosphérique [14], mais cette nappe superficielle n'est pas adaptée quand la nappe est profonde et épaisse, comme dans les bassins de la Seine et de la Somme [4].
- c) Des descriptions 2D ou 3D des écoulements souterrains ont aussi été couplées à des modèles de surface continentale et des modèles atmosphériques, mais pour l'instant uniquement à l'échelle régionale [15]. Les modèles hydrogéologiques 2D et 3D ont aussi permis de proposer des distributions de la profondeur de la nappe phréatique aux échelles continentales et globale [3,6], à partir d'une recharge forcée, issue d'un modèle de surface.
- d) Enfin, le partenaire P3 (CNRM) a repris la démarche ci-dessus, mais en augmentant le réalisme hydrogéologique, en distinguant différentes nappes 2D indépendantes, avec des propriétés hydrodynamiques adaptées en fonction de la géologie. Le couplage avec le sol est enfin limité à une fraction de maille où les remontées capillaires peuvent atteindre le sol [16,17, Decharme et al. 2019], mais l'impact de ce modèle hydrogéologique sur le climat n'avait pas été quantifié au début du projet IGEM.

De cette revue, il ressort que le couplage nappe / atmosphère reste rare à l'échelle globale, qu'il implique des résolutions horizontales grossières (avec des mailles de plusieurs milliers de km²), sans se préoccuper vraiment du réalisme mais plutôt dans des études de sensibilité, si bien qu'il est difficile de tirer des conclusions générales, vu la dispersion des types de rétroaction entre nappe et humidité du sol d'une part, et du climat simulé [7] d'autre part.

C.3 APPROCHE SCIENTIFIQUE ET TECHNIQUE

Notre projet repose sur la modélisation numérique du système climatique, en réduisant ce système aux surfaces continentales (où se trouvent les eaux souterraines) et à l'atmosphère. Vu l'état de l'art ci-dessus, nous avons comparé la sensibilité des variables atmosphériques à différentes représentations des eaux souterraines (représentatives des approches a, b, et d), dans 3 modèles climatiques différents, tous impliqués dans les programmes de simulations du climat futur analysées par le GIEC : les modèles français de l'IPSL et du CNRM, et le modèle américain CESM du NCAR, utilisé par l'équipe taiwanaise. L'intérêt de comparer trois modèles est de pouvoir isoler les impacts robustes parmi les caractéristiques spécifiques à chaque modèle, qui contribuent aux incertitudes des simulations du climat.

Nous avons réalisé et analysé de nombreuses simulations avec ces trois modèles: (S1) simulations idéalisées, non réalistes, où la profondeur de nappe est prescrite à des profondeurs fixes, allant de 1 à 10m, pour cartographier la profondeur de nappe « critique », sous laquelle le climat régional n'est pas sensible à la présence d'une nappe ; (S2) simulations réalistes, où la profondeur des nappes est dynamique et répond à la variabilité climatique. Elles couvrent le climat récent, pour évaluer nos modèles par rapport aux observations et comprendre les processus de réponse impliqués, et le climat futur pour explorer l'impact des eaux souterraines sur les manifestations du changement climatique, et inversement l'impact du changement climatique sur les ressources en eau.

En complément des simulations ci-dessous, dites couplées car elles couplent un modèle de surface et un modèle atmosphérique, nous avons aussi réalisé des simulations dites forcées, car le modèle de surface n'est pas couplé à un modèle atmosphérique mais forcé par des observations météorologiques, ce qui permet (i) une simulation beaucoup plus réaliste des variables de surface (e.g. humidité des sols ; évapotranspiration, ET ; débits des cours d'eau), (ii) de simplifier l'influence des eaux souterraines en supprimant de possibles amplifications/atténuations par le couplage avec l'atmosphère.

C.4 RESULTATS OBTENUS

Les nombreuses simulations S1 nous ont permis de cartographier la profondeur de nappe « critique », sous laquelle l'évapotranspiration (ET) n'est pas sensible à la présence d'une nappe), qui facilite la comparaison des réponses des trois modèles [Ducharne et al., soumis ; Annexe F1]. Cette analyse montre que les nappes profondes ($> 5\text{m}$, plus profond que les sols des modèles) contribuent à l'ET dans les régions arides et semi-arides, où il est donc important de décrire les eaux souterraines profondes. Ce point impose cependant une bonne caractérisation de la géométrie et des propriétés de stockage et conductivité des formations aquifères, comme analysé dans un bassin d'Afrique de l'Ouest par Rashid et al. [2019]. En revanche, la profondeur critique est inférieure à 3m dans de nombreuses régions bien arrosées, au moins saisonnièrement, comme les ceintures pluvieuses des latitudes moyennes et tropicales et les zones de mousson. Dans ces régions, une bonne représentation de l'effet des eaux souterraines sur le climat impose de pouvoir décrire une nappe dans le sol.

Cette conclusion a motivé le partenaire IPSL à développer une paramétrisation originale des interactions nappe / humidité du sol qui permet de capturer les principaux effets de la redistribution horizontale de l'eau le long des versants, pour alimenter une fraction humide de bas fond, où la nappe est peu profonde [Annexe F3 ; Tootchi, 2019] et cartographiée à l'échelle globale par Tootchi et al. [2019]. D'un point de vue hydrologique, cette paramétrisation tend à augmenter l'humidité du sol et l'ET, diminuer les débits, et rendre les pics de débits plus précoce [Annexe F4], ce qui pourrait se combiner utilement à une description plus physique du temps de transfert des eaux souterraines, qui retarde au contraire les écoulements souterrains [Schneider, 2017 ; Annexe F2].

Cette nouvelle paramétrisation a été utilisée pour réaliser les simulations S2 du partenaire IPSL, qui suggèrent, comme celles des autres partenaires, un impact assez faible des eaux souterraines sur le climat simulé (précipitations accrues, températures réduites), bien que significatif dans certaines régions, où l'humidité des sols est limitante, comme le pourtour méditerranéen ou le Sahel [Annexe F4]. Nous avons aussi montré que la présence d'eau souterraine est capable d'atténuer le réchauffement anthropique, i.e. ce réchauffement est (un peu) plus lent quand les modèles intègrent des eaux souterraines, dont le niveau est sensible au changement du climat [Wu et al., in revision ; Annexe F5].

Notre projet a aussi permis de développer un partenariat fructueux avec Taiwan, et d'organiser deux workshop internationaux qui ont massivement rassemblé la communauté travaillant sur les eaux souterraines à grande échelle, et ont installé les membres du projet comme des leaders internationaux de l'influence des eaux dans les modèles climatiques, statut réaffirmé par l'organisation d'une session à l'AGU Fall 2019. Le travail de fond mené par les partenaires français sur leurs deux modèles de surface (SURFEX et ORCHIDEE) lors du projet IGEM a enfin contribué à l'amélioration de ces modèles et des modèles climatiques associés en vue de la 6ème phase du programme international CMIP [Decharme et al., 2019 ; Ducharne et al., in prep].

C.5 EXPLOITATION DES RESULTATS

Le projet IGEM a été valorisé par 12 articles scientifiques (5 parus dans les meilleures journaux de climatologie, 3 soumises dont une en révision dans *Nature Communications*, et 4 en préparation). Nous avons présenté nos résultats par 25 communications internationales (dont 2 invitées) et 8 communications nationales (dont 3 invitées, y compris au Collège de France en juin 2019). Une autre forme de dissémination s'est faite via les deux workshops internationaux que nous avons organisés (à Paris, les 3-5 octobre 2016, à Taipei les 18-20 mars 2019) et qui ont massivement rassemblé la communauté travaillant sur les eaux souterraines à grande échelle. Nous avons enfin mis en place la page web de notre projet : <https://www.metis.upmc.fr/~ducharne/gem/anr.php>, qui fournit notamment le protocole de nos simulations pour les équipes potentiellement intéressées pour rejoindre l'inter-comparaison de modèles de climat offrant une

représentation des interactions eau souterraines – humidité des sols (manifestation d'intérêt par Hyungjun KIM, Université de Tokyo). Cette extension pourrait servir de base au lancement d'un GW-MIP (Groundwater Model Intercomparison Project), en complément des nombreux MIP structurant la phase 6 de CMIP.

C.6 DISCUSSION

Nous avons choisi d'abandonner complètement la tache T4 du projet sur l'impact des prélevements dans les nappes sur le climat. L'avancement du projet a en effet été retardé par plusieurs facteurs :

- (1) le partenaire P1 (METIS) a tardé à développer la version de son modèle permettant l'interaction des nappes sur l'humidité des sols, malgré le financement complémentaire de 2 thèses sur le sujet ; ces thèses se sont cependant révélées compliquées, et ont chacune été complétée pour 6 mois par le projet IGEM.
- (2) L'implication forte et non assez anticipée des partenaires P1 (METIS), P2 (LMD) et P3 (CNRM) dans la préparation des simulations CMIP6 de l'IPSL et du CNRM.
- (3) Les difficultés du partenaire P4 (NTU) à adopter le protocole de simulations climatiques CMIP6 pour les tâches T2 et T3.
- (4) Des travaux par les deux PIs du projet (A. Ducharne et M.-H. Lo) sur des articles non prévus initialement mais dans le cadre du projet IGEM [Rashid et al, 2019, Gleeson et al., in prep].

Nous avons cependant obtenu de nombreux résultats intéressants sur les trois premières tâches scientifiques, qu'il nous reste encore à finir de valoriser. Un certain nombre d'hypothèses initiales ont été confirmées, à savoir que l'effet des nappes sur le climat se concentre dans les zones/périodes de transition entre conditions humides et sèches. Les principales différences de réponse entre les modèles viennent de leur localisation différente de ces zones de transition, qui ne se recoupent pas parfaitement dans les différents modèles, mais aussi de leur localisation différente des nappes et des zones de rétroaction entre nappes et sols (ainsi que du caractère « sous-maille » ou pas de ces rétroactions). Ce dernier point ouvre des perspectives de recherche importantes, d'autant qu'il joue probablement sur la deuxième conclusion majeure de notre projet : dans l'état actuel de nos modèles, les nappes ne jouent pas un effet de premier ordre sur le climat simulé. Les perspectives dans ce cadre sont d'approfondir l'étude des quelques régions sensibles, en comparant la distribution spatio-temporelle des nappes simulées par les modèles de climat avec celles de modèles hydrogéologiques et/ou des observations à plus haute résolution [3], et de comparer l'impact naturel des nappes à celui de leur exploitation par l'homme susceptible d'être plus important car il augmente davantage l'humidité des sols et l'évapotranspiration dans les zones irriguées (comme initialement prévu en tache T4).

Enfin, un véritable succès de notre projet a été l'ouverture internationale permise par les deux workshops de la tache T5. Ils ont permis de rassembler la communauté des spécialistes des eaux souterraines à grande échelle (en modélisation et observation) et pour certains, de leur faire découvrir que les interactions climat/eaux souterraines ne vont pas que dans un sens. Les perspectives sont nombreuses, avec un 3^{ème} workshop « IGEM » prévu en 2022 au Canada, après une session à l'AGU Fall 2019. Les workshops IGEM ont aussi démontré l'intérêt d'une communauté plus large que celle de notre projet ANR pour une intercomparaison internationale des modèles de climat intégrant une représentation des eaux souterraines (GW-MIP, cf C.5), et pour des études croisant eaux souterraines, climat et pressions anthropiques (pompages et irrigation), qui rentreraient dans le cadre d'un prochain appel d'offre du Belmont Forum.

C.7 CONCLUSIONS

En dépit de l'abandon d'une des tâches scientifiques prévue initialement, on peut honnêtement considérer que le projet bilatéral IGEM « Impact of Groundwater in Earth System Models » est un succès. Il a en effet fait avancer notre compréhension des interactions entre les eaux souterraines et le climat simulé, et pointé certaines caractéristiques de la description des premières qui influencent ces interactions. Il a aussi

permis de structurer et même d'élargir la communauté internationale intéressée par ces questions, ce qui offre des conditions très favorables pour étudier la complexité supplémentaire induite par les activités humaines avec un partenariat renforcé.

C.8 REFERENCES

Les références produites par le projet sont listées en E.2. Les autres sont listées ci-dessous.

- [1] Anyah, Weaver, Miguez-Macho, Fan, Robock (2008). Incorporating water table dynamics in climate modeling: 3. Simulated groundwater influence on coupled land-atmosphere variability, *J. Geophys. Res.*, 113, D07103.
- [2] Campoy, Ducharme, Chéry, Hourdin, Polcher, Dupont (2013). Response of land surface fluxes and precipitation to different soil bottom hydrological conditions in a general circulation model. *JGR-Atmospheres*, 118, 10725–10739.
- [3] Fan, Y., H. Li, G. Miguez-Macho, 2013: Global patterns of groundwater table depth. *Science*, 339, 940-943.
- [4] Fan, Y., Clark, M., Lawrence, D. M., Swenson, S., Band, L. E., Brantley, S. L., et al. (2019). Hillslope hydrology in global change research and Earth system modeling, *Water Resources Research*, 55, 1737– 1772.
- [5] Gascoin, Ducharme, Ribstein, Carli, Habets (2009). Adaptation of a catchment-based land surface model to the hydrogeological setting of the Somme River basin (France). *J. Hydrology*, 368, 105-116.
- [6] de Graaf, van Beek, Gleeson; Moosdorf, Schmitz, Sutanudjaja, Bierkens (2017). A global-scale two-layer transient groundwater model: Development and application to groundwater depletion, *Advances in Water Resources* 102 (2017) 53–67.
- [7] IPCC (2014). Climate Change 2014: Synthesis Report. Contribution of Working Groups I, II and III to the Fifth Assessment Report of the Intergovernmental Panel on Climate Change [Core Writing Team, R.K. Pachauri and L.A. Meyer (eds.)]. IPCC, Geneva, Switzerland, 151 pp.
- [8] Koster, Suarez, Ducharme, Praveen, Stieglitz (2000). A catchment-based approach to modeling land surface processes in a GCM - Part 1: Model structure, *JGR*, 105 (D20): 24809-24822.
- [9] Koitala, S., Kim, H., Hirabayashi, Y., Kanae, S., & Oki, T. (2019). Sensitivity of global hydrological simulations to groundwater capillary flux parameterizations. *Water Resources Research*, 55, 402– 425.
- [10] Krakauer, N. Y., Puma, M. J., and Cook, B. I., 2013: Impacts of soil-aquifer heat and water fluxes on simulated global climate. *Hydrol. Earth Syst. Sci.*, 17, 1963-1974.
- [11] Leung, Huang, Qian, Liang (2011). Climate-soil-vegetation control on groundwater table dynamics and its feedbacks in a climate model. *Clim. Dyn.*, 36(1):57-81.
- [12] Liang, Xie, Huang (2003). A new parameterization for surface and groundwater interactions and its impact on water budgets with the variable infiltration capacity (VIC) land surface model. *JGR*, 108(D16):8613-8629.
- [13] Lo, Famiglietti (2011), Precipitation response to land subsurface hydrologic processes in atmospheric general circulation model simulations, *J. Geophys. Res.*, 116, D05107.
- [14] Mahanama, Koster (2003). Intercomparison of soil moisture memory in two land surface models. *J. Hydrometeorology*, 4:1134-1146.
- [15] Maxwell, Chow, Kollet (2007). The groundwater–land-surface–atmosphere connection: Soil moisture effects on the atmospheric boundary layer in fully-coupled simulations, *Adv. Wat. Res.*, 30, 2447-2466.
- [16] Miguez-Macho, Fan, Weaver, Walko, Robock (2007). Incorporating water table dynamics in climate modeling: 2. formulation, validation, and soil moisture simulation. *JGR*, 112(D13):D13108.
- [17] Niu, G. Y., Yang, Z. L., Dickinson, R. E., Gulden, L. E. & Su, H. Development of a simple groundwater model for use in climate models and evaluation with Gravity Recovery and Climate Experiment data. *Journal of Geophysical Research: Atmospheres* 112 (2007).
- [18] Vergnes, Decharme (2012). A simple groundwater scheme in the TRIP river routing model: global off-line evaluation against GRACE terrestrial water storage estimates and observed river discharges. *HESS*, 16, 3889-3908.
- [19] Vergnes, J.-P., B. Decharme, and F. Habets (2014). Introduction of groundwater capillary rises using subgrid spatial variability of topography into the ISBA land surface model, *J. Geophys. Res. Atmos.*, 119, 11,065–11,086.
- [20] Yuan, X., Z. H. Xie, J. Zheng, X. J. Tian, and Z. L. Yang, 2008: Effects of water table dynamics on regional climate: A case study over east Asian monsoon area. *J. Geophys. Res. Atmos.*, 113, D21112.

D LISTE DES LIVRABLES

Quand le projet en comporte, reproduire ici le tableau des livrables fourni au début du projet. Mentionner l'ensemble des livrables, y compris les éventuels livrables abandonnés, et ceux non prévus dans la liste initiale.

Les dates des livrables sont indiquées en mois après le début du projet (M1 = Oct 2014).

Date de livraison	N°	Titre	Nature (rapport, logiciel, prototype, données, ...)	Partenaires (<u>souligner le responsable</u>)	Commentaires
T0. Coordination					
M3	D0.1	Project web site	Site web	P1	https://www.metis.upmc.fr/~ducharne/gem/anr.php
M12,M26, M33,M49, M54	D0.2	Minutes of the annual meetings	Compte-rendu	P1	Sur le site web
M18,M30, M63	D.03	ANR reporting	Rapports	P1,P2,P3	Envoyés à l'ANR
T1. Sensitivity to fixed WTD					
M18	D1.1	Results of the mandatory simulations	Fichiers	P1,P2,P3,P4	Sur site ftp*
M24, M63	D1.2	Analysis & intercomparison	Draft	P1, P2,P3,P4	En annexe F.1
M34	New	Analysis for IPSL model	Article	P1,P2,P4	Wang et al (2018)
T2. Dynamic WTD – Recent period					
M53	D2.1	Simulations by the 3 models	Fichiers	P1,P2,P3,P4	Sur site ftp* pour IPSL et CNRM
M53 M55	D2.2	Validation	Article Article	P1,P4 P3	Rashid et al. (2019) for CLM land surface model Decharme et al. (2019) for CNRM model
M63	D2.3	Influence on climate, land/atmos feedback	Draft/rapport	P1,P2,P3,P4	En annexe F.4
x	D2.4	Groundwater vs ocean memory	Draft/rapport	P4	Abandonné
M33 M29	New	Sensibilité aux constantes de temps des eaux souterraines	Thèse Article	P1	Résumé et lien en annexe F.2 Schneider et al. (2017)
M58 M53	New	Paramétrisation des liens nappes/surface pour le modèle de l'IPSL	Thèse Article	P1	Résumé et lien en annexe F.3 Tootchi et al. (2019)
T3. Dynamic WTD – Climate change					
M53	D3.1	Climate change simulations by the 3 models, with and without dynamic WTD	Fichiers	P1,P2,P3,P4	Sur site ftp* pour CNRM et IPSL
M63	D3.2	Influence on climate change trajectory	Draft/rapport	P1,P2,P3,P4	En annexe F.4
M63	D3.3	Climate change impact	Draft/rapport	P1,P2,P3,P4	Wu et al. in prep, en annexe F.5
T4. Dynamic WTD with withdrawals					
x	D4.1	Formatting the withdrawals	Données	P1	Abandonné
x	D4.2	Simulations	Fichiers	P1,P2,P3,P4	Abandonné
x	D4.3	Historical influence and validation	Draft/rapport	P1,P2,P3,P4	Abandonné
x	D4.4	Future climate vs withdrawals	Draft/rapport	P1,P2,P3,P4	Abandonné
T5. International workshops					
M25	D5.1	In France	Online booklet	P1	https://www.metis.upmc.fr/~ducharne/gem/workshop1.php
M54	D5.2	In Taiwan	Online booklet	P4	https://byjoydesign.com/igem/

* <ftp://140.112.66.75/igem> , mot de passe confidentiel, transmis avec le rapport

E IMPACT DU PROJET

Ce rapport rassemble des éléments nécessaires au bilan du projet et plus globalement permettant d'apprécier l'impact du programme à différents niveaux.

E.1 INDICATEURS D'IMPACT

Nombre de publications et de communications (à détailler en E.2)

Comptabiliser séparément les actions monopartenaires, impliquant un seul partenaire, et les actions multipartenaires résultant d'un travail en commun.

Attention : éviter une inflation artificielle des publications, mentionner uniquement celles qui résultent directement du projet (postérieures à son démarrage, et qui citent le soutien de l'ANR et la référence du projet).

		Publications multipartenaires	Publications monopartenaires
International	Revues à comité de lecture	9	3
	Ouvrages ou chapitres d'ouvrage	0	0
	Communications (conférence)	18	7
France	Revues à comité de lecture	0	0
	Ouvrages ou chapitres d'ouvrage	0	0
	Communications (conférence)	4	3
Actions de diffusion	Articles vulgarisation	0	0
	Conférences vulgarisation	0	1 (Collège de France, 2019)
	Autres	0	0

Autres valorisations scientifiques (à détailler en E.3)

	Nombre, années et commentaires (valorisations avérées ou probables)
Brevets internationaux obtenus	0
Brevet internationaux en cours d'obtention	0
Brevets nationaux obtenus	0
Brevet nationaux en cours d'obtention	0
Licences d'exploitation (obtention / cession)	0
Créations d'entreprises ou essaimage	0
Nouveaux projets collaboratifs	<ul style="list-style-type: none"> • Thèse de Pedro Arboleda, financée en octobre 2019 par l'EUR IPSL sur les Rétroactions des eaux souterraines et de l'irrigation sur les extrêmes climatiques passés et futurs, et projet PIREN-Seine sur le même sujet avec un focus sur le bassin de la Seine. • Projet Belmont envisagé sur les interactions croisées entre eaux souterraines, climat et pressions anthropiques
Colloques scientifiques	<ul style="list-style-type: none"> • 2 workshops internationaux organisés dans le cadre du projet ANR : Paris, 3-5 Oct 2016 ; Taiwan, 18-20 mars 2019. • Session « IGEM » à l'AGU Fall 2019 (H128) • 3^{ème} workshop IGEM envisagé en 2022 à Saskatoon, Canada.
Autres (préciser)	

E.2 LISTE DES PUBLICATIONS ET COMMUNICATIONS

Répertorier les publications résultant des travaux effectués dans le cadre du projet. On suivra les catégories du premier tableau de la section E.1 en suivant les normes éditoriales habituelles. En ce qui concerne les conférences, on spécifiera les conférences invitées.

Nous ne listons ici que les publications et communications du projet qui impliquent au moins un partenaire financé par l'ANR.

Publications en revue à comité de lecture

Parues (5)

Decharme B., Delire C., Minvielle M., Colin J., Vergnes J.-P., Alias A., Saint-Martin D., Séférian R., Sénési S., Volodko A., (2019). Recent changes in the ISBA-CTrip land surface system for use in the CNRM-CM6 climate model and in global off-line hydrological applications. *Journal of Advances in Modeling Earth Systems*, 11. <https://doi.org/10.1029/2018MS001545>.

Rashid M, Chien RY, Ducharme A, Kim H, Yeh PJF, Peugeot C, Boone A, He X, Séguis L, Yabu Y, Boukari M, Lo MH (2019). Evaluation of groundwater simulations in Benin from the ALMIP2 project. *Journal of Hydrometeorology*, 20, 339-354, doi:10.1175/JHM-D-18-0025.1.

Tootchi A, Jost A, Ducharme A (2019). Multi-source global wetland maps combining surface water imagery and groundwater constraints. *Earth System Science data*, 11, 189-220, doi: 10.5194/essd-11-189-2019.

Wang F, Ducharme A, Cheruy F, Lo MH, Grandpeix JL (2018). Impact of a shallow groundwater table on the global water cycle in the IPSL land-atmosphere coupled model, *Climate Dynamics*, 50, 3505-3522, doi:10.1007/s00382-017-3820-9.

Schneider AS, Jost A, Coulon C, Silvestre M, Théry S, Ducharme A (2017). Global scale river network extraction based on high-resolution topography, constrained by lithology, climate, slope, and observed drainage density. *Geophysical Research Letters*, 44, 2773–2781, doi:10.1002/2016GL071844.

Soumises (3)

Gleeson T, Wagener T, Cuthbert M, Rahman S, Bierkens MFP, Döll P, Rosolem R, Zipper SC, Bresciani E, Ducharme A, Taylor R, Hill M, Wada Y, Lo MH, Luijendijk E, Maxwell R, Hartmann A, de Graaf I, Oshinlaja N, West C, S. Famiglietti JS, Kollet S, Condon L, Scanlon B, Kim H. Groundwater representation in continental to global hydrologic models (2019). A call for open and holistic evaluation, conceptualization and classification. *EarthArXiv*, submitted to *WRR* in May 2019.

Wu WY, Lo, Wada, Famiglietti, Reager, Yeh, Ducharme, Yang. Divergent effects of climate change on future groundwater availability in key mid-latitude aquifers. Submitted to *Nature Communications* in March 2018, in revision.

Ducharme A, Lo MH, Decharme B, Chien RY, Ghattas J, Colin J, Tyteca S, Cheruy F, Wu WY, Lan CW. Compared sensitivity of land surface fluxes to water table depth in three climate models. Submitted to *JGR-Atmosphere* in March 2020.

In prep (4)

Ducharme, A., Ghattas, J., Maignan, F., Ottlé, C., Vuichard, N., Guimberteau, M., Krinner, G., Polcher, J., Tafasca, S., Bastrikov, V., Cheruy, F., Guénet, B., Mizuochi, H., Peylin, P., Tootchi, A. and Wang, F. Soil water processes in the ORCHIDEE-2.0 land surface msodel: state of the art for CMIP6, in prep pour Geosci. Model Dev.

Lan CW, Hwang YT, Chien RY, Ducharme A, Lo MH. Responses of Global Atmospheric Energy Transport to Idealized Groundwater Conditions, in prep pour *J. Climate*.

Verbeke T, Ducharne A, Ghattas J, Wang F. Response of the simulated climate to the subgrid scale variability of the water table depth: evidence of non-linear amplifications in the IPSL climate model. In prep pour Geophys. Res. Lett.

Colin, J., B. Decharme, R. Séférian, D. Saint-Martin, C. Délie, R. Stchepounoff. Representing aquifers in a global climate model: impact in present-day climate and idealized climate change simulations. In prep.

Thèses de doctorat (2)

Schneider, A. (2017). Estimation of the base flow time constant for global scale applications, PhD thesis, Université Pierre et Marie Curie ([PDF](#)).

Tootchi, A. (2019). Development of a global wetland map and application to describe hillslope hydrology in the ORCHIDEE land surface model, PhD thesis, Sorbonne Université, Paris ([PDF](#)).

Communications invitées (5)

Ducharne A (2019). Cycle hydrologique et climat, relations avec les eaux souterraines. Colloque « Cycle de l'eau et climat » organisé par Edouard Bard, Collège de France, 21 juin 2019, Paris, France.

Lo MH, Ducharne A, and the IGEM project team (2018). Impact of Groundwater in Earth system Models. France-Taiwan Science Festival, 14 September 2018, Taipei (Taiwan).

Ducharne A (2017). Eau et changement climatique - Apports et limites des modèles. Séance "La gestion de l'eau face au défi des incertitudes", Académie d'Agriculture de France, 8 mars 2017 (Paris, France).

Ducharne A (2016). Modélisation de la zone critique dans les modèles de climat - Exemple du modèle ORCHIDEE de l'IPSL. "Grand témoin", Journées RBV, 19 septembre 2016 (Lyon, France).

Ducharne A (2015). Including groundwater in land surface models for hydrologic and climatic applications, Taida Institute for Mathematical Science, National Taiwan University, Taipei, November 4, 2015.

Communications internationales (23)

Wu, Lo, Wada, Reager, Famiglietti, Yeh, Ducharne (2015). Contrasting impacts of climate change on future groundwater storage. AGU Fall Meeting, 14-18 December 2015, San Francisco (USA).

Ducharne, Lo, Decharme, Wang, Cheruy, Ghattas, Chien, Lan, Colin, Tyteca (2016). Groundwater-soil moisture-climate interactions: lessons from idealized model experiments with forced water table depth. Geophysical Research Abstracts, Vol. 18, EGU2016-8541, EGU General Assembly, Wien.

Wang, Ducharne, Cheruy (2016). Evaluation of two initialization methods in a coupled land-atmosphere model. AOGS 13th Annual Meeting, August 1-5 2016 (Beijing, China).

Chien, Lo, Ducharne, Decharme, Lan, Wang (2016). Impacts of groundwater on the atmospheric convection in Amazon using multi-GCM simulations from I-GEM project, IGEM workshop, Paris, October 2016.

Ducharne, Lo, Decharme, Cheruy, Chien, Colin, Ghattas, Lan, Tyteca, Wang (2016). Groundwater-soil moisture-climate interactions: lessons from idealized model experiments with forced water table depth, IGEM workshop, Paris, October 2016.

Lan, Lo, Ducharne, Decharme, Chien, Wang (2016). Responses of atmospheric general circulation to groundwater, IGEM workshop, Paris, October 2016.

Lo, Wu, Wada, Famiglietti, Reager, Yeh, Ducharne, Wu (2016). The contrasting impacts of climate change on groundwater hydrology in the world's major aquifers, IGEM workshop, Paris, October 2016.

Wang, Cheruy, Ducharne (2016). Impact of a prescribed groundwater table on the near surface climate in the IPSL land atmosphere coupled model, IGEM workshop, Paris, October 2016.

Colin, J., B. Decharme, J.-P. Vergnes, and M. Minvielle (2016). Modeling aquifers and floodplains in climate simulations: evaluation and impact. I-GEM Workshop, Paris, October 2016.

Wang F, Ducharne A, Cheruy F, Lo MH. Impact of a prescribed groundwater table on the global water cycle in the IPSL land-atmosphere coupled model. EGU General Assembly 2017, CL4.11, April 2017 (Vienna, Austria).

Jost A, Schneider A, Oudin L, Ducharne A (2017). On the use of a physically-based baseflow timescale in land surface models. 2017 AGU Fall Meeting, H13G, 12-16 December 2017 (San Francisco, USA).

Lan, Hwang, Lo, Ducharne, Decharme, Chien (2017). Responses of Atmospheric General Circulation to Groundwater. 2017 AGU Fall Meeting, H43N, 12-16 December 2017 (San Francisco, USA).

Chien, Lo, Ducharne, Decharme, Lan, Wang, Cheruy, Colin (2017). Impacts of groundwater on the atmospheric convection in Amazon using multi-GCM simulations from I-GEM project. 2017 AGU Fall Meeting, H33B, 12-16 December 2017 (San Francisco, USA).

Verbeke T, Wang F, Ghattas J, Ducharne A (2018). Response of the simulated climate to the subgrid scale variability of the water table depth: evidence of non-linear amplifications in the IPSL climate model. Computational Methods in Water Resources (CMWR) 2018, Juin 2018, Saint Malo (France).

Schneider A, Ducharne A, Jost A (2018). Evaluation of a physically-based base flow time constant in ORCHIDEE Land-Surface Model at global scale. Computational Methods in Water Resources (CMWR) 2018, Juin 2018, Saint Malo (France).

Chien RY, Lo MH, Ducharne A, Decharme B, Lan CW, Wang F, Cheruy F, Colin J (2018). Impacts of groundwater on the Amazon precipitation using multi-GCM simulations from the I-GEM project. Computational Methods in Water Resources (CMWR) 2018, Juin 2018, Saint Malo (France).

Tootchi A, Jost A, Ducharne A, Verbeke T (2018). Assessing groundwater-stream interactions influence on ORCHIDEE land surface model dynamics: parametrization and results for Little Washita watershed. Computational Methods in Water Resources (CMWR) 2018, Juin 2018, Saint Malo (France).

Colin, J., B. Decharme, M. Minvielle, R. Séférian, D. Saint-Martin, A. Alias, M. Chevallier, C. Delire, J-F. Guérémy, M. Michou, P. Nabat, R. Roebrig, D. Salas Y Melia, S. Sénési and A. Voldoire (2018). Impact of groundwater on present-day climate and climate sensitivity in the CNRM-CM6 global climate model, Computational Methods in Water Resources (CMWR) 2018, Saint-Malo, France, June 2018.

Lan, Hwang, Lo, Ducharne, Decharme, Chien (2018). Responses of Atmospheric General Circulation to Groundwater. EGU General Assembly 2018, AS2.1/SSS13.2, April 8-13, 2018 (Vienna, Austria).

Lo MH, Ducharne A (2019). From IGEM to GW-MIP? IGEM Second International Workshop, 16-18 March 2019, Taipei (Taiwan).

Ducharne A, Verbeke T, Tootchi A, Jost A, Ghattas J, Cheruy F (2019). Subgrid-scale parametrization of groundwater-soil moisture interactions in the IPSL climate model: first results at global scale. IGEM Second International Workshop, 16-18 March 2019, Taipei (Taiwan).

Colin, J., B. Decharme, R. Séférian, D. Saint-Martin, C. Délie, R. Stcheponoff (2019). Representing aquifers in a global climate model: impact in present-day climate and

idealized climate change simulations, IGEM Second International Workshop, Taipei, March 2019.

Ducharne A, Lo MH, Decharme B, Colin J, Verbeke T, Cheruy C, Ghattas J, Chien RY, Lan CW (2019). Groundwater-soil moisture-climate interactions: compared impacts in three Earth system models. EGU General Assembly 2019, 7-12 April 2019, Vienna (Austria). CL4.29.

Verbeke T, Tootchi A, Jost A, Ghattas J, Cheruy F, Ducharne A (2019). Subgrid-scale parametrization of groundwater-soil moisture interactions in the ORCHIDEE land surface model: first results at global scale. EGU General Assembly 2019, 7-12 April 2019, Vienna (Austria). HS2.5.4.

Ducharne A, Mahenc J, Verbeke T, Jost A, Ghattas J, Cheruy F, Colin J (2019). Subgrid-scale parametrization of groundwater-soil moisture interactions in the IPSL climate model: impacts on historical and future heat waves . AGU Fall meeting 2019, 9-13 December 2019 (San Francisco, USA). Session H128.

Communications nationales (5)

Ducharne A and coauthors. I-GEM (2017). Impact of Groundwater in Earth System Models. Journées H2020 Inspiration / ANR Sols, Paris, Janvier 2017.

Colin, J., B. Decharme, J.-P. Vergnes, and M. Minvielle (2017). Modeling aquifers and floodplains in climate simulations : evaluation and impact. SURFEX user meeting, Toulouse, January 2017.

Ducharne A, Jost A, Schneider A, Tootchi A, Verbeke T, Wang F, Cheruy F, Ghattas J, et al (2017). Avancées récentes pour représenter l'effet des eaux souterraines dans le modèle ORCHIDEE de l'IPSL. 2èmes Journées de modélisation du fonctionnement des surfaces continentales, 13-14 novembre 2017, Montpellier.

Decharme B., Delire C., Minvielle M., Colin J., Vergnes J.-P., Alias A., Saint-Martin D., Séférian R., Sénési S., Volodire A. (2019). ISBA-CTrip, le nouveau système de modélisation des surfaces continentales pour les modèles de climats du CNRM ou des applications hydrologiques globales, 3ème Journées de Modélisation des Surfaces Continentales (JMSC-2019), 14-15 Novembre 2019, Paris.

Ducharne A, Verbeke T, Jost A, Tootchi A, Ghattas J, Cheruy F (2019). Quel rôle des écoulements horizontaux le long des versants ? Effets sur l'hydrologie et le climat simulés dans les modèles de l'IPSL. 3èmes Journées de modélisation du fonctionnement des surfaces continentales, 14-15 novembre 2019, Paris.

E.3 LISTE DES ELEMENTS DE VALORISATION

La liste des éléments de valorisation inventorie les retombées (autres que les publications) décomptées dans le deuxième tableau de la section E1. On détaillera notamment :

- brevets nationaux et internationaux, licences, et autres éléments de propriété intellectuelle consécutifs au projet.
- logiciels et tout autre prototype
- actions de normalisation
- lancement de produit ou service, nouveau projet, contrat,...
- le développement d'un nouveau partenariat,
- la création d'une plate-forme à la disposition d'une communauté
- création d'entreprise, essaimage, levées de fonds
- autres (ouverture internationale,..)

Elle en précise les partenariats éventuels. Dans le cas où des livrables ont été spécifiés dans l'annexe technique, on présentera ici un bilan de leur fourniture.

En dehors des publications listées en section E2, nos principaux éléments de valorisations portent sur l'ouverture internationale, par plusieurs biais :

- Conférences internationales, à commencer par les 2 workshops organisés dans le cadre du projet ANR (Paris, 3-5 Oct 2016 ; Taiwan, 18-20 mars 2019), qui ont rassemblé chacun une quarantaine de personnes de tous les continents. Les pages web de ces workshops constituent les livrables D5.1 et D5.2 du projet. Ces workshops se sont poursuivis par une session « IGEM » à l'AGU Fall 2019 (H128), et un 3ème workshop IGEM est envisagé en 2022 à Saskatoon, Canada.
- La poursuite du projet IGEM a une plus large échelle internationale est aussi en gestation, au travers de deux initiatives complémentaires : le lancement d'une intercomparaison internationale des modèles de climat intégrant une représentation des eaux souterraines (GW-MIP, Groundwater Model Intercomparison Project), basée sur le protocole développé pour les simulations S2 du projet IGEM ; l'élargissement à des études croisant eaux souterraines, climat et pressions anthropiques (pompages et irrigation), qui pourraient rentrer dans le cadre d'un prochain appel d'offre du Belmont Forum.
- La carte globale des zones humides de bas fond proposée par Tootchi et al. (2019) pour définir les fractions humides dans la nouvelle version du modèle de surface de l'IPSL a par ailleurs servi d'entrée à plusieurs autres versions de ce modèle de surface (ORCHIDEE), axées sur les zones boréales (Bowring et al., 2019, 2020) et sur les tourbières (Qiu et al., 2019). Elle est également utilisée pour diverses études liées aux zones humides à l'Université de Pékin (groupe de S. Peng), et commence à être citée dans les synthèses internationales sur les zones humides (e.g. Döll et al., 2020), qui sont particulièrement difficile à cartographier.

Bowring SPK, Lauerwald R, Guenet B, Zhu D, Guimberteau M, Tootchi A, Ducharne A, Ciais P (2020). ORCHIDEE MICT-LEAK (r5459), a global model for the production, transport and transformation of dissolved organic carbon from Arctic permafrost regions, Part 2: Model evaluation over the Lena River basin. GMD, 507–520, doi:10.5194/gmd-13-507-2020

Bowring SPK, Lauerwald R, Guenet B, Zhu D, Guimberteau M, Tootchi A, Ducharne A, Ciais P (2019). ORCHIDEE MICT-LEAK (r5459), a global model for the production, transport and transformation of dissolved organic carbon from Arctic permafrost regions, Part 1: Rationale, model description and simulation protocol. GMD, 12, 3503-3521, doi:10.5194/gmd-12-3503-2019.

Döll, P, Trautmann, T, Göllner, M, Müller, Schmied H (2020). A global-scale analysis of water storage dynamics of inland wetlands: Quantifying the impacts of human water use and man-made reservoirs as well as the unavoidable and avoidable impacts of climate change. Ecohydrology, 13, e2175, doi:10.1002/eco.2175

Qiu C, Zhu D, Ciais P, Guenet B, Peng S, Krinner G, Tootchi A, Ducharne A, Hastie A (2019). Modelling northern peatlands area and carbon dynamics since the Holocene with the ORCHIDEE-PEAT land surface model (SVN r5488). GMD, 12, 2961-2982, doi:10.5194/gmd-12-2961-2019.

A l'échelle nationale, les travaux menées par le partenaire IPSL (P1,P2) sont dès à présent poursuivis par la thèse de Pedro Arboleda, financée en octobre 2019 par l'EUR IPSL, dirigée par A. Ducharne, et intitulée « Rétroactions des eaux souterraines et de l'irrigation sur les extrêmes climatiques passés et futurs ». Cette thèse s'inscrit dans le cadre plus large d'un projet de 4 ans soutenu par le programme PIREN-Seine (www.piren-seine.fr) sur le même sujet, mais avec un accent sur la transition agro-environnementale du bassin de la Seine face au changement climatique.

E.4 BILAN ET SUIVI DES PERSONNELS RECRUTÉS EN CDD (HORS STAGIAIRES)

Ce tableau dresse le bilan du projet en termes de recrutement de personnels non permanents sur CDD ou assimilé. Renseigner une ligne par personne embauchée sur le projet quand l'embauche a été financée partiellement ou en totalité par l'aide de l'ANR et quand la contribution au projet a été d'une durée au moins égale à 3 mois, tous contrats confondus, l'aide de l'ANR pouvant ne représenter qu'une partie de la rémunération de la personne sur la durée de sa participation au projet.

Les stagiaires bénéficiant d'une convention de stage avec un établissement d'enseignement ne doivent pas être mentionnés.

Les données recueillies pourront faire l'objet d'une demande de mise à jour par l'ANR jusqu'à 5 ans après la fin du projet.

Identification				Avant le recrutement sur le projet			Recrutement sur le projet				Après le projet				
Nom et prénom	Sexe H/F	Adresse email (1)	Date des dernières nouvelles	Dernier diplôme obtenu au moment du recrutement	Lieu d'études (France, UE, hors UE)	Expérience prof. Antérieure, y compris post-docs (ans)	Partenaire ayant embauché la personne	Poste dans le projet (2)	Durée missions (mois) (3)	Date de fin de mission sur le projet	Devenir professionnel (4)	Type d'employeur (5)	Type d'emploi (6)	Lien au projet ANR (7)	Valorisation expérience (8)
WANG Fuxing	H	Fuxing.wang@shmi.se	2018	PhD	Chine (hors UE)	2.5	P2 LMD	Post-doc	12	10/09/2016	Post-doc au LMD puis permanent au SHMI (Suède)	SHMI est une sorte d'EPIC	Chercheur	Non	Oui
SCHNEIDER Ana	F	ing.anacs@gmail.com	Mars 2019	Master	Brésil, France	3	P1 METIS	Doc	41 (5.5 sur ANR)	22/07/2017	ATER puis prof vacataire en collège	ESR puis MEN	EC puis professeur du secondaire	Oui puis Non	Oui puis non
VERBEKE Thomas	H	thomas.verbeke@lsce.ipsl.fr	Nov 2019	Doctorat	France	1.5	P1 METIS	Post-doc	24	28/02/2019	Post-doc France	ESR	Ingénieur	Non	Oui
TOOTCHI Ardalan	H	ardalan.tootchi@gmail.com	Sept 2019	Master	Iran, France	0	P1 METIS	Doc	42 (6 sur ANR)	01/07/2019	Sans nouvelles				

Les informations personnelles recueillies feront l'objet d'un traitement de données informatisées pour les seuls besoins de l'étude anonymisée sur le devenir professionnel des personnes recrutées sur les projets ANR. Elles ne feront l'objet d'aucune cession et seront conservées par l'ANR pendant une durée maximale de 5 ans après la fin du projet concerné. Conformément à la loi n° 78-17 du 6 janvier 1978 modifiée, relative à l'Informatique, aux Fichiers et aux Libertés, les personnes concernées disposent d'un droit d'accès, de rectification et de suppression des données personnelles les concernant. Les personnes concernées seront informées directement de ce droit lorsque leurs coordonnées sont renseignées. Elles peuvent exercer ce droit en s'adressant à l'ANR ([Référence du formulaire : ANR-FORM-090601-01-01](http://www.agence-nationale-recherche.fr>Contact).</p>
</div>
<div data-bbox=)

F ANNEXES

Les annexes suivantes rassemblent les rapports et drafts d'articles qui composent certains livrables du projet, comme récapitulé en section D.

F.1 COMPARISON OF THE SIMULATIONS WITH FIXED WTD AMONG THE THREE CLIMATE MODELS (D1.2)

Ducharne A, Lo MH, Decharme B, Chien RY, Ghattas J, Colin J, Tyteca S, Cheruy F, Wu WY, Lan CW. Compared sensitivity of land surface fluxes to water table depth in three climate models. Submitted to JGR-Atmosphere.

1. Introduction

Soil moisture (SM) is a key variable of land/atmosphere interactions, which are now recognized as a major uncertainty source in climate simulations [Koster et al., 2004; Bierkens et al., 2007; Seneviratne et al., 2010; Dirmeyer et al., 2011; Cheruy et al., 2014]. The supply of moisture on land is limited and highly spatially variable; hence, land hydrology becomes critical in determining moisture supply to the atmosphere through the process of evapotranspiration (ET). SM exerts a positive control on ET, with usually negative feedback on air temperature, and feedback on rainfall that can either be positive (recycling) or negative, depending on boundary layer stability, convection triggering, and large-scale atmospheric circulations. These answers are often model-dependent, and the differences in convection sensitivity to ET changes can be related to convection intensity and large-scale atmospheric circulation features [Schär et al., 1999; Ducharne & Laval., 2000; Chou et al., 2009].

Groundwater can be stored in deeper reservoirs than soils, in particular in unconfined aquifer systems, in which the saturated part is called the water table (WT), characterized by slow and mostly horizontal water flows towards the river network, with well-known buffering effects on streamflow variability, thus hydrological regimes [e.g. Kollet & Maxwell, 2008; Gascoin et al., 2009]. In the following, we will restrict the term GW to water below the soil depth, or in the saturated part of the soil if the WT is high enough. In this framework, the vertical exchanges between GW and overlying soils consist of (i) drainage/recharge from the soil to the WT, and (ii) capillary rise from the WT if it is close enough to the ground surface, thus if WT depth (WTD) is small. This case is favorable to strong GW-atmosphere coupling, since the WT is a SM supply and can increase ET [Ducharne et al., 2000; Yeh et al., 2005; Anyah et al., 2008; Kollet & Maxwell, 2008; Yeh et al., 2009; Lo & Famiglietti., 2011; Campoy et al., 2013].

Our goal is to assess the potential influence of GW on ET and precipitation in a systematic way, based on idealized numerical experiments, with forced saturation below different prescribed depths (thus corresponding to different prescribed WTD), as analyzed by Wang et al. [2018] for the IPSL climate model. We mostly focus on ET, and compare the response of three different models to better distinguish robust effects from model-dependent effects, which contribute to model dispersion/uncertainties. In particular, we want to identify and compare the patterns of the "critical" WTD, inspired by the extinction depth of Shah et al. [2007], and defined here as the deepest tested WTD to achieve a significant change in ET. After presenting the three different LSMs and their host atmospheric model (section 2), we compare the responses obtained in forced and coupled mode, with a focus on land averages and the patterns of the critical WTD and land-atmosphere coupling strength (section 3). The discussion (section 4) addresses the relevance of the critical WTD diagnostic by comparison with global maps of the GW distribution, and the strengths and weaknesses of the numerical design, before a summary of the main conclusions in section 5.

2. Methods

2.1 Three land surface models

We compare the sensitivity of surface fluxes to groundwater supply in three state-of-the-art LSMs, namely the Community Land Model version 4 (CLM4) [Lawrence et al., 2011], ORCHIDEE [Krinner et al., 2005; Campoy et al., 2013], and the SURFEX modeling

system [Masson et al., 2013]. They have been developed for several decades, and used in many model inter-comparison projects, either off-line [e.g. Dirmeyer et al., 2006; Getirana et al., 2014] or coupled to atmospheric or climate models [e.g. Pitman et al., 2009; Cheruy et al., 2014], with parametrizations that evolved with time and research objective. In their reference configuration, i.e. without prescribed WT (Fig. 1, top), the three LSMs describe soil water fluxes by a 1D vertical diffusive equation, amenable to both saturated and unsaturated soils, and solved over a multi-layer discretization. Their differences are representative of the diversity of current hydrology schemes, and regard the soil depth (which displays a subgrid heterogeneity in SURFEX following the PFTs), and the runoff terms. All models include a gravitational drainage (qg) at the bottom of the soil column, equal to the hydraulic conductivity K_N at the deepest layer/node of the soil, itself a function of the local soil moisture. CLM also includes a conceptual aquifer reservoir below the soil, with a dynamic WT, which feeds a capillary rise term (qc) counteracting the gravitational drainage, and which is drained by a baseflow term (qb) [Lo et al., 2008]. Both CLM and SURFEX also includes an horizontal sub-surface runoff (qs_b) inspired by TOPMODEL. Surface runoff is also based on TOPMODEL in CLM and SURFEX (saturation excess runoff), while it is a infiltration-excess runoff in ORCHIDEE. All three LSMs include a routing model, to transform runoff into river discharge along the river network, but only ORCHIDEE uses a dynamic vegetation model (STOMATE), in which leaf area index (LAI) is positively linked to photosynthetic assimilation. Key points and references regarding these features and the related forcing/parameters are given in Table 1.

2.2 Forcing a WT at a prescribed depth

We present here how the above models were adapted to force a water table at a prescribed depth. The general idea is to force all the calculation nodes below the prescribed WTD to be saturated, in all the land points. The effective procedure depends on the original models' structure, but always relies on an upward water flux to the simulated column, called qforce (Fig. 1). This flux is diagnosed at each time step as the amount of water that is required to bring the simulated domain below the prescribed WTD to saturation. It corresponds to an addition of water to the climate system, which modifies the global water balance.

CLM4

We use the existing parametrisation which includes a conceptual aquifer, which is considered as one layer with porosity = 0.2. The water table can either rise within the explicit soil column or drop below. In the first case, the aquifer layer and soil layers up to the prescribed WTD are set to become saturated. For prescribed WTD in the aquifer layer, thus below 3.8 m, the forcing flux qforce needs to balance both the baseflow term (qb) from the prescribed WT and the net flux to the explicit soil layers (capillary rise qc , minus gravitation drainage qg).

ORCHIDEE

The soil is forced to be saturated below the selected WTD, and if the latter is deeper than the reference soil depth (2m), the soil column is extended down to the prescribed WTD, at which we locally impose saturation. This performed by adding 8 calculation nodes (regularly spaced every 12.5cm) for each additional meter of soil, ending with 86 calculation nodes for the 10m soil required to simulation a 10m WTD. The saturation of the bottom nodes would induce a leaching of the above layers by continuity if gravitational drainage was maintained, and we rather imposed an impermeable bottom. The forcing flux qforce is then defined at each time step by the amount of water that is required to bring the WT node to saturation, as well as the underlying soil for the 1 and 0.5m WTD cases. More details can be found in Wang et al. [2018].

SURFEX

For experiments with imposed WTD, the bottom flux condition, FN ($m \cdot s^{-1}$), is modified in order to account for the presence of water table under the soil moisture column ruled by the Richard's equation, following Vergnes et al. [2014]:

$$F_N = k_N \left(\frac{\psi_N - \psi_{sat}}{\Delta z_N} + 1 \right) \quad (1)$$

where ψ_N (m) is the matric potential of the last soil moisture layer, ψ_{sat} (m) the saturated matric potential assuming that the top WTD is saturated, and Δz_N (m) the

distance between the last moisture node and the WTD. In addition, when the WTD is inside the soil, the saturation is imposed in each soil moisture layer, w_i ($\text{m}^3 \text{ m}^{-3}$), under the WTD as follows:

$$w_i^{t+\Delta t} = w_i^t + \frac{q_{\text{force},i}}{\Delta z_i} \quad \text{with} \quad q_{\text{force},i} = (w_{\text{sat},i} - w_i^t) \times \max[0, \min(\Delta z_i, z_i - \text{WTD})] \quad (2)$$

where w_{sat} ($\text{m}^3 \text{ m}^{-3}$) is the soil porosity, Δz (m) the soil layer thickness, and z (m) the soil layer depth. So, the total amount of water, Q_{force} ($\text{kg m}^{-2} \text{ s}^{-1}$), brings into the soil column to maintain the WTD inside the soil is given by :

$$Q_{\text{force}} = \frac{\rho_w}{\Delta t} \sum_{i=1}^N q_{\text{force},i} \quad (3)$$

where ρ_w (kg m^{-3}) is the water density and Δt (s) the model time step.

2.3 Numerical design

Two running modes

The above land surface models can be run offline, forced by prescribed atmospheric conditions (see section 2.3), or coupled to an atmospheric model, here using the versions developped for the 5th phase of CMIP (Coupled Model Intercomparison Project, *Taylor et al. [2012]*). In both modes, the initial conditions were achieved by warm-up or spin-up procedures, let to each group's decision.

In offlline mode, all models were run globally over 1979-2010 (32 years), using the same $1^\circ \times 1^\circ$ and 3-hourly meteorological forcing, provided by the Princeton University [*Sheffield et al., 2006*]. The dataset is based on the National Center of Environmental Prediction National Center for Atmospheric Research (NCEP-NCAR) reanalysis, available 6-hourly at the 2° resolution, which was downscaled and corrected with respect to observation-based datasets of precipitation, air temperature, and radiation. In the present study, the 3-hourly precipitation from *Sheffield et al. [2006]* is further hybridized to match the monthly means from the Global Precipitation Climatology Center (GPCC) Full Data Product V6 [*Schneider et al., 2011, 2014*]. The partitioning of the resulting total precipitation into rainfall and snowfall was based on a temperature threshold, at 1°C for SURFEX and ORCHIDEE, and 0°C for CLM.

The land-atmosphere simulations (coupled mode) rely on the AMIP (Atmospheric Model Intercomparison Project), and cover 1979-2008 with prescribed interannually-varying forcing boundary conditions from observations (sea surface temperatures, sea ice content, greenhouse gases, aerosols, land-use), following *Taylor et al. [2012]*. The atmospheric models coupled to the three LSMs are the following:

- CLM4 to CAM5 (Community Atmospheric Model, version 5) [*Hurrell et al., 2013*], run at $1.9^\circ \times 2.5^\circ$ horizontal resolution, with 30 vertical layers;
- SURFEX to ARPEGE [*Volodire et al., 2013*], run at T127 horizontal resolution ($\sim 1.5^\circ$) with 91 vertical levels;
- ORCHIDEE to LMDZ5B [*Dufresne et al., 2013*]), at the low standard resolution (96x95 horizontally, $\sim 3.7^\circ \times 1.9^\circ$; 39 vertical levels), with the new version of atmospheric physics, including a profound recast of the parameterizations of boundary layer, turbulence, shallow and deep convection [*Hourdin et al., 2013*].

The corresponding climate models, sometimes used below to identify the simulations, are respectively the CESM (Community Earth System Model, version 1.0.3), CNRM-CM (version 5), and IPSL-CM (version 5B).

Exploring a wide range of prescribed WTDs

For each LSM, in both off-line and coupled modes, 7 simulations were performed (Table 2): one reference simulation (further labeled REF) using the model version described in Table 1, and 6 simulations with a prescribed WTD, at 1, 2, 3, 5, 8, and 10 m (further labeled D01, D02, D03, D05, D08, D10). An additional off-line simulation was also done for each model with a prescribed WTD at 50 cm (further labeled D005). Each modelling group was free regarding the spin-up procedure, given that equilibrium was reached before starting the compared simulations. The land/sea mask is also different between the models, and we focus the subsequent analyses on the land fractions that are common to all models, excluding Antarctica.

3. Results

3.1 Land averages

In forced mode, all three reference simulations exhibit realistic land averages of evapotranspiration (ET) and total runoff against the 2001-2010 global water budget estimates of [Rodell *et al.*, 2015] (Fig. 2). Looking at the sensitivity to the forced WTD, we first checked that the long-term mean simulated WTD was everywhere equal to the forced value (not shown). For each model, a larger q_{force} is required to sustain a shallower WT, although the magnitude of this flux is very model-dependent. The resulting impact on land mean ET is rather consistent between the models, especially for the deeper WTD. Mean ET starts to increase with a 3-m WTD, especially for CLM and SURFEX (ET increase larger than 10% in forced and coupled modes). The increase of ET when the WT becomes closer to the surface is slower for ORCHIDEE, which probably comes from the dynamic LAI in this model, via the interplay between soil evaporation and transpiration. Both transpiration and soil evaporation increase with soil moisture, but latter is more effective than the former when the soil moisture is high, as it proceeds at potential rate. Therefore, the increase of LAI with SM slows down the increase in ET, because it increases the fraction of the grid-cells contributing to transpiration, and conversely decreases the fraction contributing to soil evaporation.

For all three models, however, the terrestrial ET is almost doubled with a 50-cm WTD compared to the reference simulations. This comes from the large q_{force} required to maintain a shallow WT, even in very arid areas. The particular case of SURFEX, with an annual mean q_{force} up to 700 mm/d to sustain the 50-cm WTD, comes from the fact that all soil columns are saturated at their bottom with this WTD, and that gravitational drainage is maintained together with prescribed WTD. This leads to very high drainage, which depletes the WT, and calls for large counteracting q_{force} . The net total runoff, comprising several output fluxes (surface and subsurface runoff, and drainage) minus one input flux (q_{force}), becomes negative, thus a source of water for the soil, to enforce shallow WTDs.

Figure 4 first shows that the land average biases of the reference simulations. The mean precipitation is close to GPCC observations for CESM and CNRM-CM, but IPSL-CM overestimates it by about 12%, leading to the overestimation of the simulated latent heat flux (*i.e.* the energy for evapotranspiration). As in forced mode, this flux increases when the WTD decreases, owing to the addition of q_{force} (not shown), which leads to increase precipitation over land. For a 1m WTD, this increase is important in the CNRM-CM and IPSL-CM (+38 and 22%, respectively, compared to the reference simulations). The CESM, in contrast, displays a weak precipitation increase over land (+4%) despite a 41% increase of ET, showing a weak local recycling of enhanced ET.

3.2 Critical WTD

Definition

To map the spatial variations of the sensitivity, we introduced a new variable, the critical WTD, or WTD_c, defined at each point as the deepest WTD to induce a significant change in ET (or the equivalent latent heat flux in Fig. 4). To this end, we defined variation rates of the ET changes between two successive forced WTDs (Fig. 4b), and located at the central WTD for convenience. The resulting curves can be seen as measures of how the sensitivity of ET to a unit change in WTD evolves with WTD, and be used to compare the three models over selected domains or periods. They can also be used to define the so-called critical WTD, given a threshold on ET sensitivity, below which we can assume that ET changes resulting from WTD variations are small (Fig. 4c).

This threshold is not easy to define, and we could for instance use the relative precision of ET measurements, which is often taken as 10% [Twine *et al.*, 2000; Dirmeyer *et al.*, 2000]. Figure 4c rather uses a 5% threshold, leading to define critical WTDs of 2.5m, 4m and 6.5m for ORCHIDEE, SURFEX and CLM4, respectively, meaning that CLM4 is better able to extract deep groundwater for ET than SURFEX and ORCHIDEE, here on global average. We eventually preferred a 1% threshold, to be closer to the extinction depth of Shah *et al.* [2007], defined as the WTD at which GW-fed ET becomes zero. It must be noted that many individual grid-points show small relative variations rates between

successive WTDs, not always with the same sign, so that a small threshold also helps to get a better coverage of the WTDc, as shown below. To summarize this analysis framework, a deeper WTDc corresponds to a larger sensitivity of ET to the WTD, thus to a more water-limited ET.

Main patterns for the three models

Using a threshold of 1%, all three models show WTDc patterns (Fig. 5) which follow aridity in both forced and coupled modes. The larger critical WTDs are found in drier zones, where even deep WTDs can influence the surface fluxes in these areas where ET is water-limited. In contrast, the WTDc is small in wet zones, where deep WTDs have a negligible impact on ET, because soil moisture is not limiting, and to the limit case is found in equatorial areas, where no WTDc could be identified because ET is almost the same for all the simulations in these places where rainfall is abundant and ET is limited by radiation. The WTDc patterns are very similar with a 5% threshold (Fig. S1), despite (i) deeper WTDc since the minimum ET changes to be exceeded is 5-fold the one of the 1% threshold, and (ii) reduced coverage, since more grid-points show variations rates of ET less than 5% between any successive WTDs.

The WTDc maps also reveal strong inter-model differences. In forced mode (Fig. 5-left), thus focusing on differences induced by the land surface component of the climate models, the low critical WTDs in wet areas tend to be lower with ORCHIDEE than with the other two models, meaning that only very shallow WT have an impact on ET in the former, while the latter two are sensitive to WTs around 4m in temperate to wet climate (except Equatorial). If we exclude Sahara, where SURFEX displays very small WTDc that can be explained by the simulation design (allowing gravitational drainage from the WT, as discussed in section 3.1), CLM and SURFEX exhibit very close WTDc patterns, with large WTDc in most arid zones. The maximum values, however, are larger for CLM4, indicating a stronger, more efficient, capillary rise from deep WTs. In contrast, the deepest WTDc of ORCHIDEE are rather found in the so-called transitional zones, where soil moisture ranges between dry and wet extremes, and this probably comes from dynamic LAI. Combined with different sensitivities of soil evaporation and transpiration, this feature favors high sensitivity in areas where vegetation is present, but is not very dense, so the WT rise leads to rapid ET increases owing to the enhancement soil evaporation (as discussed in section 3.1).

Similar patterns are found in coupled mode (Fig. 5-right), but altered by the simulated climate, because the patterns of precipitation and aridity from the three climate model, although realistic, show differences with respect to observed patterns (Fig. S2). In terms of water stress ranking, the model with the largest critical WTDs becomes SURFEX (within CNRM-CM), instead of CLM4 in forced mode. This is consistent with the fact that SURFEX displays the smallest mean ET and precipitation over land (with biases of -5% and +1% with respect to the estimates of *Rodell et al.* [2015] and GPCC) in the reference coupled simulation (Figs. 3,4), thus being the most water limited. In contrast, both land ET and precipitation are overestimated in the CESM reference simulation (+10% and +2.5%, respectively), which makes its land surface component, CLM4, less sensitive to water stress than in forced mode, explaining why the WTDc becomes smaller in coupled mode. ORCHIDEE keeps the smallest WTDc of the three models, because its weak water-limitation in forced mode (corresponding to the smallest WTDc) is enhanced by the strong positive bias of ET and precipitation over land by IPSL-CM (+25% and +14% respectively). This overestimation of precipitation is particularly marked in the Congo basin and boreal zones (Fig. S2), where energy also happens to be the main limiting factor to ET. This results in a negligible impact of the WT on the simulated ET, whichever the prescribed WTD, explaining why these areas correspond to widespread zones with undefined WTDc (in white).

3.3 Land-atmosphere coupling strength

It is often accepted that the local strength of land-atmosphere coupling can be indicated by the temporal correlation between soil moisture and ET, which can transmit SM influence to the atmosphere, via different kinds of coupling processes, often involved in complex feedback loops (e.g. evaporative cooling, positive or negative influence on precipitation, subsequent impacts on incoming radiation; see *Seneviratne et al.* [2010] for a thorough review). In this framework, a positive correlation corresponds to a regime where evaporation is water-limited, and can vary substantially with SM, thus induce an

atmospheric response; in contrast, a negative correlation is found where increasing ET depletes SM, *i.e.* where ET is mostly driven by surface net radiation. To quantify the potential influence of groundwater on these interactions, we use the coupling index of Dirmeyer [2011] (adapted to monthly input data following Dirmeyer *et al.* [2013]), which multiplies the interannual correlation between SM and ET, here based on the timeseries of annual means values, by the interannual standard deviation of ET to highlight the areas where ET variations are important.

The three models show very similar coupling strengths in their reference configuration, without any forced WT (Fig. 6). In particular, the strongest coupling (highest index values) largely overlaps the semi-arid transition zones, which have been identified as hot-spot of land-atmosphere coupling since Koster *et al.* [2004]. In contrast, the coupling strength is weak in tropical and mid-latitude rainbelts and in the arid zones (with the exception of central Australia). The coupling strength exhibits similar patterns in forced and coupled simulations, but the mean value tends to be larger in coupled mode, particularly in the mid-latitude rainbelts, which is indicative of positive feedback processes between ET and precipitation in the coupled simulations. A more striking difference is the strong decrease in coupling strength, for all three models, with a WTD at 1m (Fig. 7), because it reduces the SM and ET variability. ORCHIDEE keeps a slightly stronger coupling than the other models because of a smaller ET increase between the reference and D01 simulations (Figs. 2,3), meaning that it keeps more water stress than the other models, as discussed above with respect to dynamic LAI.

It must be underlined that forcing a constant WT throughout the simulation period, which drives the strong coupling strength decrease between the reference and D01 simulations, is not realistic, since real WTDs vary both in space and time. Yet, it is expected that real GW systems display damped variability compared to precipitation variability [Entekhabi *et al.*, 1996; Russo & Lall, 2017], and that shallow WT dampen SM variability [Kollet & Maxwell, 2008; Martínez-de la Torre & Miguez-Macho, 2019]. These effects are supported by reference simulations with CLM4, which does include a dynamic WT, within a conceptual aquifer layer below the soil domain (Table 1). Despite intermodel spread, Figure 6 indicates more widespread zones of negative coupling strength with CLM4 than with the other LSMs, although the latter are less sensitive to water stress than CLM4 based on the critical WTD (Fig. 5), at least in forced mode. This weaker coupling strength with CLM4, especially in the mid-latitude and subtropical rainbelts (Eastern USA, North-western Europe, eastern China, Sahel), is consistent with reduced SM variability indices by capillary rise from the dynamic WT.

4. Discussion

4.1 Relevance of the critical WTD diagnostic

From a model development perspective, an important question is where and how deep we need to describe a water table in land surface models [Gulden *et al.*, 2007; Koitala *et al.*, 2019; Rashid *et al.*, 2019]. By providing a synthetic comparison of ET sensitivity to GW between different regions and models, the critical WTDc maps indicate that a depth of at least 5 m is required to represent the effect of GW in arid and semi-arid zones. These areas do correspond to known deep WTs, as shown for instance by the simulated WTD map published at the global scale by Fan *et al.* [2013], with a 1 km resolution and a steady state assumption (Fig. S3). Accordingly, almost half the land surface exhibits WTDs larger than 10 m, particularly in arid zones, where GW recharge is weak, and beneath mountain ranges, owing to the 2D continuity of hydraulic head, although this is not necessarily representative of small-scale observations, since the WTD can be very small along rivers or lakes draining the WT in these two kinds of areas [Lafaysse *et al.*, 2011; Martínez-de la Torre & Miguez-Macho, 2019; Tootchi *et al.*, 2019].

Among the three LSMs tested here, only CLM4 uses a dynamic WT down to 25 m in its reference simulation, and we compared the resulting mean WTD to the diagnosed WTDc, in both forced and coupled modes (Fig. 8). The mean WTD is deeper than the WTDc in most areas, particularly the most arid ones. There, the change in mean ET from a simulation with a constant 10-m WT to a simulation with a constant 8-m simulation (for the off-line configuration) is less than 1% of the mean ET with a dynamic WT, showing that GW influence is negligible, or limited to certain periods of time. In these arid zones, the map of the major aquifer systems [Strückmeier & Richts, 2008; Fig. S4) shows that,

in many parts of the world, the deep WTDs, consistently simulated by the reference CLM4 simulations and *Fan et al.* [2013], do not correspond to productive aquifer formations, or to confined aquifers (e.g. Sahara), which do not interact with the overlying soil.

Yet, there are also many places where deep WTD exist in unconfined aquifers, including zones of strong land-atmosphere coupling (like Central and Western USA, the Mediterranean rim, or India), and our WTDc maps suggest that the correct simulation of the groundwater dynamics is important to obtain realistic surface fluxes and near-surface climate in these areas. Based on the global map of *Fan et al.* [2013], around 20% of the land surface has WTDs between 2.5 and 10 m, where the critical WTD tells us that capillary can be influential, but most LSMs neglect this water source. The CLM4 case is particularly interesting regarding these transition zones, as they show a contrasted sensitivity to GW in forced and coupled mode (Fig. 8): in forced mode, the mean reference WTD is greater than the WTDc (dark blue areas), suggesting that GW has a negligible impact on land surface fluxes; the opposite relationship is found between the reference ET and the WTDc in coupled mode, showing that the GW can be involved in the land-atmosphere feedback in these areas where this feedback is effective.

Another interesting case is the one of shallow critical WTD, which comprise a majority of land points with ORCHIDEE in both forced and coupled mode (Figure 5). These shallow WTDc reveal that if the top soil include saturated layers, they can support larger ET than with gravitational drainage. But this case requires a set up allowing the WT to develop, thus to impede gravitational drainage at some depth [*Campoy et al.*, 2013] or to describe 2D GW flow to get shallow WT around rivers like in *Fan et al.* [2013]. This analysis, like the one regarding deeper WTDc, shows that the sensitivity to GW explored with our idealized simulations is only one facet of the problem, the other being to obtain realistic GW storage and residence times, WTD variations and capillary rise, which requires complex underground information not yet fully available at the global scale [*Clark et al.*, 2015; *Fan et al.*, 2015; *Cuthbert et al.*, 2019].

4.2 Strengths and weaknesses of the numerical design

Like any modeling study, ours is by essence restricted, since it discusses the modeled realm, with model dependent conclusions. The comparison of three different land surface models is useful in this context, as it helps identifying robust features (here the overall sensitivity of various land surface and atmospheric variables to the WTD, and the corresponding patterns of ET), while underlining the corresponding uncertainties, which can be quite large from a quantitative point of view. We did not focus our analyses on uncertainty quantification, since a sample of three models is hardly sufficient to estimate relevant standard deviations or dispersion criteria, but the differences in the three models shown in Figures 2 to 5 is illustrative and shows that quantitative results need to be taken with caution. It must also be reminded that the WTDc values depend on the ET threshold to define a negligible change, with substantial quantitative differences between Figures 5 and S1, although the patterns remain very consistent.

The reasons for inter-model differences are not fully clear yet but probably involve the different soil texture maps and pedotransfer function to estimate the unsaturated hydraulic parameters (*Brooks and Corey* [1966] for CLM and SURFEX, *Van Genuchten* [1980] for ORCHIDEE). The latter have a strong influence on the soil moisture redistribution [*Decharme et al.*, 2011], and may for instance explain why capillary rise seems stronger in CLM4 (section 3.2.2). The soil depth is also different among the models, like the ways to link the soil and WTs, either based on analytic capillary rise (for CLM4 and SURFEX when the WT is below the soil), or based on explicit soil moisture redistribution using Richards equation (ORCHIDEE, and the other two models when the WT is inside the soil).

Modeling choices regarding the vegetation can also impact the results, since all three models use their own vegetation map and evapotranspiration parametrizations, all based on bulk aerodynamic formulations but with different parameter sets. In particular, the rooting depth and root profiles are effective parameters to the transpiration withdrawals [*de Rosnay & Polcher*, 1998; *Feddes et al.*, 2001], and the fact that the deepest WTDc found in arid zones in CLM4 and SURFEX, but in transition zones (like the US Great Plains, and Sahel) may result from dynamic LAI in this model, combined to frequent soil

evaporation at potential rate (section 3.1). It must be noted that the feedback between the rooting depth and the WT depth [Fan *et al.*, 2017] is not taken into account in our simulations, while it is likely to exert a significant influence on the GW-ET coupling, and its control by the vegetation. The effect moderation of water-stress by GW, however, is overlooked in many rooting depth datasets inferred from LSM inversion [e.g. Kleidon, 2004; Yang *et al.*, 2016].

The present study also relies on idealized simulations, with important shortcomings, which aim at reducing the dispersion of the model response to the WTD, since the latter is prescribed and does not react to each model's hydrology. Yet, this strongly reduces the realism of the simulations, for several reasons. Firstly, important quantitative errors arise from the required forcing flux (q_{force}), which brakes water conservation in the forced-WTD simulations. Secondly, these simulations consider a shallow WTD in arid areas, where they do not exist except in small places like oases and related wetlands [Tootchi *et al.*, 2019]. Thirdly, forcing a constant WTD annihilates the WTD variability (while ET lowers the WT and recharge rises it). In particular, the links between WTD and the coupling strength, defined with respect to the standard variation of ET, are likely blurred by prescribing a constant WTD, while this variable normally fluctuates, and this contributes to the weaker coupling strength in D01.

The comparison of forced and coupled simulations is another feature of our numerical design, which brings useful informations regarding Earth system models. We found no systematic link between the mean WTDc of the two configurations, showing that the mean aridity of each climate model is a major driver of the response to WTD in coupled mode. In forced mode, the atmospheric forcing might lead to overestimated ET increase with smaller WTDs, since ET increases without negative feedback from increased atmospheric humidity. On the other hand, the absence of ET/P feedback, usually positive in most AGCMs [e.g. Lo & Famiglietti, 2011; Campoy *et al.*, 2013, Wang *et al.*, 2018] may lead to underestimated effects. The resulting overall bias is unclear, but the comparison of the dynamic WTD simulated by CLM4 to the corresponding WTDc in transition areas suggests that the latter bias dominates in these areas of strong land-atmosphere coupling (Fig. 8 and section 4.1).

5. Conclusions

Owing to theoretical 1D calculations, Shah *et al.* [2007] found extinction depths (where ET is no longer sustained by the WT) down to 8 m for forests over clay soils, but they did not test the influence of climate. Consistently with common knowledge, our results show that deep WTDs can contribute to ET in arid and semi-arid areas, and the deepest critical WTD is always below 5 m, with differences induced by the LSM, and by the atmospheric model in coupled mode. We also find that the critical WTD is below 3m, thus below commonly used soil depths in most LSMs, in widespread land areas with an active water cycle, including the mid-latitude and subtropical rainbelts for CLM4 and SURFEX, and heavily populated semi-arid areas (Mediterranean rim, US Great Plains, Sahel, India) for ORCHIDEE. Another important conclusion is that in many humid areas, it makes a difference to include a WT if it is shallow enough (where the critical WTD is shallow).

By summarizing the response to various WTDs, the critical WTD helped us ranking the sensitivity of ET to GW between different regions and models. Contrarily to classical indices of SM availability, it describes both the water-stress of the soil compartment, and the potential to extract water from the WT. The differences in mean WTDc show that CLM4 has the strongest capillary rise, followed by SURFEX then ORCHIDEE. The same model ranking is also found for land averages, so the required WTD to increase ET by more than 10% of reference ET is 3 m for CLM4 and SURFEX, while it is between 1 and 2 m for ORCHIDEE. These quantitative intermodel differences are related to the ways SM diffusion and ET withdrawals are processes by the LSMs, and the mean climate of the atmospheric models. Yet, we found similar aridity-driven patterns between three tested LSMs, in both forced and coupled configurations, despite varied biases of the water cycle by the three climate models.

An interesting perspective to the present work would be to generalize the critical WTD analyses based on precipitations or air temperature to better decypher the effect of increased SM and ET on the simulate climate. In particular, CESM shows a much weaker increase of land precipitation with shallower WT than the other climate models, and it even

exhibits a decrease of mean precipitation over land between D01 and D005 (-3%, Figure 3). This calls for further analysis of the precipitation control in the three climate models, and the non-realistic set up with a very high WTD, close to aquaplanet simulations [Levine & Schneider, 2011], may provide novel insights.

We also found that a forced WTD strongly reduces the land-atmosphere coupling strength of Dirmeyer *et al.* [2013]. Although largely driven by the lack of WTD variations in our idealized simulations, this result is consistent with the weaker coupling index in the reference CLM4 simulations, which does include a dynamic WT in an aquifer compartment below the 3.8-m soil, compared to the other two tested LSMs, without any WT in their reference simulations owing to gravitational drainage at the soil bottom. The weaker coupling strength with CLM4 is particularly found in the mid-latitude and subtropical rainbelts (Eastern USA, North-western Europe, eastern China, Sahel), *i.e.* areas with a contrasted seasonal cycle of water-stress, which can be envisioned as temporal SM transition zones. There, the presence of GW is able to buffer SM variability, thus reduce the coupling strength between SM, ET and precipitation, at timescales mostly smaller than the year. Yet, GW can induce longer-term SM memory, thus coupling, as demonstrated over Spain by Martínez-de la Torre & Miguez-Macho [2019].

Therefore, the links between the WTD, the simulated climate, and the land-atmosphere coupling processes, need further examination in simulations where the WTD variations freely respond to climate variability, vegetation dynamics, and underground hydraulic properties, in a mass conservative way. The corresponding simulations have just been realized with the three climate models tested here, and will be compared in a forthcoming paper, as pioneered by Lo & Famiglietti [2011] with the CESM.

Acknowledgements

This work was jointly supported by the Agence Nationale de la Recherche in France (grant ANR-14-CE01-0018-01) and the MOST in Taiwan (grant MOST-104-2923-M-002-002-MY4). The IPSL simulations were performed using the IDRIS computational facilities (Institut du Développement et des Ressources en Informatique Scientifique, CNRS, France).

References

- Anyah, R. O., C. P. Weaver, G. Miguez-Macho, Y. Fan, and A. Robock (2008). Incorporating water table dynamics in climate modeling: 3. Simulated groundwater influence on coupled land-atmosphere variability. *J. Geophys. Res.*, **113**, D07103.
- Bierkens, van den Hurk (2007). Groundwater convergence as a possible mechanism for multi-year persistence in rainfall, *Geophys. Res. Lett.*, **34**, L02402.
- Brook, R. H., and A. T. Corey (1966), Properties of porous media affecting fluid flow. *J. Irrig. Drain. American Soc. Civil Eng.*, **17**, 187-208.
- Calvet, J. C., J. Noilhan, J.-L. Roujean, P. Bessemoulin, M. Cabelguenne, A. Olioso and J.-P. Wigneron, 1998a: An interactive vegetation SVAT model tested against data from six contrasting sites. *Agric. Forest Meteorol.*, **92**, 73-95.
- Campoy, A., Ducharme, A., Cheruy, F., Hourdin, F., Polcher, J., and Dupont, J.-C. (2013). Response of land surface fluxes and precipitation to different soil bottom hydrological conditions in a general circulation model. *JGR-Atmospheres*, **118**, 10725–10739.
- Carsel, R., and Parrish, R. (1988). Developing joint probability distributions of soil water retention characteristics. *Water Resources Research*, **24**(5): 755-769.
- Cheruy F, Dufresne JL, Hourdin F, Ducharme A (2014). Role of clouds and land-atmosphere coupling in systematic mid-latitude summer warm biases and climate change amplification in CMIP5 simulations, *Geophys. Res. Lett.*, **41**, 6493–6500, doi:10.1002/2014GL061145.
- Chou, Chia, J. David Neelin, Chao-An Chen, Jien-Yi Tu, 2009: Evaluating the "Rich-Get-Richer" Mechanism in Tropical Precipitation Change under Global Warming. *J. Climate*, **22**, 1982–2005.
- Clark, M. P., Fan, Y., Lawrence, D. M., Adam, J. C., Bolster, D., Gochis, D. J., Hooper, R. P., Kumar, M., Leung, L. R., Mackay, D. S., Maxwell, R. M., Shen, C., Swenson, S. C., and Zeng, X. (2015), Improving the representation of hydrologic processes in Earth System Models, *Water Resour. Res.*, **51**, 5929– 5956, doi:10.1002/2015WR017096.
- Cuthbert, M.O., Gleeson, T., Moosdorf, N. et al. (2019). Global patterns and dynamics of climate-groundwater interactions, *Nature Clim Change* **9**, 137–141, doi:10.1038/s41558-018-0386-4
- Decharme, B., R. Alkama, E. Douville, M. Becker, A. Cazenave (2010) Global evaluation of the ISBA-TRIP continental hydrologic system. Part 2: Uncertainties in river routing simulation related to flow velocity and groundwater storage. *J. Hydromet.*, **11**, 601-617.

- Decharme, B., E. Martin, and S. Faroux (2013). Reconciling soil thermal and hydrological lower boundary conditions in land surface models, *J. Geophys. Res. Atmos.*, **118**, doi:10.1002/jgrd.50631.
- Decharme, B., Brun, E., Boone, A., Delire, C., Le Moigne, P., and Morin, S.: Impacts of snow and organic soils parameterization on North-Eurasian soil temperature profiles simulated by the ISBA land surface model, *The Cryosphere Discuss.*, **9**, 6733-6790, doi:10.5194/tcd-9-6733-2015, 2015.
- de Rosnay, P., and Polcher, J. (1998). Modelling root water uptake in a complex land surface model coupled to a GCM, *HESS*, **2**, 239-255.
- de Rosnay, P., Polcher, J., Bruen, M., and Laval, K. (2002). Impact of a physically based soil water flow and soil-plant interaction representation for modeling large-scale land surface processes. *Journal of Geophysical Research*, **107**(D11):4118.
- Dirmeyer, P.A., Zeng, F.J., Ducharne, A., Morrill, J., and Koster, R.D. (2000). Sensitivity of surface fluxes to soil water content in three land surface schemes, *J. Hydromet.*, **1**, 121-1.
- Dirmeyer, P. A., Gao, X., Zhao, M., Guo, Z., Oki, T., and Hanasaki, N. (2006). GSWP-2: Multimodel Analysis and Implications for Our Perception of the Land Surface, *BAMS*, **87**, 1381-1397, doi:10.1175/BAMS-87-10-1381
- Dirmeyer, P. A. (2011). The terrestrial segment of soil moisture-climate coupling, *Geophys. Res. Lett.*, **38**, L16702, doi:10.1029/2011GL048268.
- Dirmeyer, P. A., Jin, Y., Singh, B., and Yan, X. (2013). Trends in Land-Atmosphere Interactions from CMIP5 Simulations, *J. Hydrometeorol.* **14**, 829–849, doi: 10.1175/JHM-D-12-0107.1.
- Ducharne A, Koster RD, Suarez MJ, Praveen K, Stieglitz M (2000). A catchment-based approach to modeling land surface processes in a GCM - Part 2: Parameter estimation and model demonstration, *JGR*, **105** (D20): 24823-24838.
- Ducharne A, Laval K (2000). Influence of the realistic description of soil water-holding capacity on the global water cycle in a GCM, *Journal of Climate*, **13**, 4393-4413.
- Dufresne, J., Foujols, M., Denvil, S., and 58 others (2013). Climate change projections using the IPSL-CM5 Earth System Model: from CMIP3 to CMIP5, *Clim. Dyn.*, **40**, 2123-2165, doi:10.1007/s00382-012-1636-1.
- Entekhabi, D., Rodriguez-Iturbe, I., Castelli, F. (1996). Mutual interaction of soil moisture state and atmospheric processes. *J. Hydrology*, **184**, 3-17.
- Fan, Y., H. Li, G. Miguez-Macho (2013). Global patterns of groundwater table depth. *Science*, **339**, 940-943.
- Fan, Y., S. Richard, R. S. Bristol, S. E. Peters, S. E. Ingebritsen, N. Moosdorf, A. Packman, T. Gleeson, I. Zaslavsky, S. Peckham, L. Murdoch, M. Fienan, M. Cardiff, D. Tarboton, N. Jones, R. Hooper, J. Arrigo, D. Gochis, J. Olson, and D. Wolock (2015). DigitalCrust – a 4D data system of material properties for transforming research on crustal fluid flow, *Geofluids*, **15**, 372– 379, doi: doi.org/10.1111/gfl.12114
- Fan, Y., G. Miguez-Macho, E.G. Jobbagy, R.B. Jackson and C. Otero-Casal (2017). Hydrologic regulation of plant rooting depth, *PNAS*, **114**, 10572-10577, doi : doi/10.1073/pnas.1712381114.
- Fan, Y., Clark, M., Lawrence, D. M., Swenson, S., Band, L. E., Brantley, S. L., et al. (2019). Hillslope hydrology in global change research and Earth system modeling, *Water Resources Research*, **55**, 1737– 1772, https://doi.org/10.1029/2018WR023903
- FAO/IIASA/ISRIC/ISSCAS/JRC, 2012. *Harmonized World Soil Database (version 1.2)*. FAO, Rome, Italy and IIASA, Laxenburg, Austria. (<http://www.iiasa.ac.at/research/LUC/External-World-Soil6database/HTML/>).
- Faroux S., A. T. Kaptué Tchuenté, J.-L. Roujean, V. Masson, E. Martin, and P. Le Moigne (2013) ECOCLIMAP-II/Europe: a twofold database of ecosystems and surface parameters at 1-km resolution based on satellite information for use in land surface, meteorological and climate models. *Geosci. Model Dev.*, **6**, 563-582.
- Feddes, R.A., H. Hoff, M. Bruen, T. Dawson, P. de Rosnay, P. Dirmeyer, R.B. Jackson, P. Kabat, A. Kleidon, A. Lilly, and A.J. Pitman (2001). Modeling Root Water Uptake in Hydrological and Climate Models. *Bull. Amer. Meteor. Soc.*, **82**, 2797–2810, doi:10.1175/1520-0477(2001)082<2797:MRWUIH>2.3.CO;2
- van Genuchten, M. (1980). A closed-form equation for predicting the hydraulic conductivity of unsaturated soils. *Soil Science Society of America Journal*, **44**(5), 892-898.
- Gascoin, Ducharne, Ribstein, Carli, Habets (2009). Adaptation of a catchment-based land surface model to the hydrogeological setting of the Somme River basin (France). *J. Hydrology*, **368**, 105-116.
- Getirana, A., Dutra, E., Guimbeteau, M., Kam, J., Li, H.L., Decharme, B., Zhang, Z., Ducharne, A., Boone, A., Balsamo, G., Rodell, M., Toure, A.M., Xue, Y., Drapeau, G., Arsenault, A., Kumar, S., Leung, L.R., Peters-Lidard, C., Ronchail, J., and Sheffield, J. (2014). Water balance in the Amazon basin from a land surface model ensemble, *J. Hydromet.*, **15**, 2586–2614, doi:10.1175/JHM-D-14-0068.1
- Gulden, L. E., Rosero, E., Yang, Z.-L., Rodell, M., Jackson, C. S., Niu, G.-Y., Yeh, P. J.-F., and Famiglietti, J. (2007). Improving land-surface model hydrology: Is an explicit aquifer model better than a deeper soil profile? *Geophys. Res. Lett.*, **34**, L09402, doi:10.1029/2007GL029804.

- Hourdin, F. et al. (2013). LMDZ5B: the atmospheric component of the IPSL climate model with revisited parameterizations for clouds and convection *Clim. Dyn.*, **40**, 2193–2222.
- Hurrell, J.W., M.M. Holland, P.R. Gent, S. Ghan, J.E. Kay, P.J. Kushner, J. Lamarque, W.G. Large, D. Lawrence, K. Lindsay, W.H. Lipscomb, M.C. Long, N. Mahowald, D.R. Marsh, R.B. Neale, P. Rasch, S. Vavrus, M. Vertenstein, D. Bader, W.D. Collins, J.J. Hack, J. Kiehl, and S. Marshall (2013). The Community Earth System Model: A Framework for Collaborative Research. *Bull. Amer. Meteor. Soc.*, **94**, 1339–1360, doi:10.1175/BAMS-D-12-00121.1
- Koirala, S., Kim, H., Hirabayashi, Y., Kanae, S., & Oki, T. (2019). Sensitivity of global hydrological simulations to groundwater capillary flux parameterizations. *Water Resources Research*, **55**, 402– 425, doi:10.1029/2018WR023434
- Kleidon, A. (2004). Global Datasets of Rooting Zone Depth Inferred from Inverse Methods. *J. Climate*, **17**, 2714–2722, doi:10.1175/1520-0442(2004)017<2714:GDORZD>2.0.CO;2
- Krinner, G., N. Viovy, N. de Noblet-Ducoudré, J. Ogée, J. Polcher, P. Friedlingstein, P. Ciais, S. Sitch, and I. C. Prentice (2005). A dynamic global vegetation model for studies of the coupled atmosphere-biosphere system, *Global Biogeochem. Cycles*, **19**, GB1015.
- Kollet, S., and R. Maxwell (2008). Capturing the influence of groundwater dynamics on land surface processes using an integrated, distributed watershed model. *WRR*, **44**(2):W02402.
- Koster, R. D., et al. (2004). Regions of strong coupling between soil moisture and precipitation. *Science*, **305**, 1138–1140.
- Lafaysse, M., B. Hingray, P. Etchevers, E. Martin, C. Obled (2011). Influence of spatial discretization, underground water storage and glacier melt on a physically-based hydrological model of the Upper Durance River basin, *Journal of Hydrology*, **403**, 116–129, doi:10.1016/j.jhydrol.2011.03.046.
- Lawrence, P.J., and Chase, T.N. (2007). Representing a MODIS consistent land surface in the Community Land Model (CLM 3.0). *J. Geophys. Res.*, **112**, G01023.
- Lawrence, D. M., et al. (2011). Parameterization improvements and functional and structural advances in Version 4 of the Community Land Model, *Journal of Advances in Modeling Earth Systems*, **3**(1), M03001.
- Levine, X.J., Schneider, T. (2011). Response of the Hadley Circulation to Climate Change in an Aquaplanet GCM Coupled to a Simple Representation of Ocean Heat Transport. *Journal of the Atmospheric Sciences*, **68**(4): 769–783. DOI:10.1175/2010jas3553.1
- Lo, M.-H., P. J.-F. Yeh, and J. S. Famiglietti (2008). Constraining water table depth simulations in a land surface model using estimated baseflow, *Adv. Water Resour.*, doi:10.1016/j.advwatres.2008.06.007.
- Lo, M.-H., and J. S. Famiglietti (2011). Precipitation response to land subsurface hydrologic processes in atmospheric general circulation model simulations. *J. Geophys. Res. Atmos.*, **116**, D05107.
- Martínez-de la Torre, A. and Miguez-Macho, G. (2019). Groundwater influence on soil moisture memory and land-atmosphere fluxes in the Iberian Peninsula. *Hydrol. Earth Syst. Sci.*, **23**, 4909–4932, doi:10.5194/hess-23-4909-2019.
- Masson, V., et al. (2013). The SURFEXv7.2 land and ocean surface platform for coupled or offline simulation of earth surface variables and fluxes, *Geosci. Model Dev.*, **6**, 929–960.
- Milly, P.C.D. (1992). Potential Evaporation and Soil Moisture in General Circulation Models. *J. Climate*, **5**, 209–226.
- Mualem, Y. (1976). A new model for predicting the hydraulic conductivity of unsaturated porous media. *Water Resources Research*, **12**(3), 513– 522.
- Niu, G.-Y., Yang, Z.-L., Dickinson, R. E., and Gulden, L. E. (2005). A simple TOPMODEL-based runoff parameterization (SIMTOP) for use in global climate models, *J. Geophys. Res.*, **110**, D21106, doi:10.1029/2005JD006111.
- Pitman, AJ, de Noblet-Ducoudré, N, Cruz, FT, Davin, EL, Bonan, GB, Brovkin, V, Claussen, M, Delire, C, Ganzeveld, L, Gayler, V and others (2009). Uncertainties in climate responses to past land cover change: First results from the LUCID intercomparison study, *Geophys. Res. Lett.*, **36**, L14814, doi:10.1029/2009GL039076.
- Rashid, M., R. Chien, A. Ducharme, H. Kim, P.J. Yeh, C. Peugeot, A. Boone, X. He, L. Séguis, Y. Yabu, M. Boukari, and M. Lo (2019). Evaluation of Groundwater Simulations in Benin from the ALMIP2 Project. *J. Hydrometeorol.*, **20**, 339–354, doi:10.1175/JHM-D-18-0025.1
- Reynolds, C. A., T. J. Jackson, and W. J. Rawls (2000). Estimating soil water-holding capacities by linking the Food and Agriculture Organization Soil map of the world with global pedon databases and continuous pedotransfer functions, *Water Resour. Res.*, **36**(12), 3653–3662.
- Rodell, M., H. K. Beaudoin, T. S. L'Ecuyer, W. S. Olson, J. S. Famiglietti, P. R. Houser, R. Adler, M. G. Bosilovich, C. A. Clayson, D. Chambers, E. Clark, E. J. Fetzer, X. Gao, G. Gu, K. Hilburn, G. J. Huffman, D. P. Lettenmaier, W. T. Liu, F. R. Robertson, C. A. Schlosser, J. Sheffield, and E. F. Wood (2015). The Observed State of the Water Cycle in the Early Twenty-First Century. *J. Climate*, **28**, 8289–8318.
- Russo, T., Lall, U (2017). Depletion and response of deep groundwater to climate-induced pumping variability. *Nature Geosci* **10**, 105–108, doi:10.1038/ngeo2883
- Schär, Lüthi, Beyerle, Heise (1999). The soil-precipitation feedback: A process study with a regional climate model, *J. Climate*, **12** (3), 722–741.

- Schneider, U., Becker, A., Finger, P., Meyer-Christoffer, A., Rudolf, B., Ziese, M. (2011). GPCC Full Data Reanalysis Version 6.0 at 1.0°: Monthly Land-Surface Precipitation from Rain-Gauges built on GTS-based and Historic Data, doi:10.5676/DWD_GPCC/FD_M_V6_100
- Schneider, U., Becker, A., Finger, P., Meyer-Christoffer, A., Ziese, M., Rudolf, B. (2014). GPCC's new land surface precipitation climatology based on quality-controlled in situ data and its role in quantifying the global water cycle. *Theoretical and Applied Climatology*, **115**, 15-40.
- Seneviratne, Corti, Davin, Hirschi, Jaeger, Lehner, Orlowsky, Teuling (2010). Investigating soil moisture-climate interactions in a changing climate: A review, *Earth-Science Reviews*, **99**, 125-161.
- Shah, N., Nachabe, M., and Ross, M. (2007). Extinction depth and evapotranspiration from ground water under selected land covers. *Groundwater*, **45**, 329-338.
- Sheffield, J., G. Goteti, and E. F. Wood (2006). Development of a 50-yr high-resolution global dataset of meteorological forcings for land surface modeling, *J. Climate*, **19** (13), 3088-3111.
- Strückmeier, and Richts (2008). Groundwater Resources Map of the World 1:25,000,000. BGR & UNESCO.
- Taylor, K.E., R.J. Stouffer, and G.A. Meehl, 2012: An Overview of CMIP5 and the Experiment Design. *Bull. Amer. Meteor. Soc.*, **93**, 485–498, doi:10.1175/BAMS-D-11-00094.1
- Tootchi, A., Jost, A., and Ducharne, A. (2019). Multi-source global wetland maps combining surface water imagery and groundwater constraints, *Earth Syst. Sci. Data*, **11**, 189–220, doi:10.5194/essd-11-189-2019, 2019.
- Twine, T.E., W.P. Kustas, J.M. Norman, D.R. Cook, P.R. Houser, T.P. Meyers, J.H. Prueger, P.J. Starks, M.L. Wesely, 2000: Correcting eddy-covariance flux underestimates over a grassland, *Agricultural and Forest Meteorology*, **103**, 279-300. [https://doi.org/10.1016/S0168-1923\(00\)00123-4](https://doi.org/10.1016/S0168-1923(00)00123-4).
- Valcke, S., T. Craig and L. Coquart, 2015. OASIS3-MCT User Guide, OASIS3-MCT_3.0, Technical Report TR/CMGC/15/38, Cefracs, France.
- Vergnes, J.-P., B. Decharme, and F. Habets (2014). Introduction of groundwater capillary rises using subgrid spatial variability of topography into the ISBA land surface model, *J. Geophys. Res. Atmos.*, **119**, 11,065–11,086, doi:10.1002/2014JD021573.
- Voldoire, A., E. Sanchez-Gomez, D. Salas y Mélia, and 23 others (2013). The CNRM-CM5.1 global climate model: description and basic evaluation, *Climate Dynamics*, **40**, 2091. Doi: 10.1007/s00382-011-1259-y
- Wang, F., Ducharne, A., Cheruy, F., Lo, M.-H., and Grandpeix, J.-L. (2018). Impact of a shallow groundwater table on the global water cycle in the IPSL land-atmosphere coupled model, *Climate Dynamics*, **50**, 3505-3522, doi:10.1007/s00382-017-3820-9
- Yang, Y., Donohue, R. J., and McVicar, T. R. (2016). Global estimation of effective plant rooting depth: Implications for hydrological modeling, *Water Resour. Res.*, **52**, 8260– 8276, doi:10.1002/2016WR019392
- Yeh, Pat J-F., Elfatih A. B. Eltahir, 2005: Representation of Water Table Dynamics in a Land Surface Scheme. Part I: Model Development. *J. Climate*, **18**, 1861–1880.
- Yeh, Pat J-F., J. S. Famiglietti, 2009: Regional Groundwater Evapotranspiration in Illinois. *J. Hydrometeor*, **10**, 464–478.

Table 1. Main features of the three land surface models for the reference simulations.

	CLM	ORCHIDEE	SURFEX
Main references	<i>Lawrence et al. [2011]</i>	<i>Krinner et al. [2005]</i> <i>Campoy et al. [2013]</i>	<i>Decharme et al. [2013]</i> <i>Decharme et al. [2015]</i>
Vegetation	Vegetation map	Based on MODIS [<i>Lawrence and Chase, 2007</i>]	IPSL-CM5 maps [<i>Dufresne et al., 2013</i>]
	Nb. of PFTs (including bare soil)	17	13
	LAI	Prescribed	Computed (STOMATE module)
Soil hydrology	Soil texture	Based on sand and clay content for each soil layer, from the IGBP soil dataset (Global Soil Data Task 2000).	12 USDA classes, based on the map of <i>Reynolds et al. [2000]</i>
	Soil hydraulic properties	<i>Brooks and Corey [1966]</i>	<i>Van Genuchten [1980]</i> <i>Mualem [1976]</i>
	Independent soil tiles in one grid-cell	No	Yes: up to 3
	Vertical discretization	Soil depth =3.4 m, with 10 layers of increasing depth	Soil depth = 2 m, with 22 layers
	Surface runoff	A TOPMODEL-based model for surface runoff [<i>Niu et al., 2005</i>], including saturation-excess and infiltration-excess mechanisms	Infiltration-excess, with sub-grid variability
	Separate aquifer	Yes: conceptual aquifer below the soil (bedrock at 25 m)	No
	Drainage and baseflow	Gravitational drainage + subsurface runoff based on the SIMTOP scheme [<i>Niu et al., 2005</i>] + baseflow from aquifer	Gravitational drainage at soil bottom Gravitational drainage at soil bottom and lateral Topmodel-based baseflow in the root zone
Atmospheric model	CAM5 [<i>Hurrell et al., 2013</i>] at $1.9^\circ \times 2.5^\circ$ horizontal resolution, with 30 vertical layers	ARPEGE [<i>Volodioire et al., 2013</i>] at T127 horizontal resolution ($\sim 1.5^\circ$) with 91 vertical levels	LMDZ5B [<i>Dufresne et al., 2013</i>], at low standard resolution (96x95 horizontally, $\sim 3.7^\circ \times 1.9^\circ$; 39 vertical levels)

Table 2. Simulations names.

Model	Configuration	Reference simulation	Prescribed WTD simulations
CLM	Forced: fC	fC_REF	fC_D005, fC_D01, fC_D02, fC_D03, fC_D05, fC_D08, fC_D10
	AMIP: aC	aC_REF	aC_D01, aC_D02, aC_D03, aC_D05, aC_D08, aC_D10
ORCHIDEE	Forced: fO	fO_REF	fO_D005, fO_D01, fO_D02, fO_D03, fO_D05, fO_D08, fO_D10
	AMIP: aO	aO_REF	aO_D01, aO_D02, aO_D03, aO_D05, aO_D08, aO_D10
SURFEX	Forced: fS	fS_REF	fS_D005, fS_D01, fS_D02, fS_D03, fS_D05, fS_D08, fS_D10
	AMIP: aS	aS_REF	aS_D01, aS_D02, aS_D03, aS_D05, aS_D08, aS_D10

Table S1. Pluriannual land mean ET for the different simulations and % change with respect to the reference simulations (in italic). The simulation names are defined in Table 2.

WTD (m)	Forced						Coupled					
	CLM4		SURFEX		ORCHIDEE		CLM4		SURFEX		ORCHIDEE	
	mm/d	%	mm/d	%	mm/d	%	mm/d	%	mm/d	%	mm/d	%
REF	1.32	<i>100.0</i>	1.28	<i>100.0</i>	1.31	<i>100.0</i>	2.11	<i>141.4</i>	2.52	<i>201.4</i>	2.36	<i>138.7</i>
10	1.29	<i>97.8</i>	1.30	<i>101.0</i>	1.35	<i>102.7</i>	1.96	<i>131.1</i>	2.23	<i>177.7</i>	1.82	<i>106.8</i>
8	1.30	<i>98.2</i>	1.30	<i>101.4</i>	1.35	<i>102.8</i>	1.77	<i>118.4</i>	1.53	<i>121.8</i>	1.76	<i>103.5</i>
5	1.35	<i>101.9</i>	1.33	<i>103.4</i>	1.36	<i>103.7</i>	1.47	<i>98.3</i>	1.35	<i>107.3</i>	1.73	<i>101.8</i>
3	1.62	<i>122.8</i>	1.44	<i>112.4</i>	1.38	<i>105.4</i>	1.47	<i>98.3</i>	1.29	<i>102.6</i>	1.72	<i>100.9</i>
2	1.97	<i>149.2</i>	1.99	<i>155.0</i>	1.42	<i>108.4</i>	1.47	<i>98.1</i>	1.27	<i>101.4</i>	1.70	<i>100.0</i>
1	2.42	<i>182.9</i>	2.55	<i>198.7</i>	1.91	<i>145.4</i>	1.49	<i>100.0</i>	1.25	<i>100.0</i>	1.70	<i>100.0</i>
0.5	2.61	<i>197.1</i>	2.70	<i>210.0</i>	2.75	<i>209.9</i>	-	-	-	-	-	-

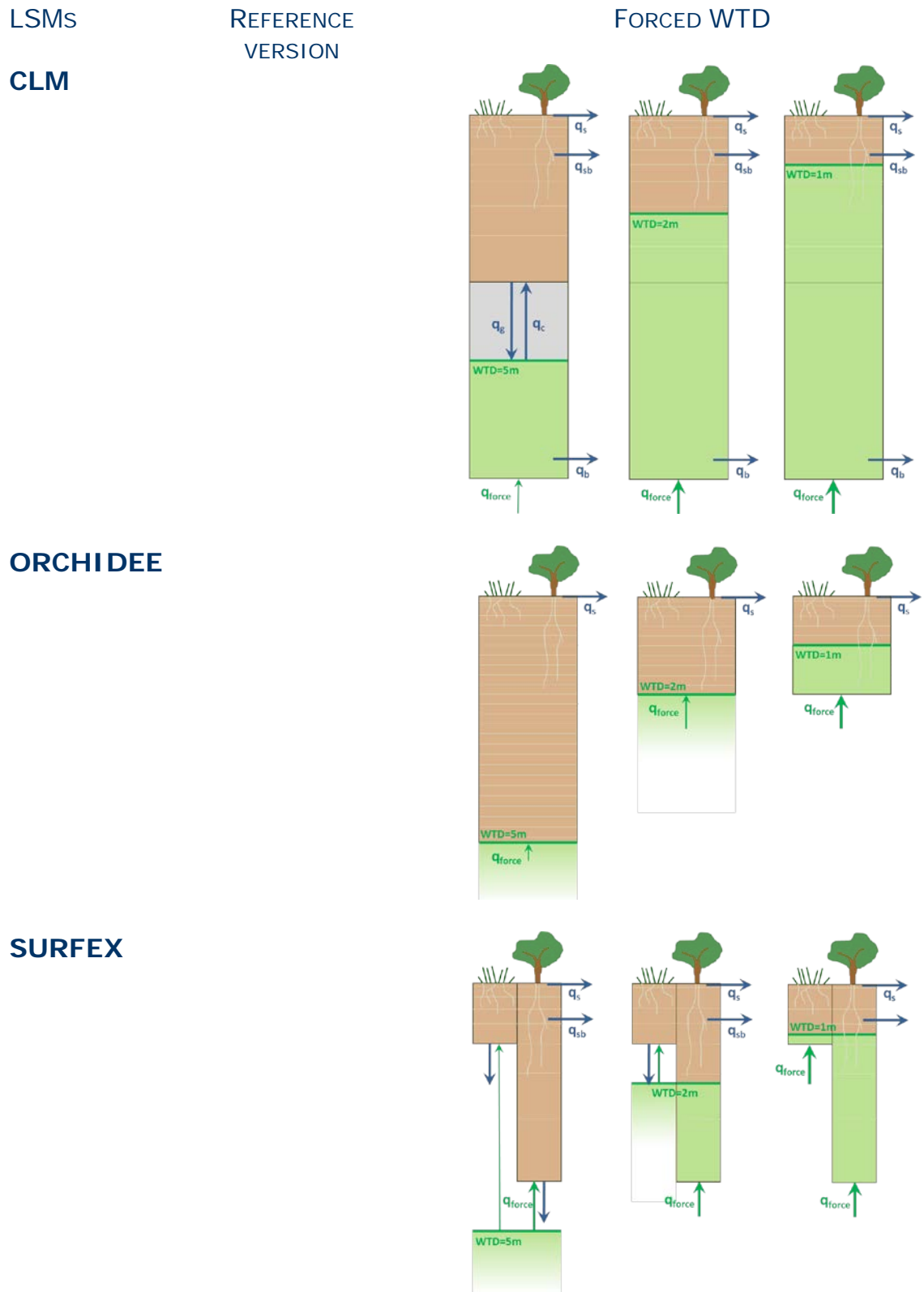


Figure 1. Main features of the models, in the reference configuration (left) and with forced WTD (right).

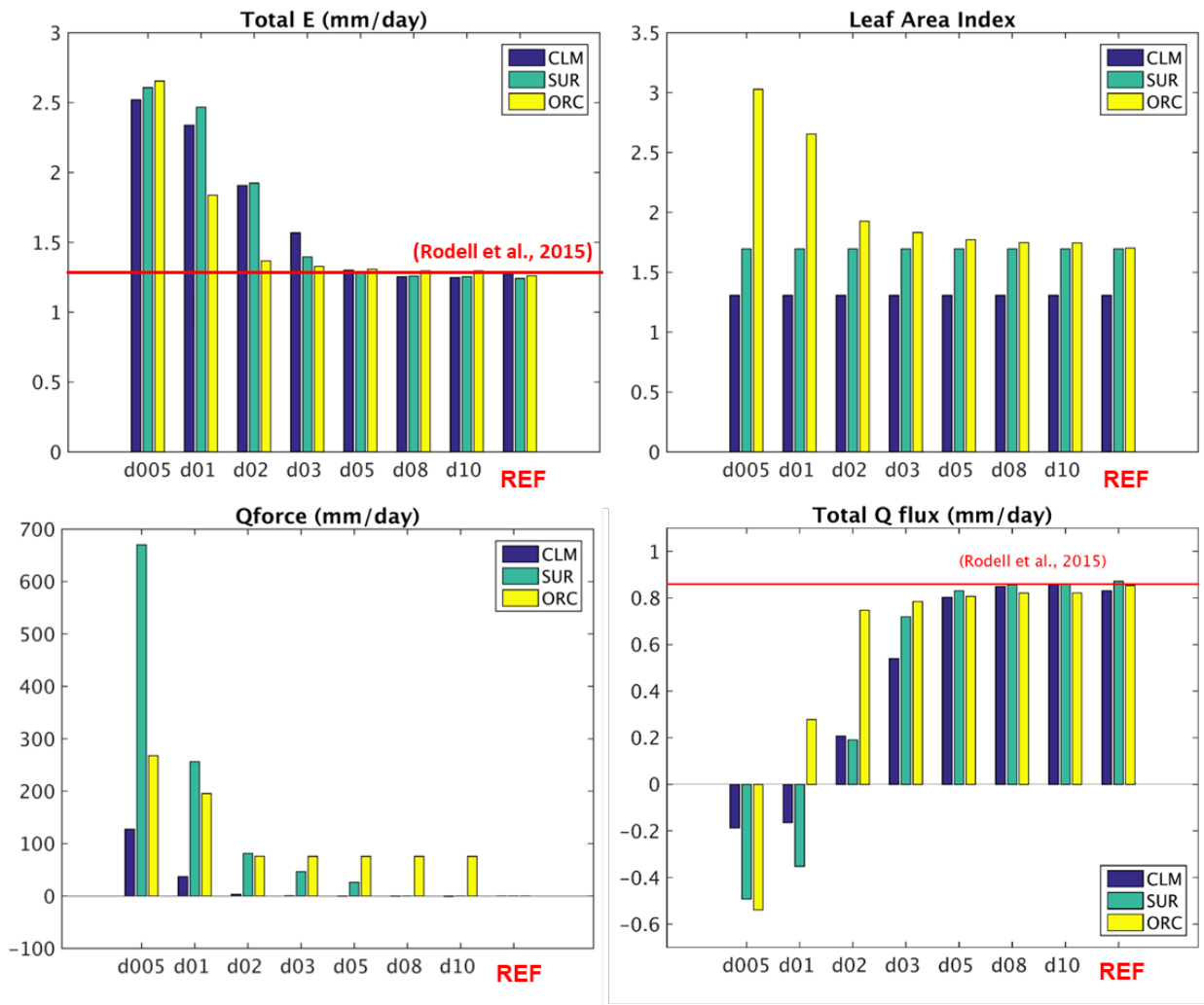


Figure 2. Land average sensitivity to forced WTD in off-line simulations, on pluriannual means (1979-2010) of evapotranspiration, LAI, qforce, and total runoff. The red lines indicate the land-average estimates of [Rodell et al., 2015].

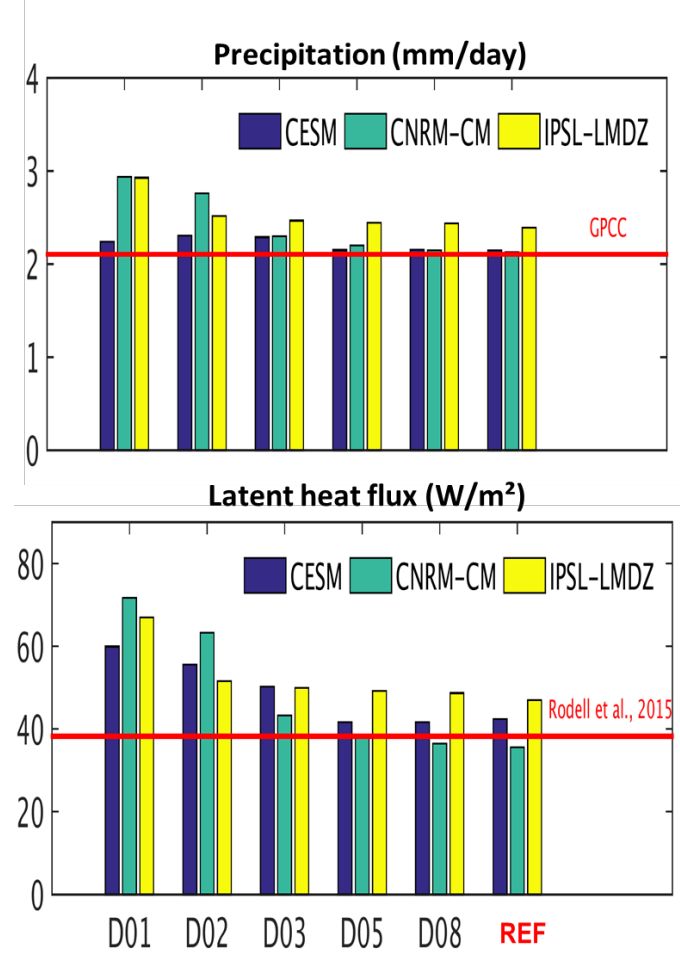


Figure 3. Land average sensitivity to forced WTD in coupled simulations, on pluriannual means (1979-2008) of precipitation and latent heat flux. The red lines indicate the land-average estimates of GPCC [Schneider *et al.*, 2011] and [Rodell *et al.*, 2015].

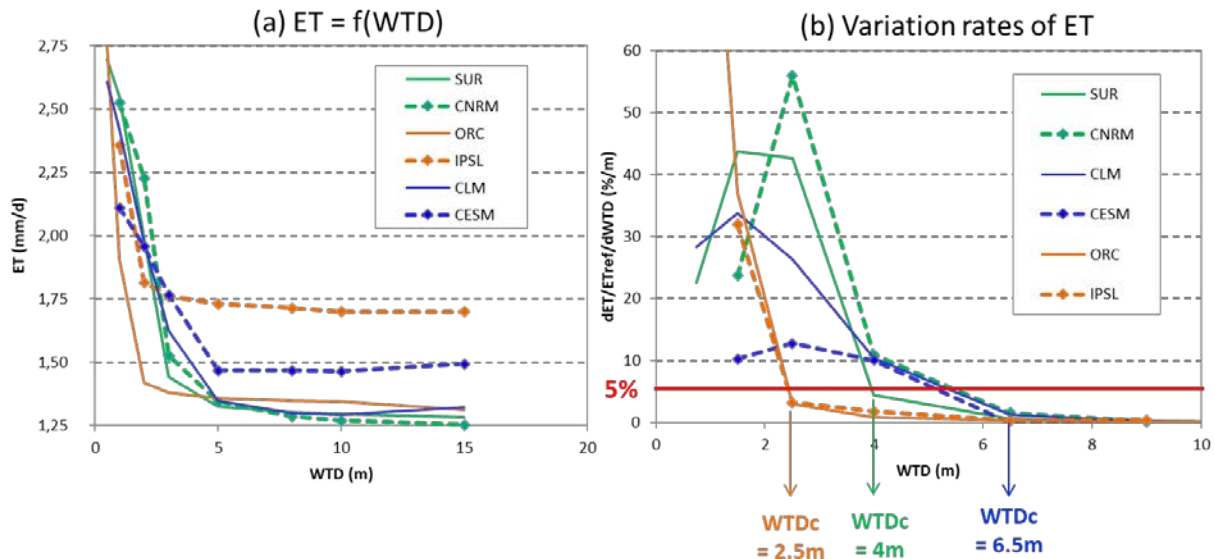


Figure 4. Response of land surface averages of ET (pluriannual means) to forced WTD for the three land surface models (results from forced/coupled simulations appear in plain/dashed lines): (a) variation of mean ET with prescribed WTD (the reference simulation is assigned a WTD of 15 m); (b) variation rates of ET with respect to WTD, expressed in % of reference ET per meter, showing how we can define a critical WTD for each model using a 5% threshold to define small ET variations.

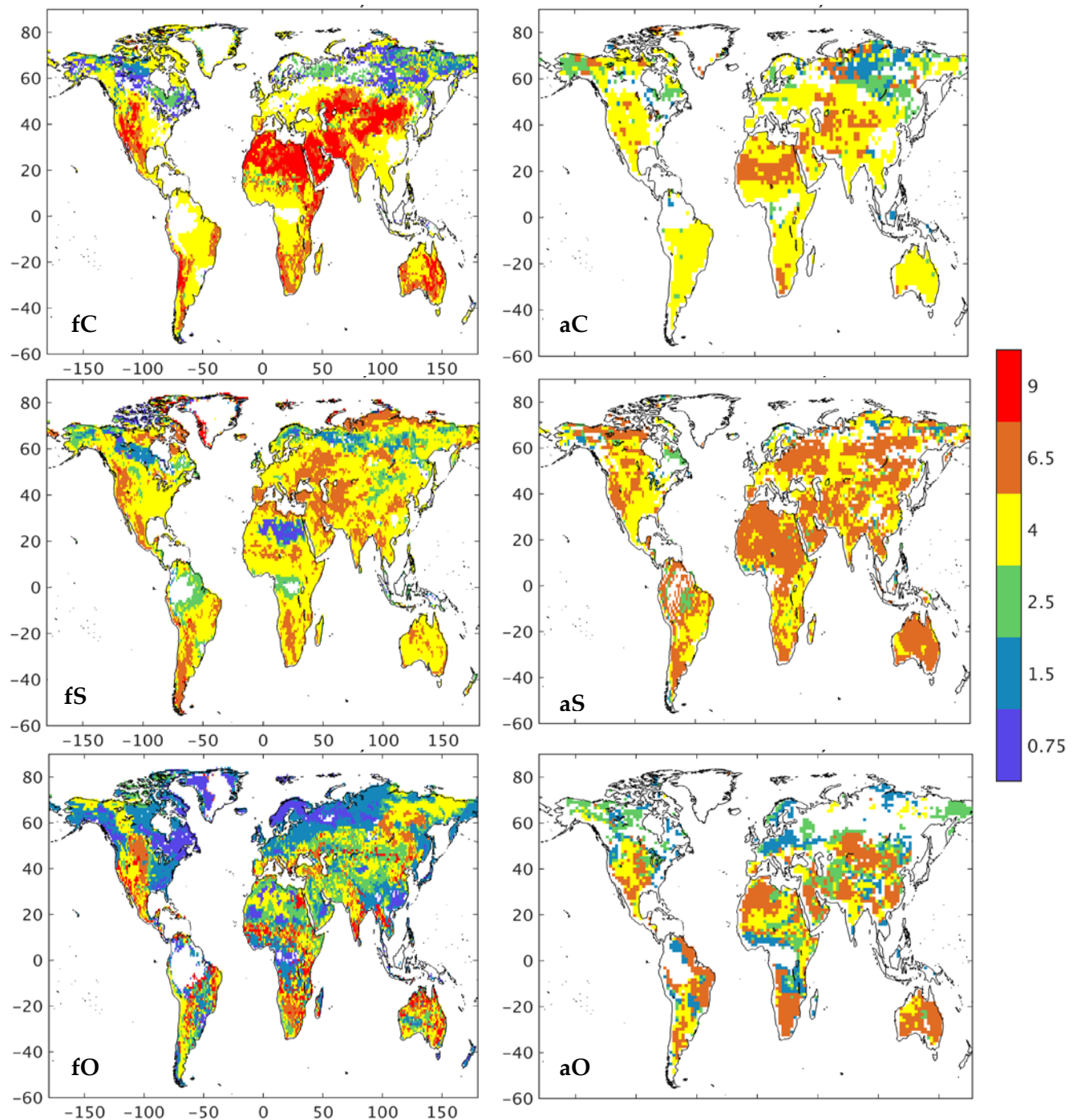


Figure 5. Maps of the critical WTDc for the three models, with a threshold of 1% of the reference ET: top: CLM; middle: SURFEX; bottom: ORCHIDEE; Forced/AMIP configuration on the left/right. White areas correspond to areas where the relative changes in ET with WTD are smaller than 1% whichever the WTD.

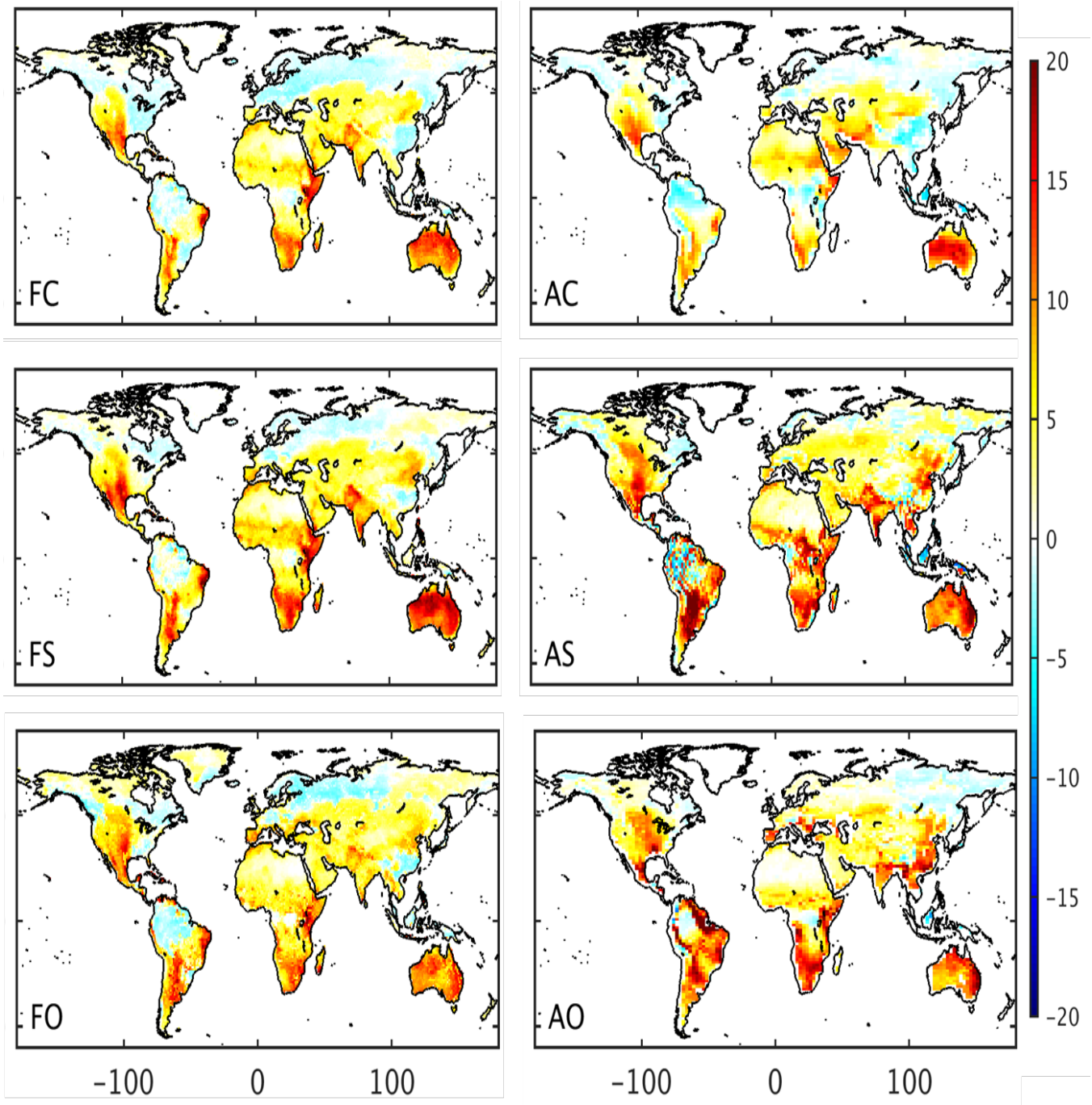


Figure 6. Coupling strength of Dirmeyer *et al.* [2013] (in W/m^2) for the six reference simulations, based on annual means: top: CLM; middle: SURFEX; bottom: ORCHIDEE; Forced/AMIP configuration on the left/right.

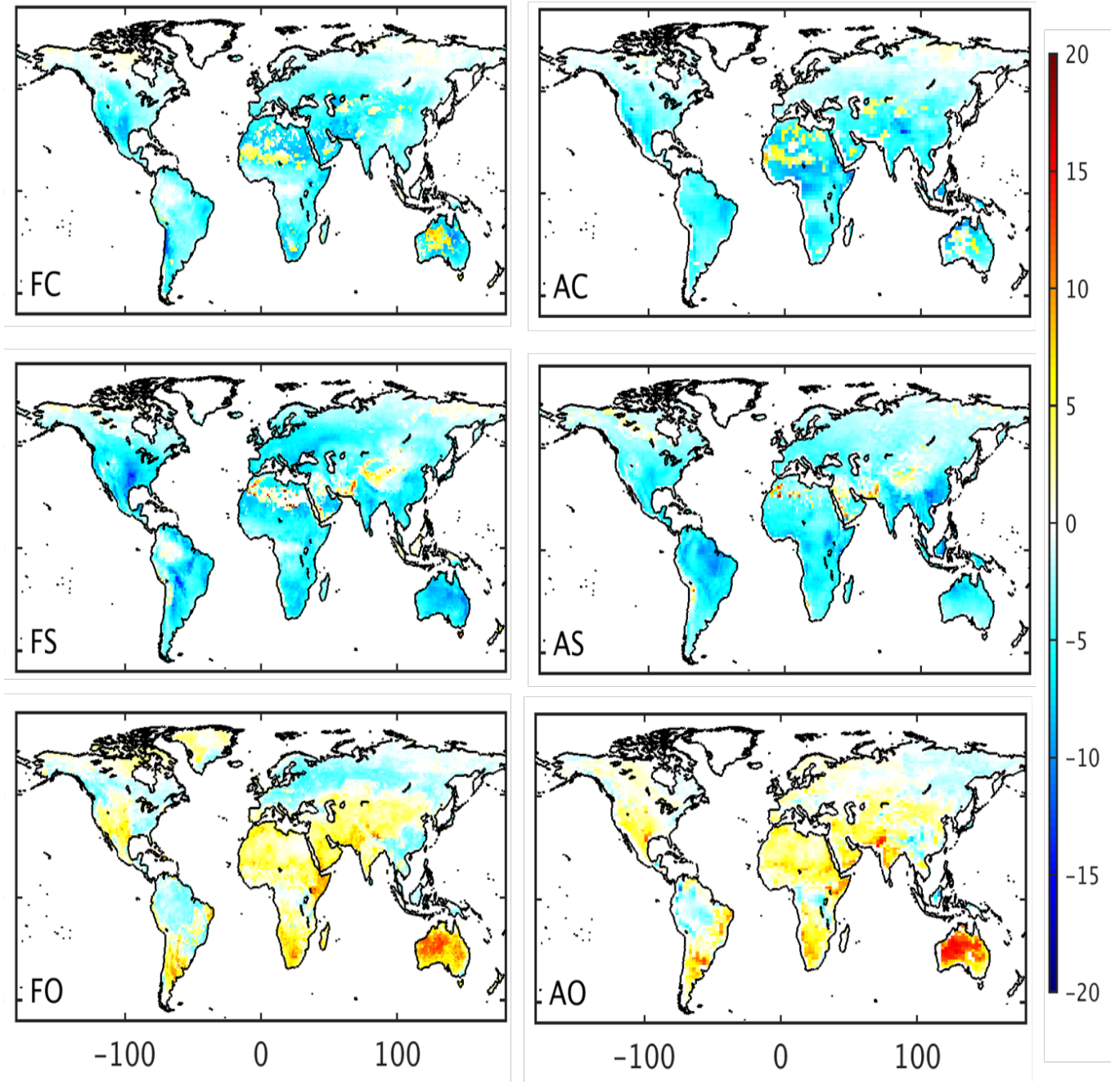


Figure 7. Coupling strength of Dirmeyer *et al.* [2013] (in W/m²) for the six simulations D01 (1m WTD), based on annual means: top: CLM; middle: SURFEX; bottom: ORCHIDEE; Forced/AMIP configuration on the left/right.

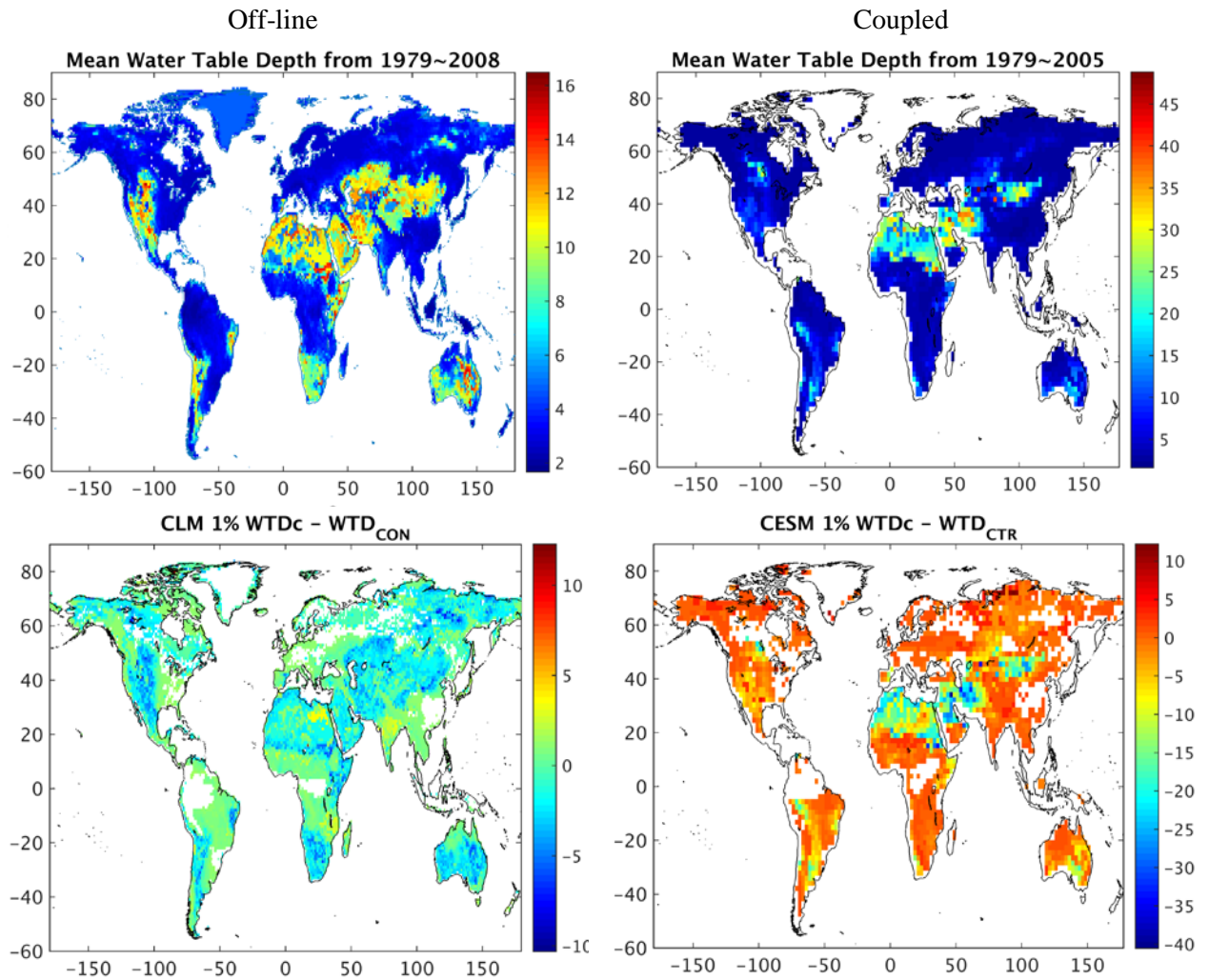


Figure 8. Comparison between critical WTD (with a 1% threshold) and mean WTD in the reference simulation with CLM4. Offline results on the left, coupled results on the right. All values in m. White areas where no WTD_c could be defined.

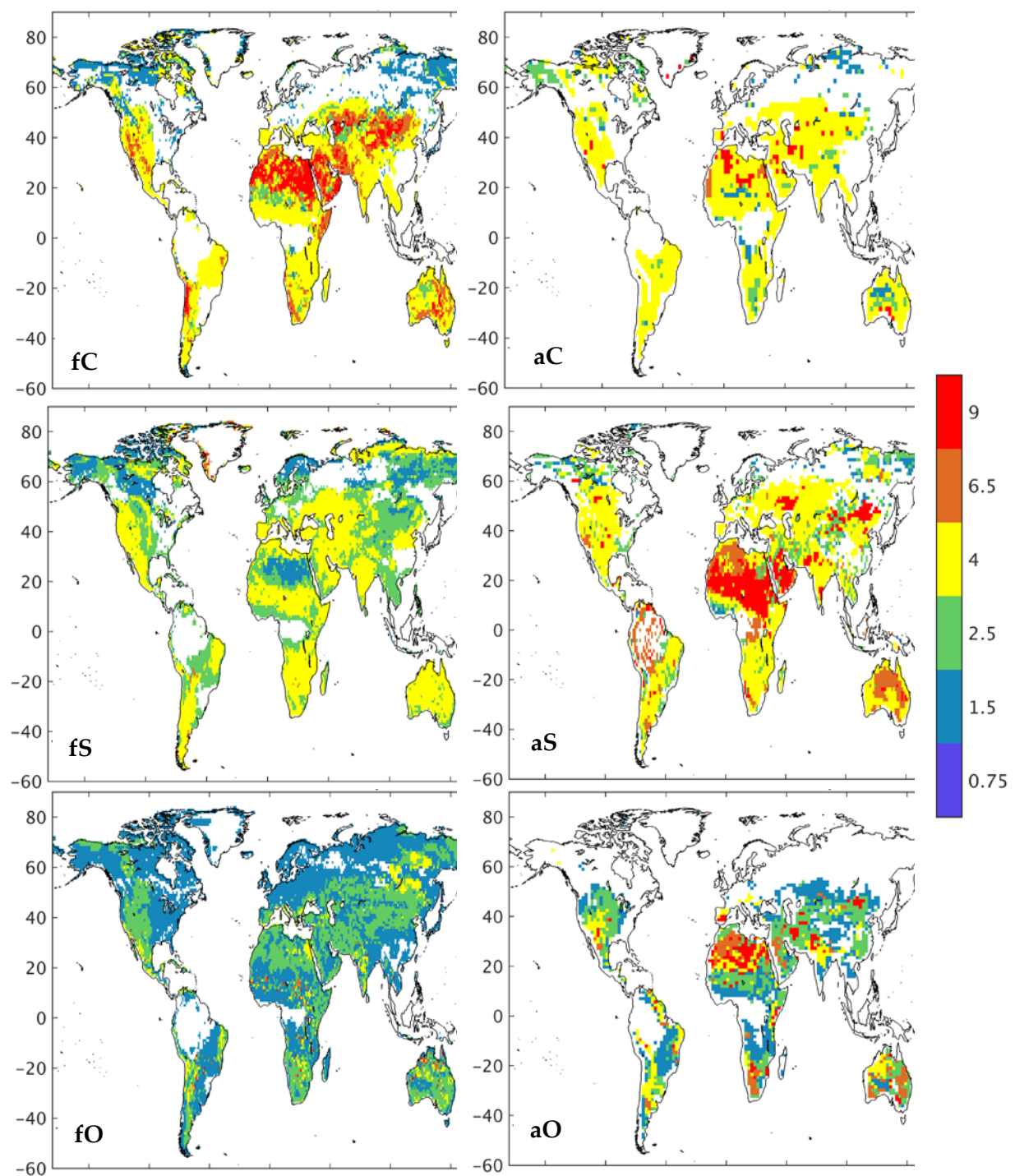


Figure S1. Maps of the critical WTDc for the three models, with a threshold of 5% of the reference ET: top: CLM; middle: SURFEX; bottom: ORCHIDEE; Forced/AMIP configuration on the left/right. White areas correspond to areas where the relative changes in ET with WTD are smaller than 5% whichever the WTD.

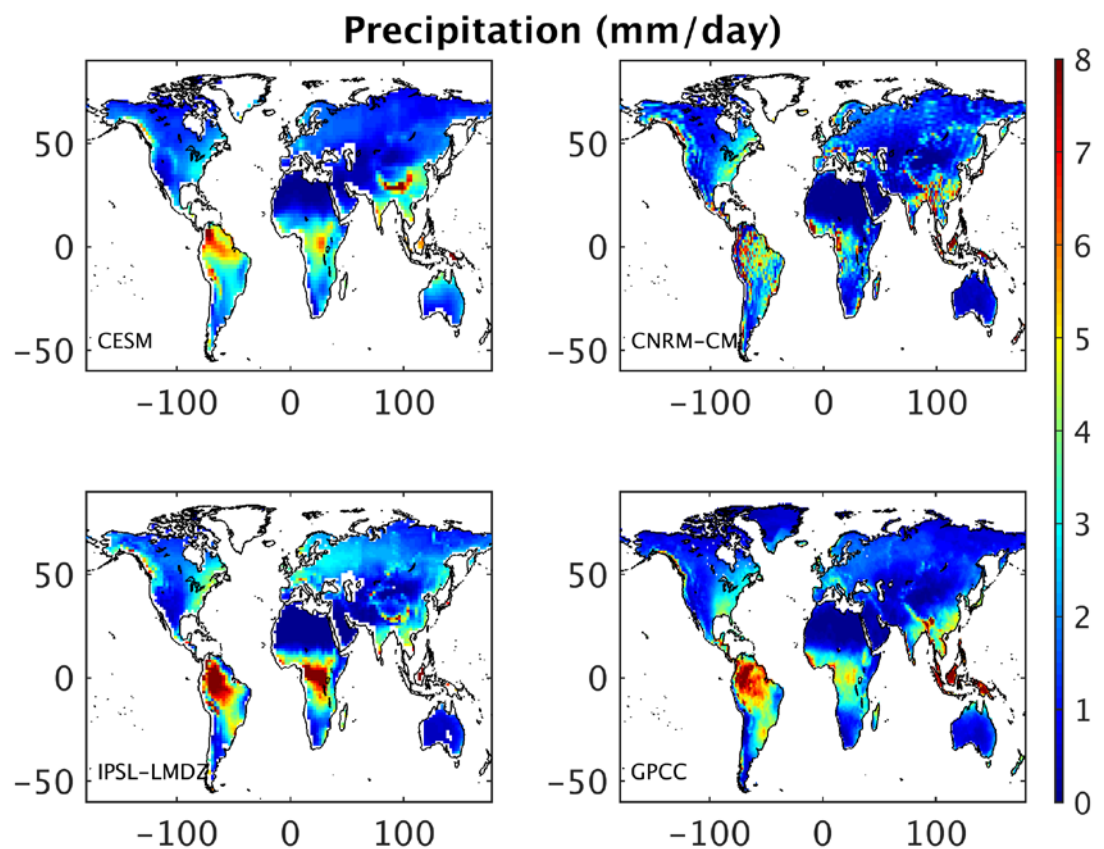
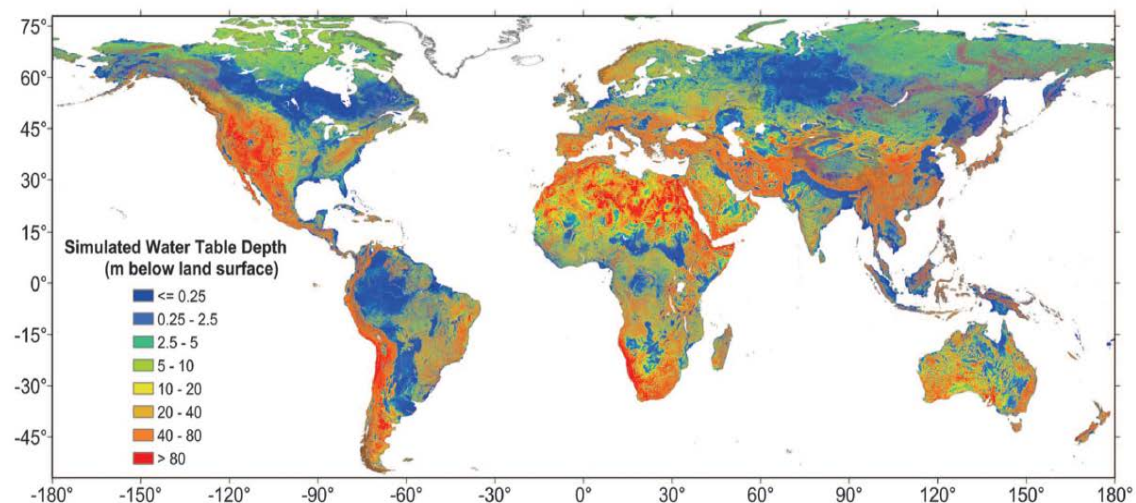


Figure S2. Pluriannual yearly mean precipitation (in mm/d over 1979-2008) from the three climate models and the GPCC [Schneider *et al.*, 2014].

(a)



(b)

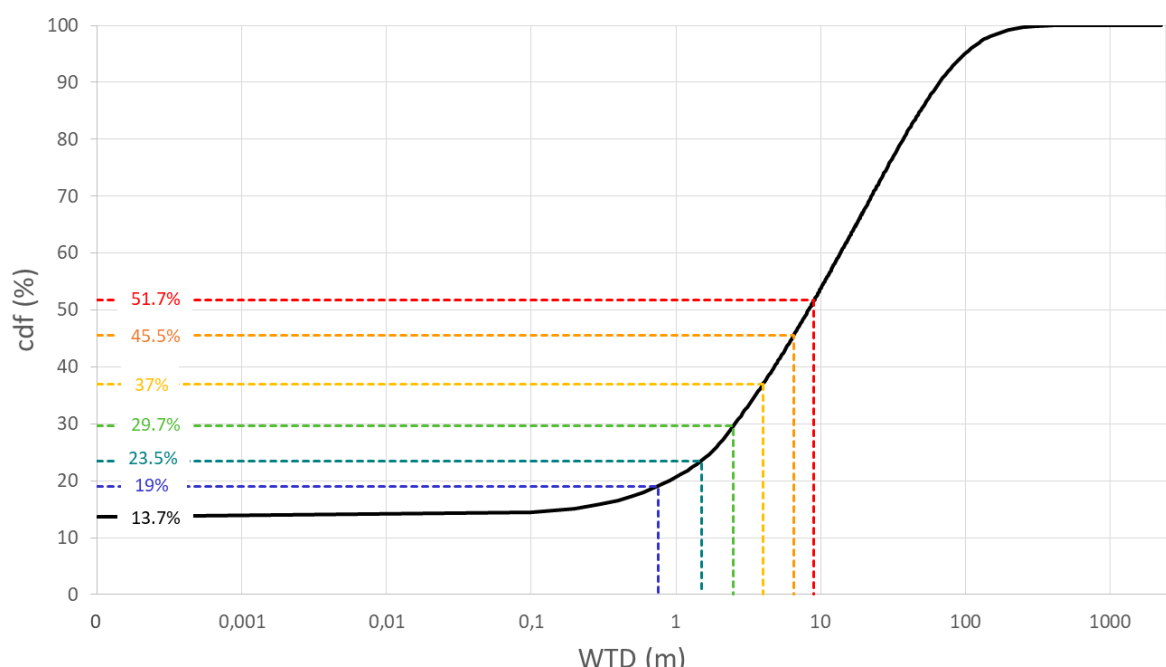


Figure S3. Simulated WTD from *Fan et al. [2013]*: (a) global map; (b) cumulative distribution function (cdf). The colored dashed lines correspond to the critical WTDs values used in Fig. 5. viz. 0.75. 1.5. 2.5. 4. 6.5 and 9 m. The 13.7% assigned to zero comprise inundated areas with WT above the soil surface.

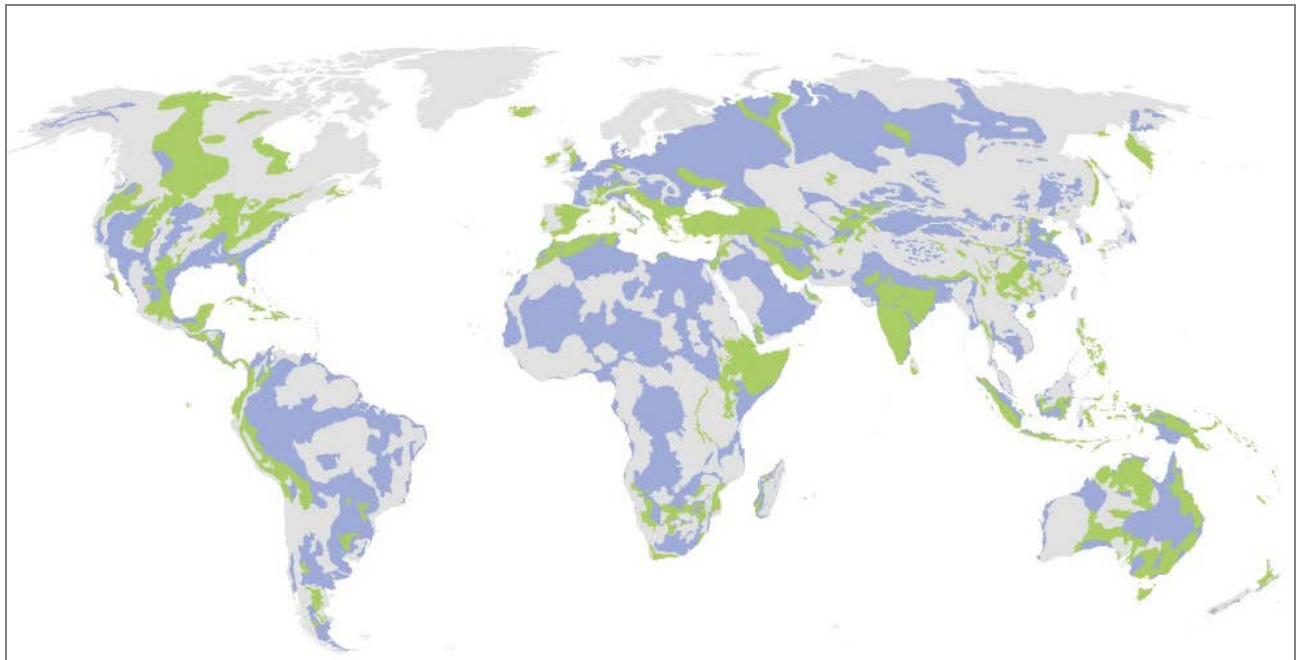


Figure S4. Classification of the aquifer formations of the world by Strückmeier & Richts [2008]. Blue underlines large and rather uniform aquifer systems, usually in large sedimentary basins that may offer good conditions for groundwater exploitation; green corresponds to complex hydrogeological environments, including some productive aquifers in heterogeneous folded or faulted regions (including karst aquifers). Grey is used for other areas, with relatively dense bedrock exposed to the surface, so the aquifers; when present; are local and shallow.

F.2 SENSIBILITE AUX CONSTANTES DE TEMPS DES EAUX SOUTERRAINES (NOUVEAU LIVRABLE)

La thèse d'Ana Schneider a été partiellement financée par le projet ANR IGEM (co-financement KIC-Climat pour les 3 premières années). Elle a été encadrée par Agnès Ducharne et Anne Jost (P1 METIS), et soutenue le 22 juin 2017 à l'UPMC. La thèse visait à améliorer la caractérisation de la vitesse d'écoulement des eaux souterraines (via une constante de temps) dans le modèle de surface ORCHIDEE de l'IPSL, à partir de la formule à bases physiques de Boussinesq, et des bases de données globales des propriétés du milieu souterrain. Une autre information nécessaire est la densité du réseau de drainage, qui a été caractérisée globalement en rendant compte de la variabilité spatiale forte de cette grandeur (Schneider et al., 2017), contrairement aux autres bases de données existantes. En ce qui concerne les simulations ORCHIDEE, la conclusion principale est que les constantes de temps proposées, beaucoup plus longues que les valeurs par défaut, sont trop importantes, et réduisent trop fortement les contrastes saisonniers des débits simulés. Les perspectives sont de modifier les paramètres d'entrée (qui correspondent probablement à des zones trop profondes) ou de modifier le calcul des débits en rajoutant un compartiment plus dynamique, ce qui renvoie aux développements suivants menés dans la thèse d'Ardalan Tootchi (Annexe F.4).

Ana Schneider (2017). Estimation of the base flow time constant for global scale applications, Thèse de doctorat de l'Université Pierre et Marie Curie, 172 pp. [Lien vers le manuscrit de thèse en PDF](#)

Résumé : La constante de temps du débit de base (τ) représente le temps moyen pour que l'eau souterraine arrive à la rivière depuis la zone de recharge dans un bassin donné. C'est un élément clé pour simuler le débit de base dans les modèles simples des eaux souterraines, tels qu'ORCHIDEE. τ a été estimée à l'échelle globale à partir d'une solution de l'équation de Boussinesq pour les aquifères libres en pente. τ dépend de la porosité efficace, de la transmissivité, de la pente de l'aquifère et de la densité de drainage (δ).

Calculées à partir de bases de données globales, les valeurs de τ sont surestimées par rapport à celles obtenues par analyse des courbes de récession. Une analyse de sensibilité a montré que la transmissivité et δ sont les principales sources d'incertitude de τ . L'extraction d'un nouveau réseau de drainage, qui dépend de la lithologie, du climat, de la pente et des δ observées, a permis d'obtenir des δ conformes aux valeurs observées aux échelles régionales et à la variabilité spatiale. L'utilisation de ces nouvelles δ et la combinaison de deux jeux de données de conductivité hydraulique pour le sol et l'aquifère a réduit τ de deux ordres de grandeur, mais les valeurs calculées restent surestimées. L'utilisation de τ dans le modèle de surface ORCHIDEE a montré une forte sensibilité du débit simulé à l'augmentation de τ , qui dégrade les débits simulés par rapport aux observations. Cette méthodologie nécessite des valeurs plus adaptées de transmissivité et porosité efficace par rapport aux jeux de données globaux actuellement disponibles pour obtenir des valeurs de τ plus proches de celles attendues et qui permettent de reproduire les débits observés.

Schneider AS, Jost A, Coulon C, Silvestre M, Théry S, Ducharne A (2017). Global scale river network extraction based on high-resolution topography, constrained by lithology, climate, slope, and observed drainage density. Geophysical Research Letters, 44, 2773–2781, doi:[10.1002/2016GL071844](https://doi.org/10.1002/2016GL071844)

Abstract: To improve the representation of surface and groundwater flows, global land surface models rely heavily on high-resolution digital elevation models (DEMs). River pixels are routinely defined as pixels with drainage areas that are greater than a critical drainage area (A_{cr}). This parameter is usually uniform across the globe, and the dependence of drainage density on many environmental factors is often overlooked. Using the 15" HydroSHEDS DEM as an example, we propose the calibration of a spatially variable A_{cr} as a function of slope, lithology, and climate, to match drainage densities from reference river networks at a 1:50,000 scale in France and Australia. Two variable A_{cr} models with varying complexities were derived from the calibration, with satisfactory performances compared to the reference river networks. Intermittency assessment is also proposed. With these simple tools, river networks with natural heterogeneities at the 1:50,000 scale can be extracted from any DEM.

F.3 PARAMETRISATION DES LIENS NAPPES/SURFACE DANS LE MODELE DE L'IPSL (NOUVEAU LIVRABLE)

La thèse d'Ardalan Tootchi a été partiellement financée par le projet ANR IGEM (co-financement par le GIS R2DS de la région Ile de France pour les 3 premières années). Elle a été encadrée par Agnès Ducharne et Anne Jost (P1 METIS), et soutenue le 1er juillet 2019 à Sorbonne Université. Cette thèse a été une contribution importante au développement de la nouvelle paramétrisation des liens nappe/surface dans le modèle de surface ORCHIDEE de l'IPSL, qui repose sur la séparation dans chaque maille d'une fraction basse (« lowland »), correspondant aux zones riveraines des cours d'eau, et alimentée les écoulements (en souterrain et en surface) issus de la fraction haute. Les développements du code ont été menés par Thomas Verbeke (post-doc IGEM), et la thèse d'Ardalan Tootchi a permis de construire la carte des fractions basses à l'échelle du globe (Tootchi et al., 2019) et de tester le nouveau modèle dans le bassin de la Seine, en mode forcé par des données météorologique, donc sans couplage avec le climat.

Ardalan Tootchi (2019) Development of a global wetland map and application to describe hillslope hydrology in the ORCHIDEE land surface model, Sorbonne Université. [Lien vers le manuscrit de thèse en PDF](#)

Résumé : Les zones humides jouent un rôle important dans le fonctionnement du système Terre aussi bien à l'échelle locale, via un effet tampon sur les crues et épurateur de l'eau (dénitrification), que régionalement, du fait de leurs interactions avec l'atmosphère et de leur contribution majeure aux émissions de méthane. Leur représentation dans les modèles climatiques planétaires requiert une connaissance approfondie à la fois de leur distribution géographique et de leur hydrologie. Il y a un vaste désaccord sur l'estimation de l'étendue globale des zones humides, comprise entre 3% et 21% de la surface terrestre continentale, selon les méthodes employées. Ces contradictions s'expliquent par une représentation incomplète par les modèles hydrogéologiques des zones régulièrement inondées identifiées par l'imagerie satellitaire,

qui peine en revanche à détecter les zones humides alimentées par les eaux souterraines. Peu visibles, elles sont également sous-estimées par la plupart des inventaires. La première étape de la thèse s'est donc focalisée sur la construction d'une carte mondiale des zones humides visant à concilier ces différences, par la distinction de ces deux types de zones humides, obtenus par combinaison des méthodes d'imagerie des eaux de surface et de modélisation des eaux souterraines. La proportion de zones humides à la surface du globe (21%) se situe dans la fourchette haute des estimations précédentes et concorde avec de nombreuses études régionales récentes, notamment en France et aux Etats-Unis. Dans une seconde étape, cette carte a servi d'entrée à une nouvelle version du modèle ORCHIDEE, qui décrit les surfaces continentales dans le modèle de climat de l'IPSL. La carte permet de distinguer dans chaque maille du modèle une fraction humide qui correspond aux fonds de vallée et reçoit les écoulements de la fraction haute, ce qui y rend possible le développement d'une nappe proche de la surface dont la profondeur répond au climat. Cette nouvelle version, dite ORCHIDEE-WET, a été testée dans le bassin de la Seine par comparaison à des observations de débit, d'évapotranspiration et de profondeur de nappe et afin de mieux comprendre l'effet des paramètres mal contraints tels que la profondeur du sol ou la formulation du flux nappe-rivière. Les effets principaux sont une augmentation de l'évaporation, une baisse des débits et un effet refroidissant, dont les conséquences sur le climat présent mais aussi futur sont une perspective importante à ce travail.

Tootchi A, Jost A, Ducharne A (2019). Multi-source global wetland maps combining surface water imagery and groundwater constraints. Earth System Science data, 11, 189-220, doi: 10.5194/essd-11-189-2019.

Abstract: Many maps of open water and wetlands have been developed based on three main methods: (i) compiling national and regional wetland surveys, (ii) identifying inundated areas via satellite imagery and (iii) delineating wetlands as shallow water table areas based on groundwater modeling. However, the resulting global wetland extents vary from 3 % to 21 % of the land surface area because of inconsistencies in wetland definitions and limitations in observation or modeling systems. To reconcile these differences, we propose composite wetland (CW) maps, combining two classes of wetlands: (1) regularly flooded wetlands (RFWs) obtained by overlapping selected open-water and inundation datasets; and (2) groundwater-driven wetlands (GDWs) derived from groundwater modeling (either direct or simplified using several variants of the topographic index). Wetlands are statically defined as areas with persistent near-saturated soil surfaces because of regular flooding or shallow groundwater, disregarding most human alterations (potential wetlands). Seven CW maps were generated at 15 arcsec resolution (ca. 500 m at the Equator) using geographic information system (GIS) tools and by combining one RFW and different GDW maps. To validate this approach, these CW maps were compared with existing wetland datasets at the global and regional scales. The spatial patterns were decently captured, but the wetland extents were difficult to assess compared to the dispersion of the validation datasets. Compared with the only regional dataset encompassing both GDWs and RFWS, over France, the CW maps performed well and better than all other considered global wetland datasets. Two CW maps, showing the best overall match with the available evaluation datasets, were eventually selected. These maps provided global wetland extents of 27.5 and 29 million km², i.e., 21.1 % and 21.6 % of the global land area, which are among the highest values in the literature and are in line with recent estimates also recognizing the contribution of GDWs. This wetland class covers 15 % of the global land area compared with 9.7 % for RFW (with an overlap of ca. 3.4 %), including wetlands under canopy and/or cloud cover, leading to high wetland densities in the tropics and small scattered wetlands that cover less than 5 % of land but are highly important for hydrological and ecological functioning in temperate to arid areas. By distinguishing the RFWS and GDWs based globally on uniform principles, the proposed dataset might be useful for large-scale land surface modeling (hydrological, ecological and biogeochemical modeling) and environmental planning. The dataset consisting of the two selected CW maps and the contributing GDW and RFW maps is available from PANGAEA at <https://doi.org/10.1594/PANGAEA.892657> (Tootchi et al., 2018).

F.4 INFLUENCE OF GROUNDWATER ON PRESENT AND PAST CLIMATE (D2.3 AND D3.2)

By Ducharme A, Colin J, Decharme B, Cheruy F, Ghattas J, P Arboleda, Lo MH.

1. Introduction

Groundwater (GW) constitutes by far the largest volume of liquid freshwater on Earth. The most active part is soil moisture (SM), recognized as a key variable of land/atmosphere interactions, especially in so-called transition zones, where/when SM varies between wet and dry values (Koster et al., 2004; Seneviratne et al., 2010; Cheruy et al., 2014). But GW can also be stored in deeper reservoirs than soils, in particular unconfined aquifer systems, in which the saturated part is called the water table. The latter is characterized by slow and mostly horizontal water flows towards the river network, with well-known buffering effects on streamflow variability (e.g. Gascoin et al., 2009). Where/when the water table is shallow enough, it can also sustain SM by means of capillary rise, thus increase evapotranspiration (ET), with potential impact on the climate system (including temperatures and precipitation). This feedback is frequently overlooked, although it has been demonstrated in both regional and global scale climate models (Maxwell et al., 2007; Lo & Famiglietti, 2011; Campoy et al., 2013; Wang et al., 2018; Ducharme et al., submitted). The large residence time of GW may also increase the Earth system's memory, with consequences on the persistence of extreme events, hydro-climatic predictability, and anthropogenic climate change, particularly the magnitude of regional warming.

Here, our main goal is to explore the impacts of GW-SM interactions on historical and future climate, by comparing integrations from three different climate models used in CMIP6 (Coupled Model Intercomparison Project Phase 6, Eyring et al., 2016). Their land surface component explicitly describe the spatio-temporal dynamics of GW with GW-SM interactions, but these processes are based on different physical assumptions representative of the state of the art (e.g. scale of GW flow, active depth, input parameters, see a full review in Gleeson et al., 2019). For each climate model, we compare two transient land-atmosphere simulations, one with GW-SM interaction, and a reference simulation, where the related processes are deactivated. Each transient simulation covers 1980-2100, using the SSP5-8.5 radiative forcing after 2015 (O'Neill et al., 2016). The required sea forcing, identical for each transient simulation, comes from observations for 1979-2014, and is deduced from an SSP5-8.5 fully coupled (land-ocean-atmosphere) CNRM-CM simulation.

Within this framework, we want to assess the sensitivity of the simulated climate to GW-SM interaction in a systematic way, by trying to identify robust features among the three models. Our main objectives are twofold: (1) Compare GW-SM and REF simulations to observations to assess if accounting for GW related processes improves some simulated land or climate parameters; (2) Compare future and historical periods to assess if the GW-SM interaction is able to alter the manifestations of climate change. For instance, can we get weaker regional warming in areas with significant GW-SM interactions? The projected simulations have been performed (deliverable D3.1), but their analysis is still preliminary, and has mostly focus on the IPSL simulations, with complementary offline simulations, i.e. driven by a prescribed meteorological forcing.

2. Numerical design

2.1 Models

The three IGEM climate models used in this work are restricted to their land surface and atmosphere components. They correspond to the same models as used in Ducharme et al. (submitted) with prescribed water table depths (WTDs), except for the evolutions developed between CMIP5 and CMIP6.

2.1.3 IPSL-CM6

The land-atmosphere model used here is a subset of the IPSL-CM6 model (Boucher et al., 2020), restricted to the land-surface and atmospheric components, as evaluated

under the CMIP6 configuration by Cheruy et al. (2020). This model is run at the 144x142 horizontal resolution ($2.5^\circ \times 1.3^\circ$), with 79 vertical levels.

In the standard version of ORCHIDEE, the land surface component of the IPSL climate model, the sole effect of GW is on river discharge (Kriinner et al., 2005, Ducharne et al., in prep). This effect is brought by the routing scheme, which define one linear reservoir in each grid-cell to represent GW storage and base flow, with no GW flow between grid-cells, and no feedback on local soil moisture (SM). To describe this feedback, we introduced a new subgrid fraction, corresponding to the lowland parts of the grid-cell, and acting as a buffer between the upland areas, supplying most GW recharge, and the river system eventually draining GW flow. For simplicity, this fraction is constant over time in each grid-cell, and prescribed from a global-scale wetland map recently designed for this purpose at the 500-m resolution (Tootchi et al., 2019). This map (Figure 1) overlaps two classes of wetlands, viz. regularly flooded wetlands (RFWs) from open-water and inundation datasets, and groundwater-driven wetlands (GDWs) derived from high-resolution GW modeling (Fan et al., 2013), and the resulting total wetland extent is 22 % of the global land area (excluding Antarctica and Greenland). This value is among the highest ones in the literature, along with recent estimates also recognizing the contribution of GDWs. The lowland fraction of each grid cell is described as a separate hydrological element, with physically-based water flow relying on a fine vertical discretization (22 soil layers). It is effectively wet when/where GW flow is sufficient, in which case a water table can build up, and feed base flow to the river, as well as enhanced evapotranspiration compared to the upland fraction, where the 2-m soil is disconnected from the (deep) water table. For the time being, the land cover is assumed to be the same in the upland and lowland fraction, by lack of clear guiding rules to do otherwise (Fan et al., 2019).

This new version is called ORCHIDEE-GWF (GW-fed Fraction), it was detailed and evaluated in the Seine river basin by Tootchi (2019), and we analyze here its impact on the climate simulated by the IPSL-CM6 climate model, by comparison with a reference simulation REF using the standard version of ORCHIDEE (effect of GW on river discharge, but no effect on SM and ET). It must also be underlined that, for the sake of simplicity, several options have been turned off in both versions ORCHIDEE, since they may have interacted with the studied GW-SM interactions. In particular, the simulations do not account for river flooding nor soil freezing in permafrost areas. Plant phenology, however, is prognostic, so the LAI evolves as result of photosynthesis, itself coupled to transpiration.

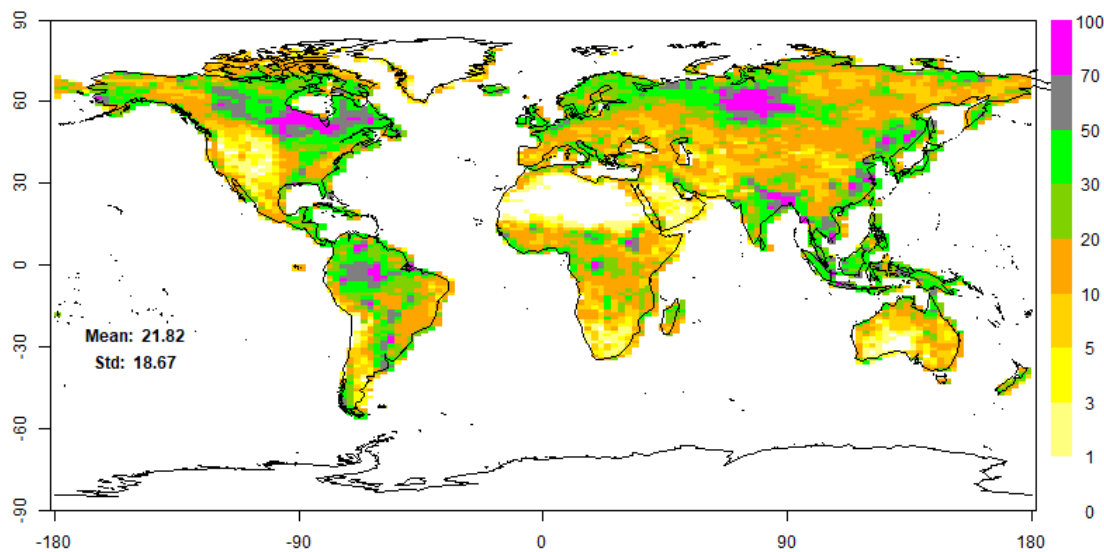


Figure 1. Map of the lowland fraction (in % of land area in each grid cell) used in the IPSL-CM6 simulation with ORCHIDEE-GWF. Upscaled from Tootchi et al (2019) to the $2.5^\circ \times 1.3^\circ$ resolution.

2.1.2 CNRM-CM6

The land-atmosphere model used here is a subset of the CNRM-CM6 model (Volodire et al., 2019). It is run at a $1.5^\circ \times 1.5^\circ$ horizontal resolution (T127 truncation) with 91 vertical levels.

The land surface component is the ISBA-CTRI model, as recently described and evaluated by Decharme et al. (2019). A mixed form of the Richards equation is used to describe the vertical water-mass transfer within the soil, with 14 layers of increasing thickness down to the 12-m depth. This LSM also includes a 2D diffusive GW scheme, which is used represent horizontal GW flow between grid cells in unconfined aquifers (Vergnes & Decharme, 2012). The latter (Figure 2) are defined based on the global map of the groundwater resources of the world from the Worldwide Hydrogeological Mapping and Assessment Programme (WHYMAP; <http://www.whymap.org>), and cover 43% of the land surface, excluding Antarctica and Greenland.

The simulated WTD acts as a lower boundary condition for the vertical soil moisture diffusion, a subgrid scale parametrization is implemented owing to the coarse resolution of the grid-scale: it is assumed that upward capillary fluxes from the aquifer can only take place in lowlands of the grid-cells (flat valleys and alluvial plains), where the WTD is shallow enough (Vergnes et al., 2014). The fraction over which capillary rise effectively occurs (f_{wtd}) is derived over time in each grid-cell including an aquifer, by comparing the mean WTD to the accumulated normalized distribution of high-resolution elevation inside the grid-cell, based on a 7.5-arc-second (~250 m) DEM (GMTED2010; Danielson & Gesch, 2011). The water table, in the simulated aquifers, is drained by the rivers and contributes baseflow to the routing scheme. This GW scheme is turned off in the reference simulation to assess the effect of GW-SM on the simulated climate, so this reference simulation includes does not include any GW process (no capillary rise to the soil, no baseflow contribution to the river discharge). River-floodplain interaction, however, is activated in both versions.

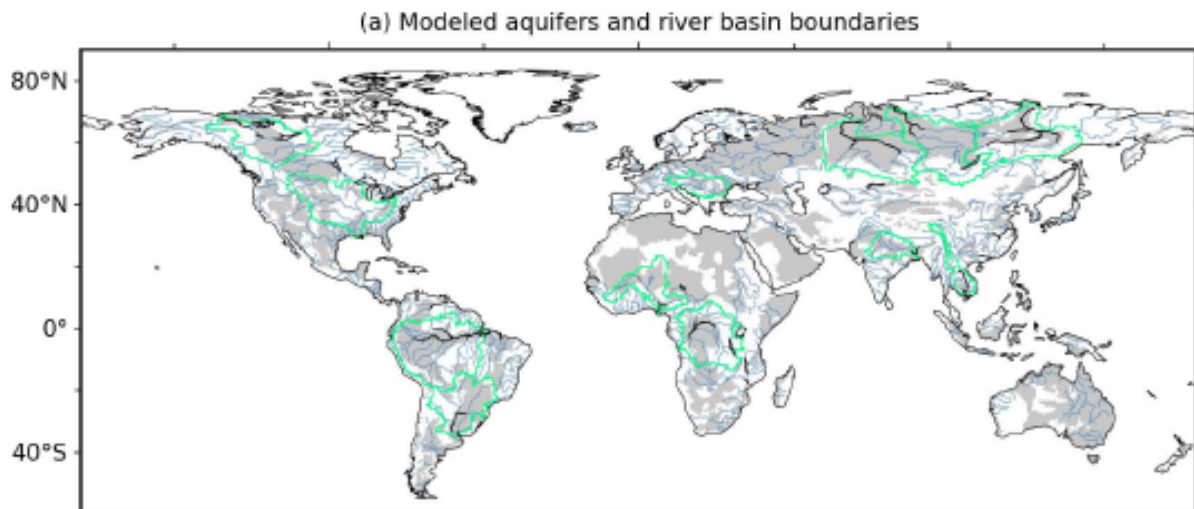


Figure 2. Modeled aquifers (in grey) and river basin boundaries (in green) in the CNRM-CM6 model. From Vergnes & Decharme (2012).

2.1.1 CESM2

The land-atmosphere model used here is a subset of the CESM2 climate model (Danabasoglu et al. 2019). It is run at a $1.9^\circ \times 2.5^\circ$ horizontal resolution with 30 vertical layers.

The land surface component is the Community Land Model version 5 (CLM5, Lawrence et al., 2019), but for the sake of comparison with the simulations performed for the Task 1 of the IGEM project (Ducharne et al., submitted), and the ones analyzed in the first ever assessment of GW on the simulated precipitation (Lo & Famiglietti, 2011), the new GW scheme of Swenson and Lawrence (2015) used in CLM5 has been replaced by the GW scheme of Niu et al. (2007), used in CLM versions 2 to 4. This GW scheme defines a conceptual aquifer layer below the 3.8-m soil column, where vertical water flow is classically calculated based on Richards equation, discretized into 10 soil layers. The conceptual aquifer is considered as one layer with a specific yield $S_y = 0.2$, and an exponentially decaying hydraulic conductivity.

The WTD evolves at each time step as a result of recharge from the soil (which can be negative if the upward capillary flux from the water table is larger than the downward drainage from the unsaturated soil), and baseflow from the saturated layer(s), which

contributes to the simulated river discharge. If the water table position is below the 3.8-m soil, capillary rise is deduced from the hydraulic head gradient between the soil bottom and the water table. This GW is purely 1D vertical, with no GW flow between grid-cells, and no subgrid scale variability of capillary rise, which occurs over the full land fraction of each grid-cells. The reference simulation to assess the effect of GW-SM on the simulated climate has no conceptual aquifer layer, so the boundary condition at the bottom of the 3.8-m soil is gravitational drainage (no capillary flux).

2.2 Land-atmosphere simulations over 1979-2100

To reduce the sources of differences between climate models, we focus on land-atmosphere simulations, all performed under the protocol of the Atmospheric Model Intercomparison Project (AMIP), with prescribed interannually-varying forcing boundary conditions from observations (sea surface temperatures - SST, sea ice cover - SIC, greenhouse gases, aerosols, land-use), following Taylor et al. (2012), but updated for the 1979-2014 historical period for CMIP6.

To extend this period over the entire 21st century, we preferred the most severe CMIP6 radiative forcing, namely SSP5-8.5, to get a strong climate change signal at the end of the 21st century. The required SST/SIC forcing datasets have been provided over 2015-2100 by the CNRM (partner P3), and consist of bias-corrected SST and SIC output from a fully coupled (land-ocean-atmosphere) simulation by the CNRM-CM6 climate model, performed for ScenarioMIP (O'Neill et al., 2016) under historical then SSP5-8.5 radiative forcing. To prevent from inhomogeneities in climate variability between the historical and future periods (respectively constrained by observed SST in AMIP, and modeled bias-corrected SST under SSP5-8.5), the future simulations were preceded by historical simulations forced with an equivalent SST/SIC forcing, i.e. modelled by the fully coupled CNRM-CM6 climate model under observed historical radiative forcing, then bias-corrected with the same method as used to prepare the future SST/SIC forcing.

Eventually, we performed three pairs of transient simulations with each land-atmosphere (LA) model involved in the IGEM project, each pair comprising a simulation with GW-SM interactions, and a reference one, REF, where the related processes are deactivated:

- 1) AMIP simulations, over 1979-2014, well suited for validation since the inter-annual climate variability is well constrained by the observed SST forcing;
- 2) LA-Historical simulations, over 1979-2014, which only differ from the AMIP simulations by their modelled bias-corrected SST/SIC forcing;
- 3) LA-Future simulations over 2015-2100, directly pursuing the LA-Historical simulations, and forced by radiative forcing from SSP5-8.5, and by corresponding modeled bias-corrected SST/SIC.

The spin-up (to initialize the AMIP and LA-Historical simulations in 1979) was let to each groups' expertise.

It must be noted that, contrarily to the classical AMIP protocol, we kept a constant land-cover in all land-atmosphere simulations throughout the entire period (1979-2100) so the climate change signal is simple, and the possible attenuation of warming by GW does not involve feedbacks via land-cover change. Each land cover map is representative of the early 21st century conditions, from the datasets used for CMIP6 by each model. Each model used its standard soil texture map, and the corresponding soil hydraulic parameters.

2.3 Complementary off-line simulations with ORCHIDEE

A pair of REF and GW-SM simulations was also performed in off-line mode over 1979-2010 (32 years, after a 20-yr warm up) with the ORCHIDEE LSM, as a complement to the ISPL-CM6 land-atmosphere simulations. The two off-line simulations were forced with the same soil and land cover maps as the land-atmosphere ones. The meteorological forcing is the one used for the IGEM T1 simulations (Ducharne et al., submitted), based on the 1°x1° and 3-hourly dataset developed by the Princeton University [Sheffield et al., 2006], by downscaling and bias-correcting the National Center of Environmental Prediction National Center for Atmospheric Research (NCEP-NCAR) reanalysis. The 3-hourly precipitation from Sheffield et al. [2006] is further hybridized to match the monthly means from the Global Precipitation Climatology Center (GPCC) Full Data Product V6 [Schneider et al., 2011, 2014].

3. Results

3.1 Off-line evaluation of the ORCHIDEE-GWF version

3.1.1 Sensitivity to GW-SM interactions

Figure 3a shows the simulated WTD in the lowland fractions, with white values if there is no WTD along the entire simulation, thus in very arid areas (Sahara). As expected, the WTD is very shallow (blue) in wet climates, much deeper (yellowish) in arid zones. In semi-arid climates, deep WTDs are often found in places with very large lowland fractions (see Figure 1), for instance in the Sahelian band (inner Niger delta, around lake Chad, and in the Sudd Swamp), or in the Ob basin, because the relative contribution from the upland is smaller than in the surrounding places with smaller lowland fraction, thus too small to induce a shallow water table. Since these areas are notorious wetlands, it may be postulated that they are sustained by large scale water flows, and that 2D water redistribution, owing to river flooding and/or 2D GW flow, may be lacking in the simulation.

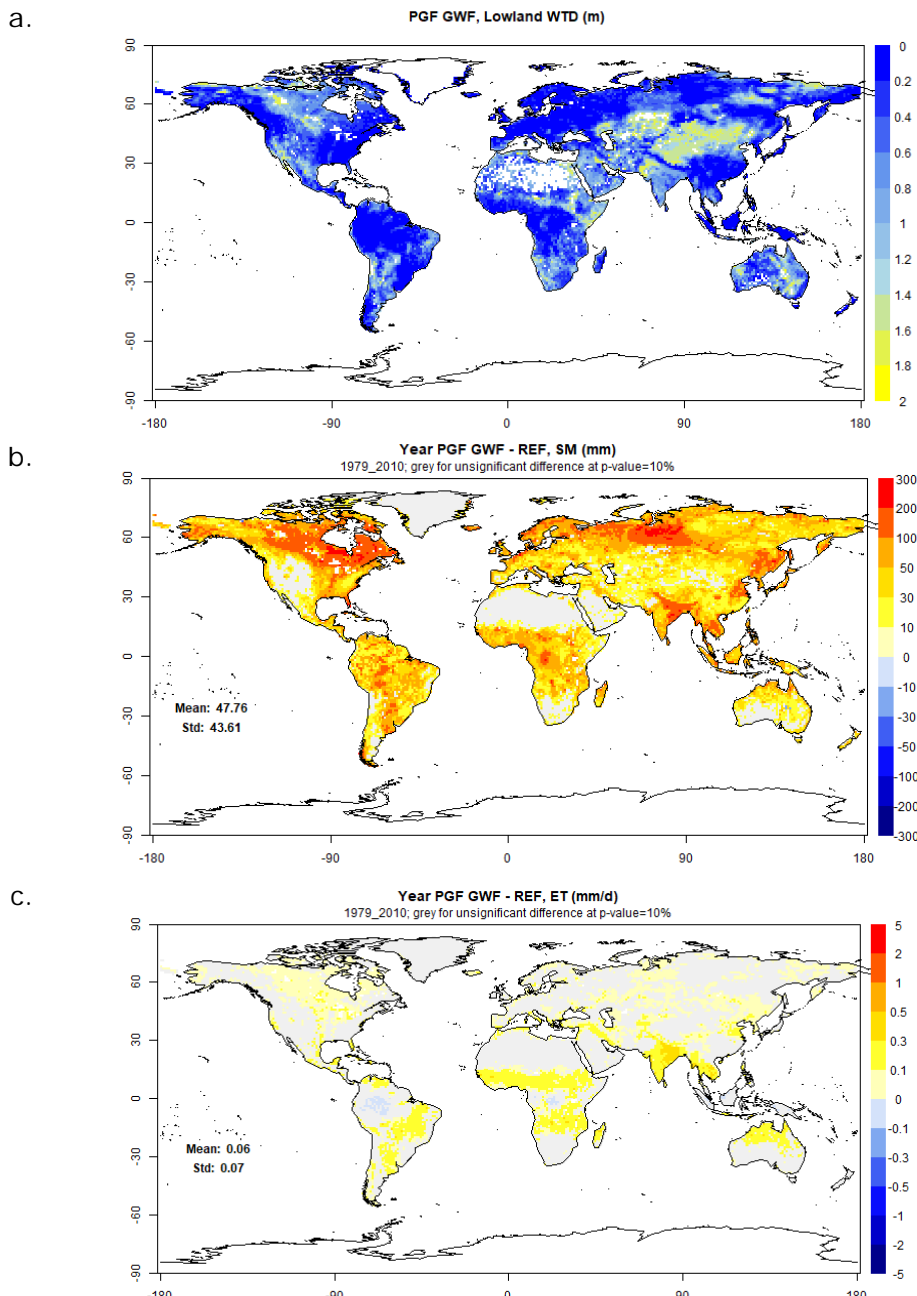


Figure 3. Multi-annual mean differences between the GW-SM and REF simulations with the ORCHIDEE LSM (off-line simulations). Grey shows areas with unsignificant mean changes based on a Student test, with a p-value < 10%.

These scaling problems vanish when looking at grid-cell mean SM, which is everywhere increased by GW flow convergence from upland to lowland (Figure 3b), particularly where the lowland fraction is high (boreal, coastal, and tropical humid areas), with an average of +11% over land. As a result, ET also increases with ORCHIDEE-GWF (+5% on average over land), mostly in transition zones (Figure 3c), where ET is both water limited and not energy limited. In contrast, several areas with a large SM increase with ORCHIDEE-GWF do not show significant ET increases: the boreal areas since water is not limiting in these energy limited areas, and reversely, tropical humid areas, like the Amazon and Congo river basins, or the maritime continent, where ET is not water limited despite the high net radiation. ET is even found to decrease in these areas, which is probably related to the dynamic LAI in this model, via the interplay between soil evaporation and transpiration. Both transpiration and soil evaporation increase with SM, but the latter is more effective than the former when SM is high, as it proceeds at potential rate. Therefore, the increase of LAI with SM slows down the increase in ET, because it increases the fraction of the grid-cells contributing to transpiration, and conversely decreases the fraction contributing to soil evaporation.

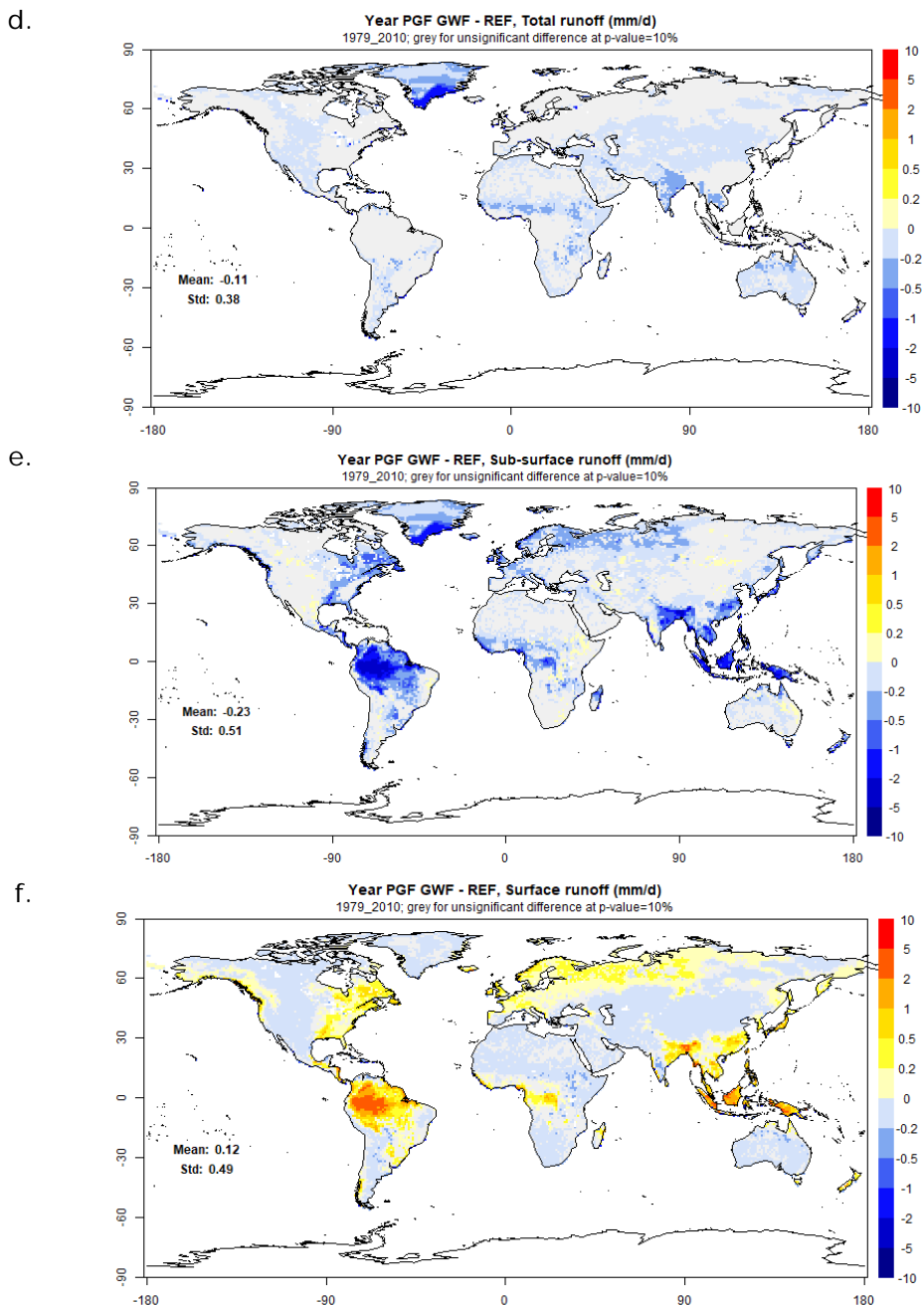


Figure 3 (continued). Multi-annual mean differences between the GW-SM and REF simulations with the ORCHIDEE LSM (off-line simulations). Grey shows areas with unsignificant mean changes based on a Student test, with a p-value < 10%.

Finally, total runoff decreases with ORCHIDEE-GWF (Figure 3d, -11% on average over land), as a direct result of ET decrease in water conservative simulations, both forced by the same precipitation. The rather weak total runoff decrease is the result of much stronger and opposite changes in drainage and surface runoff (respectively -38% and +33% on average over land). Drainage decreases very ubiquitously (Figure 3e), since it is reduced to the baseflow from the lowland water table (the drainage from the lowland fraction becomes a subgrid flux in ORCHIDEE-GWF). Surface runoff shows more contrasted change patterns (Figure 3f), with strong increases where SM increases a lot (humid climates). The SM increase comes from the lowland fraction, which can become very humid, and generate together a water table, and a lot of surface runoff. The decrease of surface runoff in the other land areas has the same explanation as the one of drainage, since the surface runoff produced by the upland fraction is a subgrid flux in ORCHIDEE-GWF, unless it induces surface runoff from the lowland fraction as described above in very humid conditions.

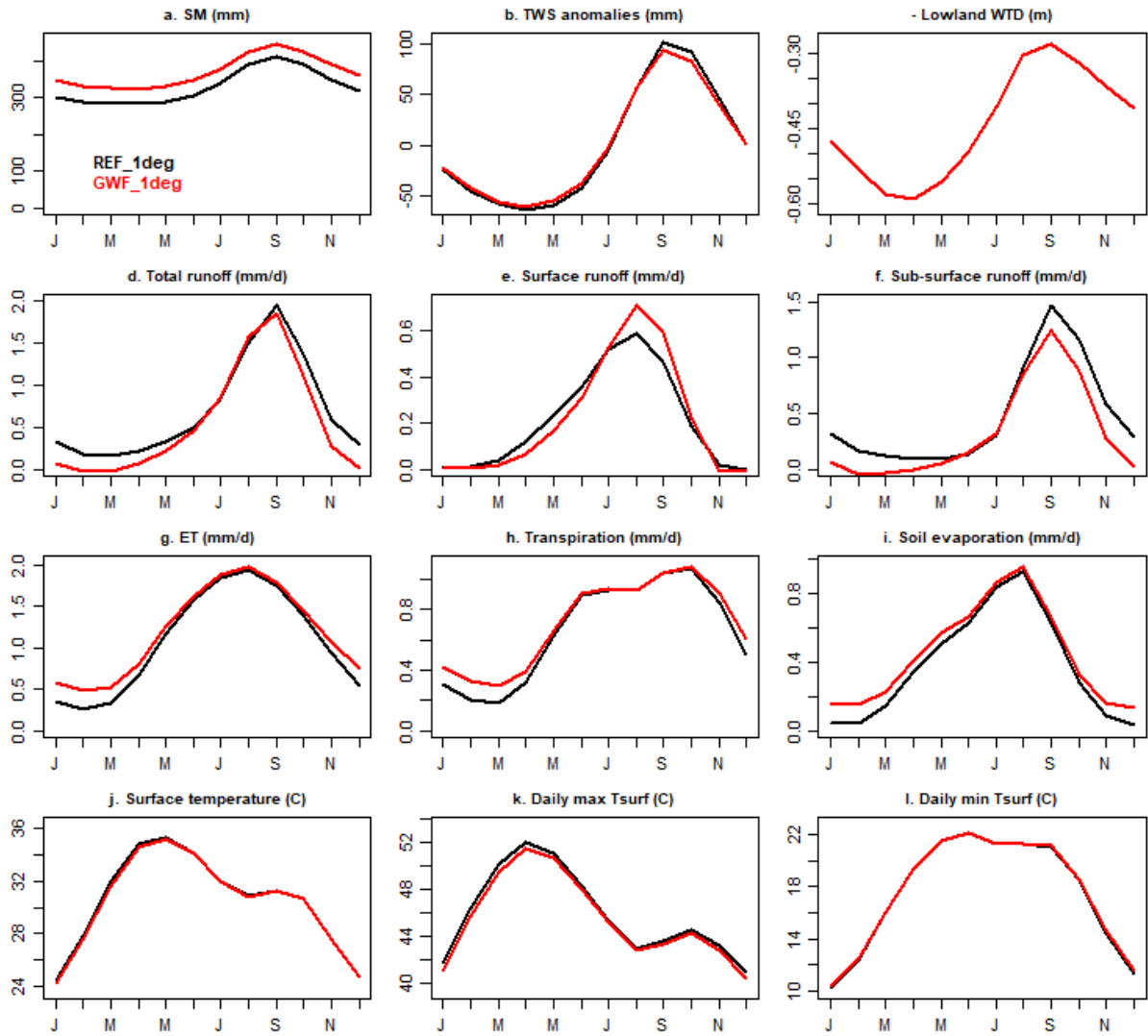


Figure 4. Multi-annual mean seasonal cycles of important land surface variables, on average over the Niger River basin (located in Figure 5a, with an average lowland fraction of 11.8 %). The red and black curves correspond respectively to the GW-SM and REF versions of the ORCHIDEE LSM (off-line simulations over 1979-2010). TWS is the total water storage (given in mm, i.e. kg/m², summing up SM, intercepted water over the canopy, the snow mass, and the water mass in the reservoirs of the routing scheme); this variable is plotted in anomaly with respect to the long-term mean of each simulation.

These hydrological changes also occur seasonally, as illustrated in the Niger river basin (Figure 4), largely overlapping the Sahelian band, where the annual mean changes are amongst the highest over the planet (Figure 3). There the annual mean changes of the main water budget variables between REF and GW-SM are: +11% for SM; +11% for ET; -22% for total runoff, despite a large increase of surface in summer, during the rainy

season, from the lowland fraction where the WTD almost reaches the surface (Figure 4c; showing a water table at less than 30 cm from the surface in August and September). We also get a decrease of the surface temperature (Figure 4j, -0.4°C on annual average), with two causes: the increase of ET and related evaporative cooling, but also the one of soil heat capacity with increasing SM. Another noticeable impact is the respective decrease and increase of mean maximum and minimum daily temperature (Figure 4k,l), with an average of -0.85 and +0.5 °C respectively between REF and GW-SM). These variations, which correspond to a decrease of the diurnal amplitude of surface temperature, come from the larger soil heat capacity, soil heat conductivity, and resulting thermal inertia, when the soil is more humid (Aït-Mesbah et al., 2015; Cheruy et al., 2017), as in the lowland fraction.

3.1.2 Evaluation of the simulated river discharge

An important question when developing a new parametrization is to assess if it increases the realism of the model. Following Vergnes & Decharme (2012) for the GW model of the CNRM climate model, we started this work by a comparison to the simulated river discharge (Figure 5).

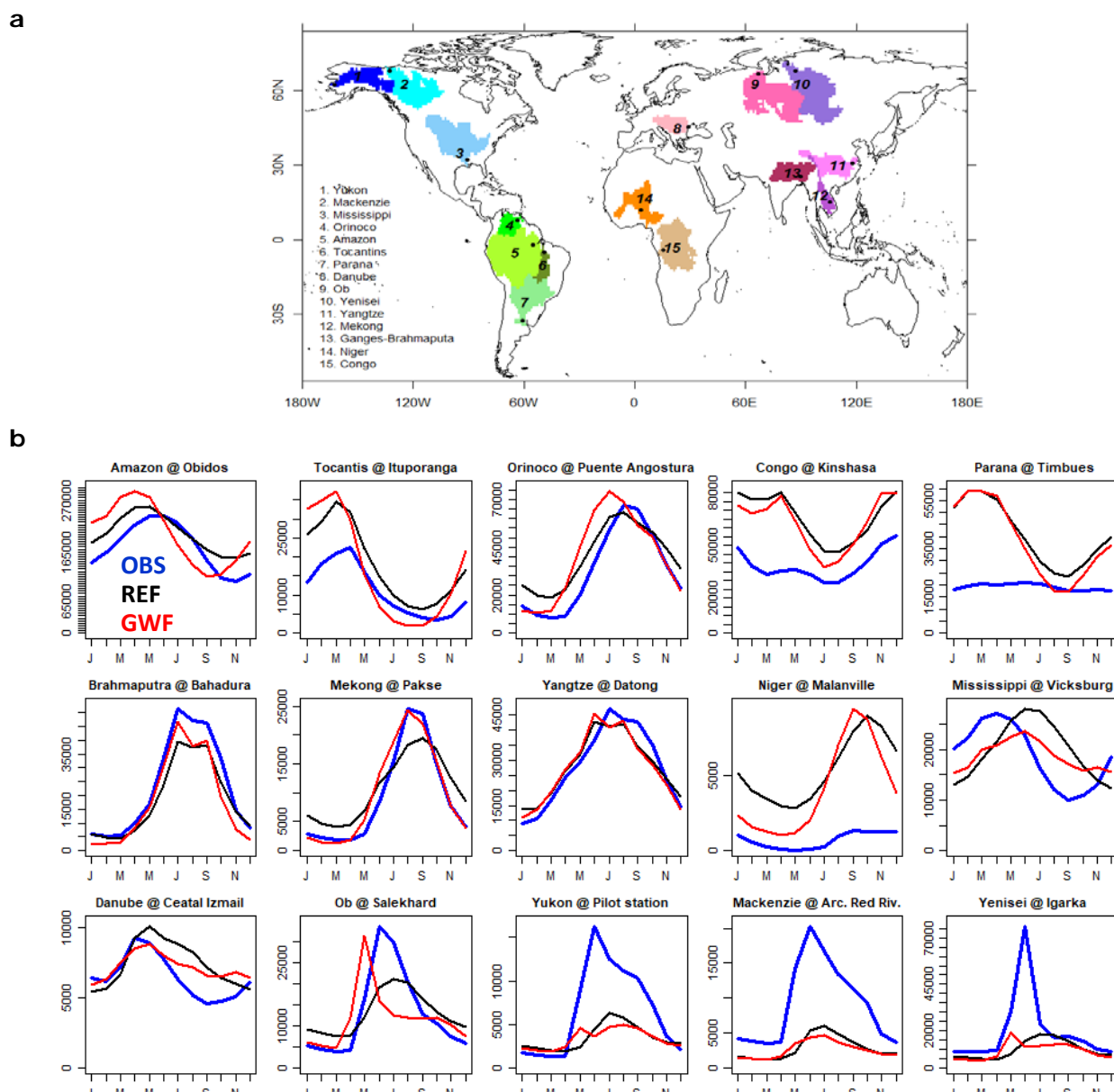


Figure 5. Selected major river basins: a. global map, b. multi-annual mean hydrographs (over 1980-2010) hydrographs, with observations from the Global Runoff data Centre in blue, and offline simulations by the GW-SM and REF versions of the ORCHIDEE LSM in black and red respectively. It must be underlined that the dates with no data in the observed records are censored from the simulated time series, to make the comparison meaningful.

It must be noted, however, that this validation effort still need to be extended to other important land variables, like ET, total water storage anomalies, or surface soil moisture, for which global gridded observation-based products do exist, and also to important atmospheric variables (air temperature, precipitation, radiation), using the land-atmosphere simulations analyzed in section 3.2.

Figure 5 and Table 1 show that the reference ORCHIDEE simulation (in black, with a buffer effect on discharge by the linear GW reservoir of the routing scheme) severely underestimates river discharge of (1) the Niger river, since the inner delta is not accounted, nor the resulting river discharge depletion because of enhanced ET, and (2) the boreal rivers, because the neglect of permafrost favors infiltration and severely reduces runoff. In other river basins, REF compares fairly well with observations, despite significant errors, which may be attributed to several factors: errors in the meteorological forcing, neglect of the significant natural or anthropogenic pressures on river discharge (lakes, dams, and withdrawals), errors in the time constants of the routing scheme, and errors in the simulated water budget.

Looking now at the effect of the GW-SM interaction in the lowland fraction, it is systematically two-fold, with (1) a discharge decrease (because ET increases), (2) advanced peak discharge and low flows, because soil saturation is faster owing to the wet lowlands. Despite exceptions in the Mississippi and Danube, which need further investigation, another significant impact consists of increased seasonal amplitude of river discharge in a majority of basins, likely linked to the second effect, and confirming that accounting for wet areas reduces the effective residence of water in the river basins. This overall effect is also visible in the reduced amplitude of seasonal TWS anomalies in the Niger River basin (Figure 4b), to be confirmed over all land masses, and compared to remote-sensing observation by the GRACE satellite.

Table 1. Performance criteria when comparing the simulated river discharge to the GRDC observations in the selected 15 river basins: relative bias (in %), relative RMSE (in %), relative bias in seasonal amplitude compared to the observation (in %), correlation coefficient between the mean hydrographs (12 mean values for simulation and observation), correlation coefficient between the full time series (excluding the date with no data in the observed record). The evaluated simulations are the same as in Figure 5 (REF and GW-SM versions ORCHIDEE of off-line). The basins are sorted based on their annual mean SM in the river basin in REF (penultimate column), while the last column gives the mean lowland fraction in each basin ($R^2=0.25$ between mean SM and lowland fraction). The green/orange cells indicate basins/criteria for which GW-SM is better/worse than REF.

River@Station	RelB%		RelRMSE%		CorClim		CorPluri		RelAmpli%		SM (mm)	Lowland (%)
	REF	GWF	REF	GWF	REF	GWF	REF	GWF	REF	GWF		
Niger @ Malanville	636,66	471,23	713,06	609,66	0,91	0,76	0,8	0,71	376,99	546,74	329	11,8
Mackenzie @ Arc. Red Riv.	-68,4	-71,19	83,48	87,38	0,88	0,97	0,83	0,87	-70,68	-78,8	414	37,4
Yukon @ Pilot station	-46,87	-49,21	76,47	80,24	0,81	0,83	0,71	0,69	-70,44	-79,41	436	19,8
Mississippi @ Vicksburg	5,06	-0,94	41,06	27,29	0,12	0,52	0,37	0,65	-7,5	-51,94	459	16,2
Yenisei @ Igarka	-49,07	-52,38	98,86	101,02	0,48	0,48	0,45	0,44	-80,24	-78,39	470	22,8
Congo @ Kinshasa	71,21	62,6	75,63	67,58	0,65	0,75	0,54	0,62	30,68	59,76	496	21,0
Ob @ Salekhard	0,7	-8,99	45,23	70,31	0,91	0,46	0,79	0,43	-54,27	-10,51	502	49,2
Brahmaputra @ Bahadura	-20,19	-21,57	28,13	26,49	0,99	0,98	0,95	0,94	-24,89	-4,69	506	42,7
Parana @ Timbues	115,5	101,42	130,78	126,36	0,41	0,39	0,53	0,48	979,17	1175,34	514	27,1
Danube @ Ceatal Izmail	14	10,56	24,97	17,96	0,62	0,8	0,71	0,77	1,14	-38,48	538	15,2
Tocantis @ Ituporanga	63,07	50,6	72,07	91,4	0,97	0,85	0,89	0,78	49,06	86,9	545	29,4
Mekong @ Pakse	16,14	6,1	40,19	20,96	0,95	0,97	0,92	0,95	-32,47	1,64	553	36,6
Yangtze @ Datong	1,1	-0,57	16,2	17,85	0,95	0,92	0,91	0,88	-24,66	-8,89	605	28,5
Amazon @ Obidos	15,36	15,03	18,79	31,97	0,93	0,6	0,9	0,61	-22	31,1	631	37,4
Orinoco @ Puente Angostura	22,78	20,71	30,32	40,43	0,98	0,87	0,96	0,85	-24,39	9,4	666	43,7

In terms of performance, it is not straightforward to assess which version is better, given the often large biases of the reference simulation. This is particularly true in 6 of the 15 selected basins, where the performance changes seem very negligible in front of the errors (Parana, Brahmaputra, Yangtze, and three boreal rivers, namely the Yukon, Mackenzie, and Yenisei). In the remaining nine basins, the GW-SM version tends to improve the simulated volume (cf. bias in Table 1), which is consistent with the improvement of mean simulated ET over land (excluding Greenland and Antarctica): from 1.17 mm/d in REF to 1.23 mm/d in GW-SM, thus closer to state-of-the art observation-based estimates (1.37 mm/d according to GLEAM, Martens et al., 2017; 1.45 mm/d according to Rodell et al., 2015).

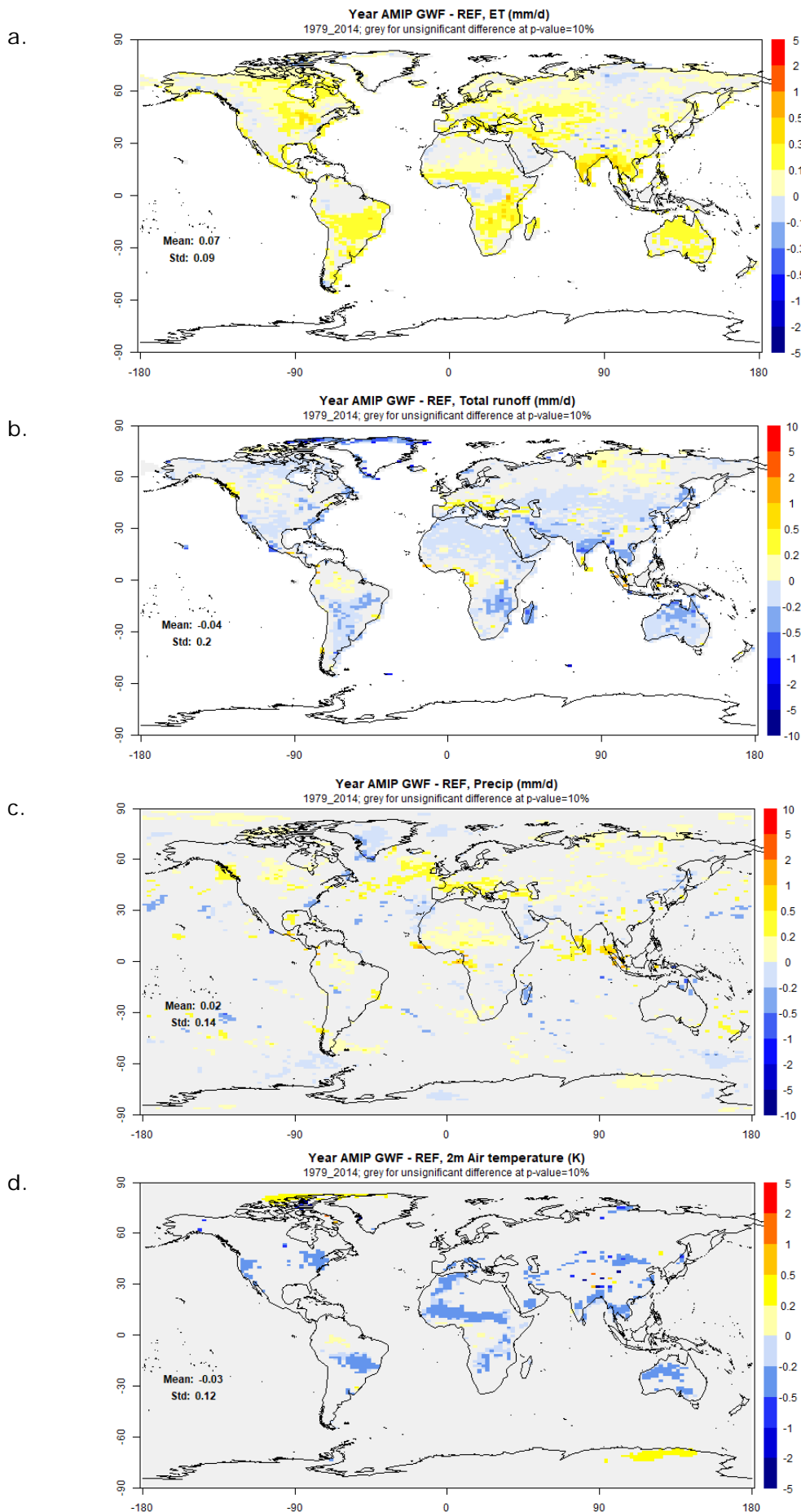


Figure 6. Multi-annual mean differences between the GW-SM and REF simulations with the IPSL-CM6 (land-atmosphere simulations). Grey shows areas with unsignificant mean changes based on a Student test, with a p-value < 10%.

The seasonal amplitude increase with GW-SM interactions represents an improvement in the most humid basins, although the timing of the corresponding hydrographs (cf. correlation coefficients in Table 1) is deteriorated, while the reverse may be speculated in drier basins, where water is limiting, at least seasonally. These associations, although sensible from a physical point of view, need to be verified across a larger sample of river basins.

3.2 Impact of GW-SM interaction on the simulated climate

3.2.1 Historical climate (AMIP simulations)

Over the historical period, the impact of GW-SM interactions on the simulated ET by the ORCHIDEE LSM is very similar in forced and coupled (AMIP) modes, although the significant changes seem larger in coupled mode (Figure 6a). In contrast, the total runoff decrease owing to GW-SM interactions (Figure 6b) is much smaller in coupled mode (-2.7% on land average compared to -11% in forced mode), as a result from the feedback of increased ET to precipitation (Figure 6c).

This feedback is mostly positive (thus increasing precipitation, and counteracting the total runoff decrease), but very weak on annual average, although focused significant precipitation increases can be found in some well-known semi-arid/transition zones, like Sahel and the Mediterranean rim. The near surface atmospheric cooling arising from the previously analyzed surface temperature cooling (due to evaporative cooling and increased soil thermal inertia) is also very weak, with multi-annual means of -0.3°C and -0.1°C on average over land and the entire Earth, respectively.

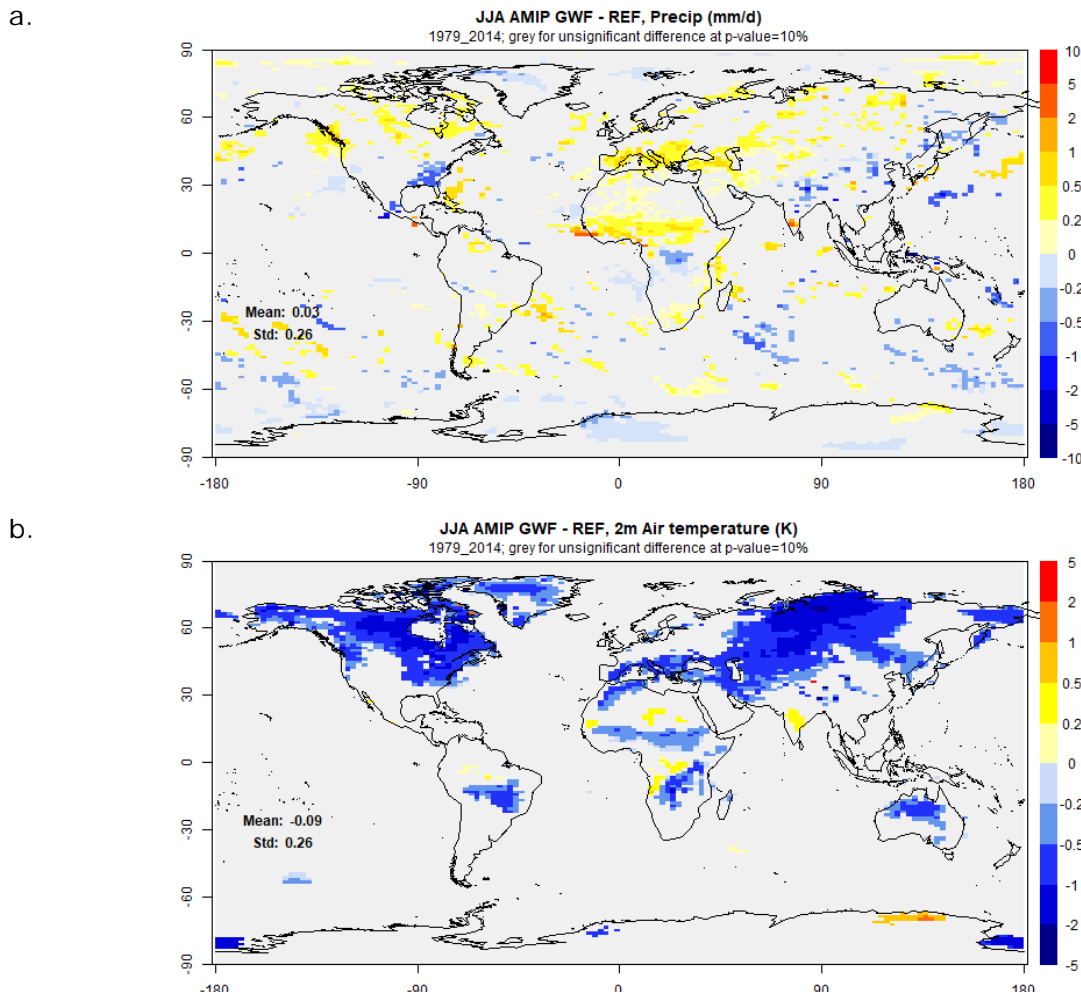


Figure 7. Multi-annual mean differences in boreal summer (June-July-August) between the GW-SM and REF simulations with the IPSL-CM6 (land-atmosphere simulations). Grey shows areas with unsignificant mean changes based on a Student test, with a p-value < 10%.

A stronger impact of GW-SM interactions is found in boreal summer (June-July-August, Figure 7), owing to the larger land masses in the Northern Hemisphere. This leads to a stronger increase of precipitation over the Mediterranean rim and Sahel (Figure 7b) than on a yearly basis. Following the analysis of Wang et al. (2018) with a prescribed 1-m WT, the strong precipitation increase found in JJA over Sahel corresponds to the propagation of the West African monsoon further north into land, due to increased meridional temperature gradient between the equator and higher latitudes, given the much higher and widespread air temperature decrease in the northern middle latitudes (where the cooling can exceed -1°C, especially in areas with high lowland fractions, cf. Figure 1) than around the Equator (Figure 7b).

As shown in Figure 8, this enhancement of the West-African monsoon and the related precipitation corrects a long lasting defect of the IPSL climate model (Cheruy et al., 2020), with a much more realistic GW parametrization (dynamic WTD in selected lowland fractions) than in Wang et al. (2018), in which the WT is uniformly and constantly imposed at 1m from the surface. Besides, the significant cooling found in the boreal areas with GW-SM in JJA is prone to alleviating the warm bias diagnosed in the IPSL-CM6 model by Cheruy et al. (2020) in these areas.

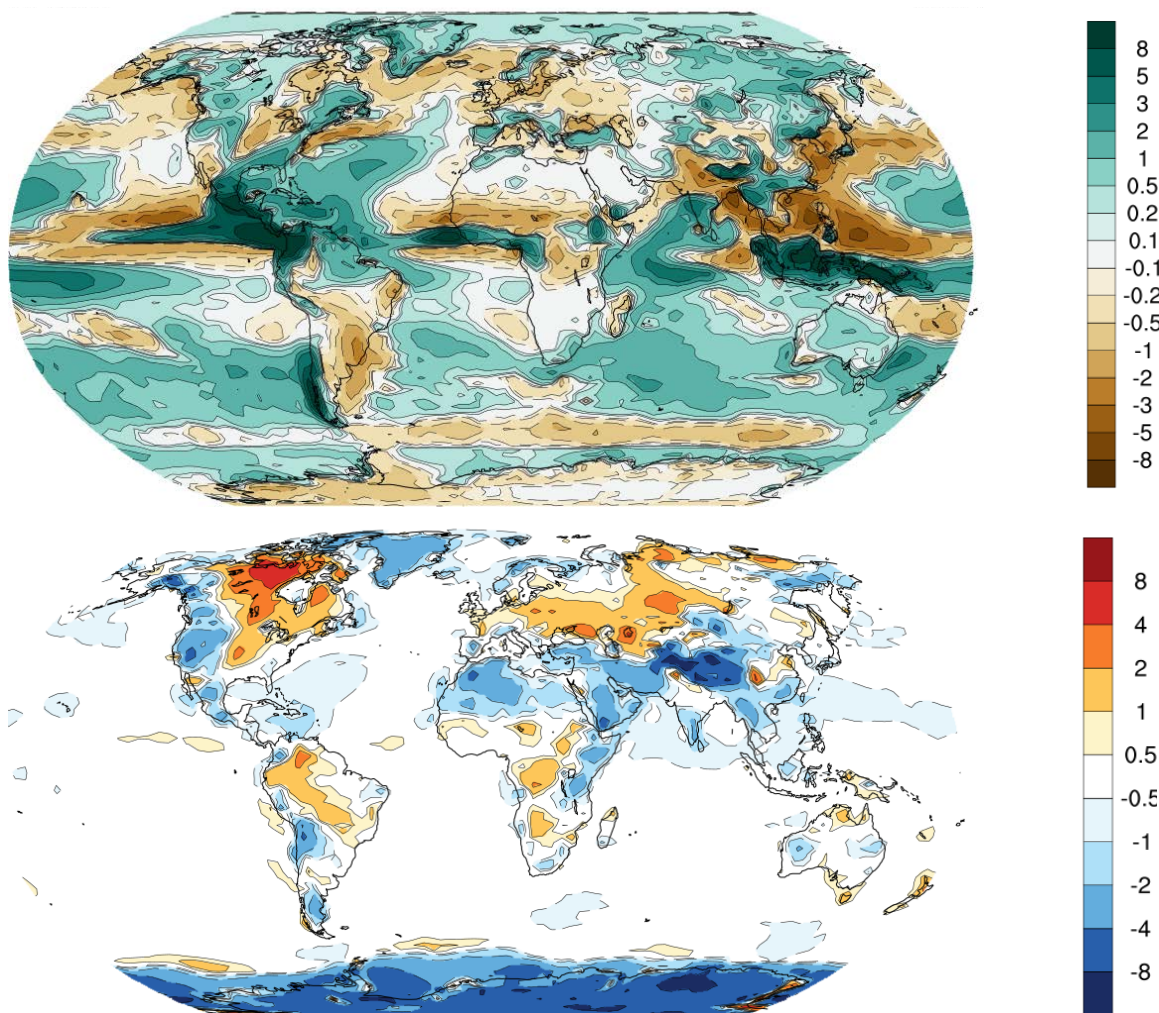


Figure 8. Mean multi-annual bias of the IPSL-CM6 model in JJA: (top) for precipitation, in mm/d, with respect to GPCP observations; (bottom) for 2m-temperature, in °C, with respect to the ERA-I reanalysis. The simulations are performed following the CMIP6 AMIP protocol with a very close version to REF for both ORCHIDEE and the atmospheric model. The biases are calculated over 1979-2014 period. Taken from Cheruy et al. (2020).

The impact of GW-SM interaction, already weak in the IPSL-CM AMIP simulation, is even weaker in the CNRM-CM AMIP simulations, as illustrated for 2-m air temperature in Figure 9, with very tiny spots of significant cooling. The warmer pockets found with GW-SM in arctic areas in DJF are also found in the IPSL-CM simulations (not shown), without any clear explanation for the moment. A thorough comparison of the different model responses is now needed, encompassing the three climate models of the IGEM project, with similar methods, especially for statistical assessment.

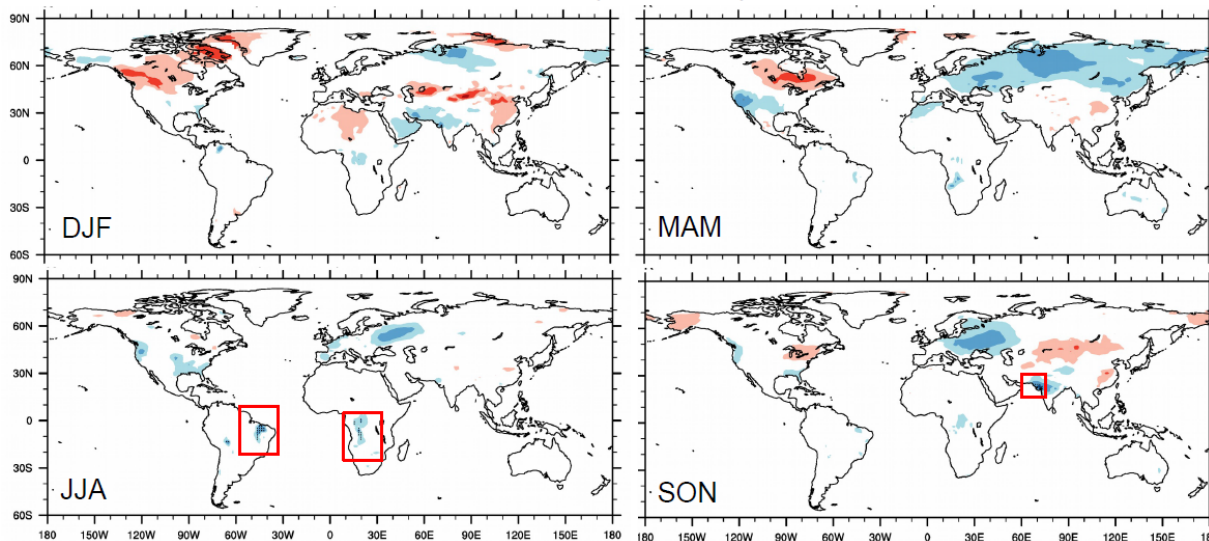


Figure 9. GW impact on mean 2m temperature over the four seasons in the CNRM-CM6 AMIP simulations (multi-annual mean of GW-REF over 1980-2014). Hashed areas correspond to statistically significant differences with a p-value < 5%, using the Wilks (2016) global test, and are highlighted by red boxes.

3.2.2 Future climate

The climate change expected from the SSP5-8.5 radiative forcing scenario is summarized in Figure 9 for the IPSL-CM simulations, but the large spread of future climate projections must be underlined. For instance, the equilibrium climate sensitivity (ECS, the global surface temperature response to CO₂ doubling) of the CMIP6 climate models ranges from +2°C to almost +6°C, with a multi-model mean ECS around +4.1°C (Zelinka et al., 2020). Based on the same paper, the three fully coupled climate models linked to the IGEM models are in the warmer half, with an ECS of +4.6°C with IPSL-CM6A-LR, +5.2°C with CNRM6-CM6-1, and +5.5°C with CESM2. For the SSP-5.8-5, the spread of global mean increase in 2m air temperature between 1980 and 2100 is approximately between +3.7°C and +7°C (Forster et al., 2020), to be compared with the IPSL-CM6 projection of ca. +6°C (using bias-corrected SST from the CNRM-CM6 model).

Associated to this strong warming, and in line with many other future projections (e.g. IPCC, 2014), the REF simulation performed with IPSL-CM6 shows an increase of precipitation (ca + 8% on average over the entire globe) and an increase in the number of dry days (with precipitation < 1 mm/d) per month (Figure 9). The combination of these two trends is consistent with the intensification of the water cycle, with more precipitation on global average, but concentrated in the wet areas and wet moments, to the detriment of the dry areas and dry moments, as summarized by the “dry gets drier, wet gets wetter” paradigm (e.g. Chou et al., 2013; Greve et al., 2014).

Figure 9 also shows that the impact of GW-SM interaction found over the historical period (section 3.2.1) persists throughout the 21st century: 2-m air temperature remains consistently lower with GW-SM than with REF, and so does the mean of daily maximum temperature (with a larger effect, as previously noted for surface temperature, owing to enhanced thermal inertia); precipitation, in contrast, is higher with GW-SM, logically decreasing the number of dry days. Figure 10 offers a more precise illustration of the effect of the GW-SM interaction on the trend of 2-m air temperature, focused on land masses only (because sea surface temperatures are forced in our simulations). It also compares the response of two models, IPSL-CM6 and CNRM-CM6, which both show a very similar decreasing trend of the temperature difference between GW-SM and REF,

meaning that the warming trend along the 21st century is slower in both models when the GW-SM interaction is accounted for.

This mitigation is very weak on average land, since the simulated warming of +6°C over the 21st century is only reduced by 0.1°C over the same period. However, the geographic distribution of the attenuation of anthropogenic warming owing to GW-SM interaction in the IPSI-CM6 climate model (Figure 11) reveals several regions where the projected warming at the end of the 21st century may be significantly reduced, by at least 0.5°C on annual average, like in Western Europe. To summarize, the global mean impact of GW-SM interaction, albeit small on average over land, offers a significant mitigation of climate change in some areas, and the above analysis will shortly be extended to the three climate models, and to a larger number of climate variables, including the number of dry days, and several kinds of extreme event, like heatwaves and droughts (Lorenz et al., 2015; Teuling et al., 2013; Moon et al., 2018; Padron et al., 2020).

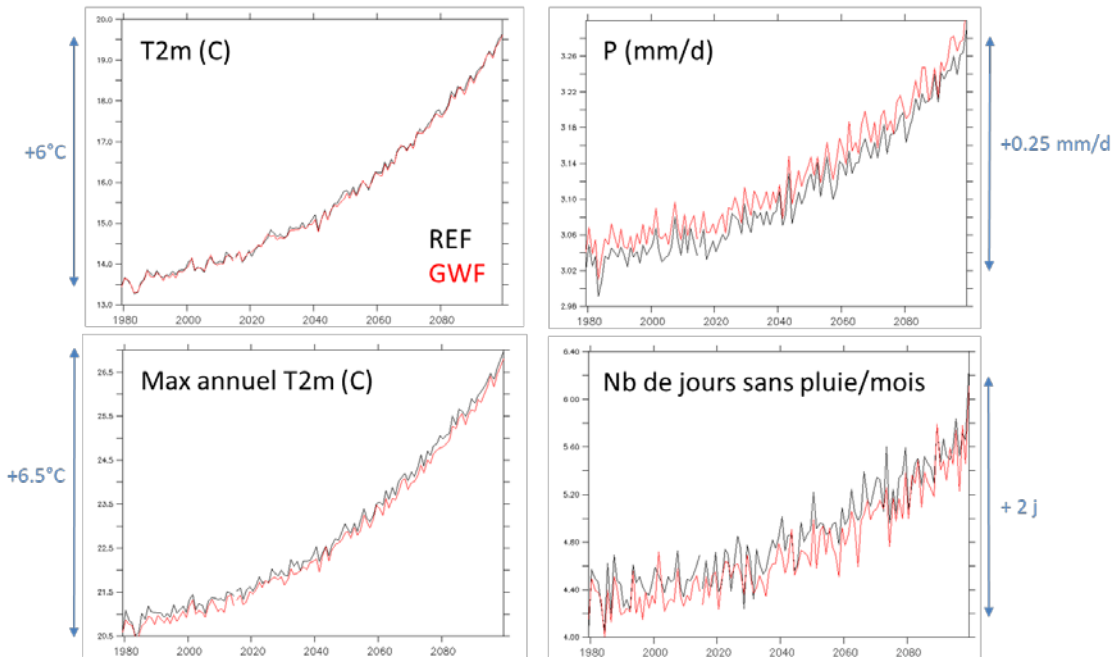


Figure 9. Evolution of yearly means between 1980 and 2100 according to the GW-SM and REF simulations with the IPSL-CM6 LA simulations (global averages).

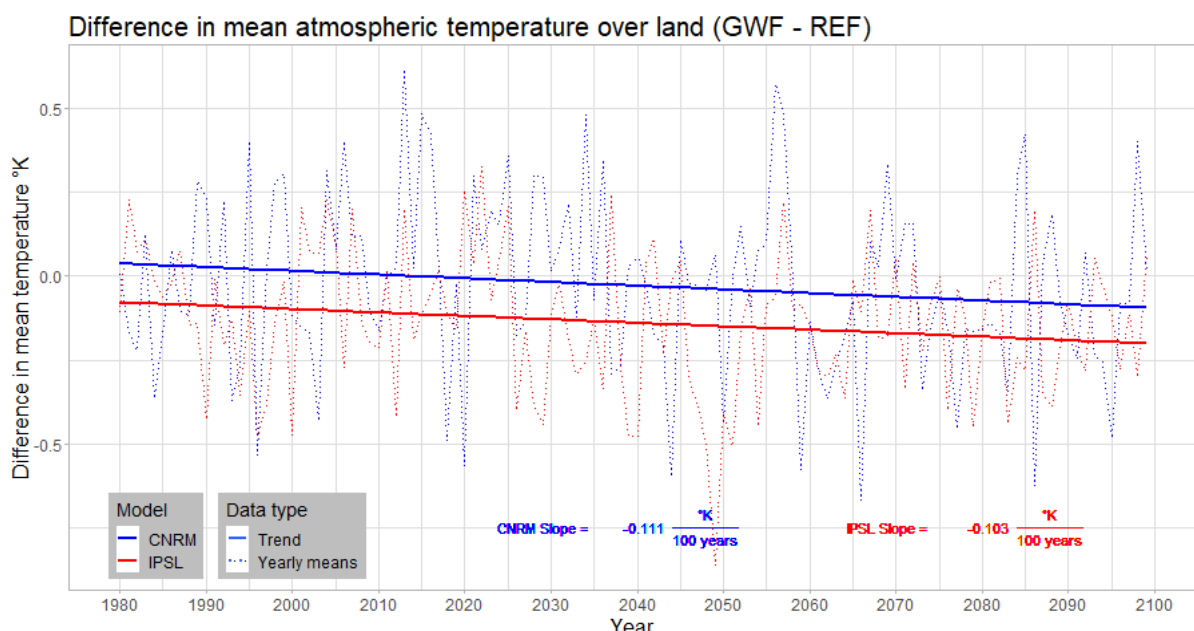


Figure 10. Attenuation of global warming (SSP5-8.5 radiative forcing scenario) on average over land (-0.1°C/100 years) owing to the GW-SM interactions, in simulations with the CNRM-CM6 model (blue) and IPSL-CM6 (red). The trends are extracted based on a linear regression model.

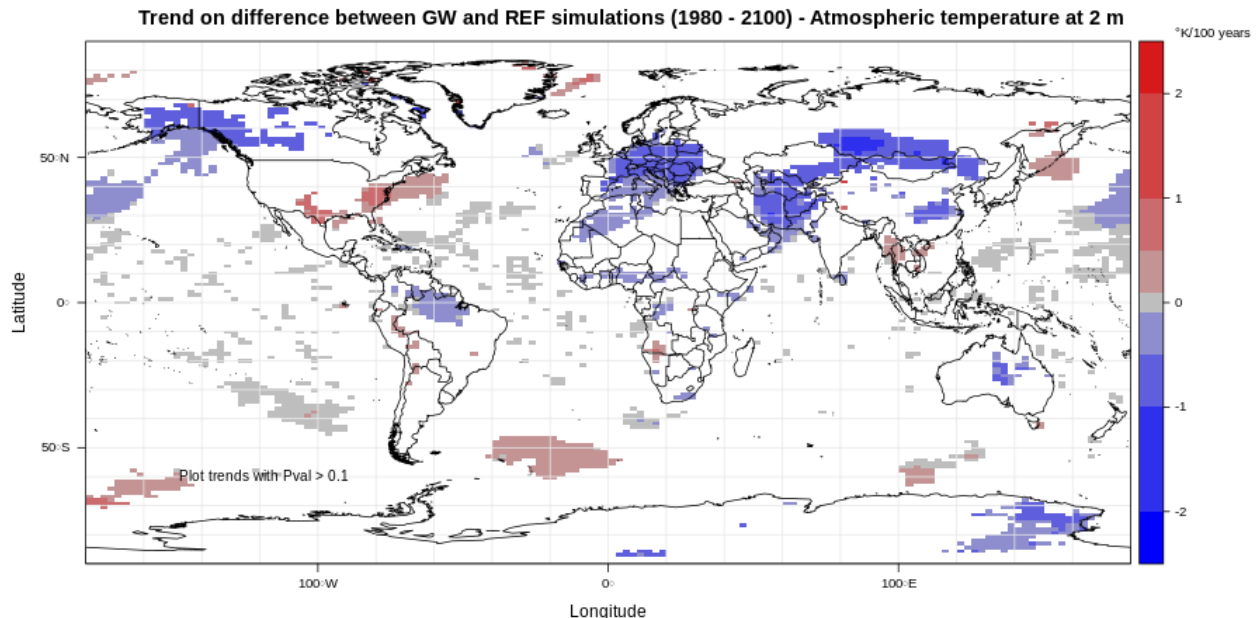


Figure 11. Patterns of global warming attenuation owing to the GW-SM interactions in the IPSL-CM6 simulations (under SSP5-8.5 radiative forcing scenario). This map generalizes to each grid-cell the trend displayed in Figure 10 for the land average of 2-m air temperature difference between GW-SM and REF. Trends (expressed in °C per 100 years) are extracted based on a linear regression model, and the significance is assessed at the 10% level.

4. Conclusions

This report focuses a lot on the IPSL-CM6, for which an original parametrization of GW-SM interactions has been developed during the IGEM project to capture the main effects of hillslope water redistribution in a simple and numerically efficient way. The off-line evaluation of this new model needs to be extended to a wide range of variables, and the results obtained on river discharge (section 3.1.2) call for an improved calibration, for instance by increasing the GW residence time to compensate the earlier peak and low flows, but floodplains and permafrost need to be activated for such a calibration to be meaningful.

At the land surface, the main impacts of GW-SM interaction logically consist of increased SM and ET, and decreased total runoff and surface temperature (direct cooling by ET and larger heat capacity in wet fractions). The subsequent impacts on precipitation and air temperature are weak but significant in some areas, with patterns linked to general circulation, and modulated by lowland fractions and land-atmosphere feedback.

A thorough comparison of the different model responses is now needed, encompassing the three climate models of the IGEM project with similar methods, especially for statistical assessment (e.g. Wilks, 2016). In particular, since the overall sensitivity is weak, a better significance assessment may require ensemble simulations. Important scientific questions will be addressed owing to this multi-model analysis: (i) can we highlight areas where the GW-SM interaction improves the land-surface or atmospheric simulations, although it might be difficult owing to the small sensitivity in front of the large uncertainties of both observations and simulated variables; (ii) do we get weaker regional warming in areas with significant GW-SM interactions? (iii) can this kind of physical mitigation of regional warming be cancelled with increasing land aridity?

Acknowledgements

This work was jointly supported by the Agence Nationale de la Recherche in France (grant ANR-14-CE01-0018-01) and the MOST in Taiwan (grant MOST-104-2923-M-002-002-MY4). The IPSL simulations were performed using the IDRIS computational facilities (Institut du Développement et des Ressources en Informatique Scientifique, CNRS, France).

References

- Aït-Mesbah, S., J. L. Dufresne, F. Cheruy, and F. Hourdin (2015), The role of thermal
Référence du formulaire : ANR-FORM-090601-01-01

- inertia in the representation of mean and diurnal range of surface temperature in semiarid and arid regions, *Geophys. Res. Lett.*, 42, 7572–7580, doi:10.1002/2015GL065553.
- Boucher O, Servonnat J, and 76 others (2020). Presentation and evaluation of the IPSL-CM6A-LR climate model. Submitted to JAMES.
- Campoy, A., Ducharne, A., Cheruy, F., Hourdin, F., Polcher, J., and Dupont, J.-C. (2013). Response of land surface fluxes and precipitation to different soil bottom hydrological conditions in a general circulation model. *JGR-Atmospheres*, **118**, 10725–10739.
- Cheruy, F., Dufresne, J. L., Ait Mesbah, S., Grandpeix, J. Y., & Wang, F. (2017). Role of soil thermal inertia in surface temperature and soil moisture-temperature feedback. *Journal of Advances in Modeling Earth Systems*, **9**, 2906–2919. <https://doi.org/10.1002/2017MS001036>
- Cheruy F, Ducharne A, Hourdin F, Musat I, Vignon E, Gastineau G, Bastrikov V, et 13 others (2020). Improved near surface continental climate in IPSL-CM6 by combined evolutions of atmospheric and land surface physics. Submitted to JAMES.
- Cheruy F, Dufresne JL, Hourdin F, Ducharne A (2014). Role of clouds and land-atmosphere coupling in systematic mid-latitude summer warm biases and climate change amplification in CMIP5 simulations, *Geophys. Res. Lett.*, **41**, 6493–6500, doi:10.1002/2014GL061145.
- Chou, C., Chiang, J., Lan, C. et al. Increase in the range between wet and dry season precipitation. *Nature Geosci* **6**, 263–267 (2013). <https://doi.org/10.1038/ngeo1744>
- Danabasoglu, G., Lamarque, J.-F., Bacmeister, J., Bailey, D. A., DuVivier, A. K., Edwards, J., et al. (2020). The Community Earth System Model Version 2 (CESM2). *Journal of Advances in Modeling Earth Systems*, **12**, e2019MS001916. <https://doi.org/10.1029/2019MS001916>
- Danielson, J.-J., & Gesch, D.-B. (2011). Global multi-resolution terrain elevation data 2010 (GMTED2010). U.S. Geological Survey Open- File Report 2011–1073, 26. Retrieved from <https://pubs.usgs.gov/of/2011/1073/pdf/of2011-1073.pdf>
- Decharme, B., Delire, C., Minvielle, M., Colin, J., Vergnes, J.-P., Alias, A., et al. (2019). Recent changes in the ISBA-CTrip land surface system for use in the CNRM-CM6 climate model and in global off-line hydrological applications. *Journal of Advances in Modeling Earth Systems*, **11**, 1207– 1252. <https://doi.org/10.1029/2018MS001545>
- Ducharne A, Lo MH, Decharme B, Chien RY, Ghattas J, Colin J, Tyteca S, Cheruy F, Wu WY, Lan CW. Compared sensitivity of land surface fluxes to water table depth in three climate models. Submitted to JGR-Atmosphere.
- Ducharne, A., Ghattas, J., Maignan, F., Ottlé, C., Vuichard, N., Guimbertea, M., Krinner, G., Polcher, J., Tafasca, S., Bastrikov, V., Cheruy, F., Guénet, B., Mizuochi, H., Peylin, P., Tootchi, A. and Wang, F. Soil water processes in the ORCHIDEE-2.0 land surface msodel: state of the art for CMIP6, in prep pour Geosci. Model Dev.
- Eyring, V., Bony, S., Meehl, G. A., Senior, C. A., Stevens, B., Stouffer, R. J., and Taylor, K. E.: Overview of the Coupled Model Intercomparison Project Phase 6 (CMIP6) experimental design and organization, *Geosci. Model Dev.*, **9**, 1937–1958, <https://doi.org/10.5194/gmd-9-1937-2016>, 2016.
- Fan, Y., Li, H. & Miguez-Macho, G. Global Patterns of Groundwater Table Depth. *Science* **339**, 940-943, doi:10.1126/science.1229881 (2013).
- Fan, Y., Clark, M., Lawrence, D. M., Swenson, S., Band, L. E., Brantley, S. L., et al. (2019). Hillslope hydrology in global change research and Earth system modeling, *Water Resources Research*, **55**, 1737– 1772, <https://doi.org/10.1029/2018WR023903>
- Faroux, S., Kaptué Tchuenté, A. T., Roujean, J.-L., Masson, V., Martin, E., & Le Moigne, P. (2013). ECOCLIMAP-II/Europe: A twofold database of ecosystems and surface parameters at 1 km resolution based on satellite information for use in land surface, meteorological and climate models. *Geoscientific Model Development*, **6**(2), 563–582. <https://doi.org/10.5194/gmd-6-563-2013>
- Forster, P.M., Maycock, A.C., McKenna, C.M. et al (2020). Latest climate models confirm need for urgent mitigation. *Nat. Clim. Chang.* **10**, 7–10, <https://doi.org/10.1038/s41558-019-0660-0>
- Gascoin, Ducharne, Ribstein, Carli, Habets (2009). Adaptation of a catchment-based land surface model to the hydrogeological setting of the Somme River basin (France). *J. Hydrology*, **368**, 105-116.
- Greve, P., Orlowsky, B., Mueller, B. et al. (2014). Global assessment of trends in wetting and drying over land. *Nature Geosci* **7**, 716–721. <https://doi.org/10.1038/ngeo2247>

- IPCC (2014). Climate Change 2014: Synthesis Report. Contribution of Working Groups I, II and III to the Fifth Assessment Report of the Intergovernmental Panel on Climate Change [Core Writing Team, R.K. Pachauri and L.A. Meyer (eds.)]. IPCC, Geneva, Switzerland, 151 pp.
- Koster, R. D., et al. (2004). Regions of strong coupling between soil moisture and precipitation. *Science*, **305**, 1138-1140.
- Krinner, G., N. Viovy, N. de Noblet-Ducoudré, J. Ogée, J. Polcher, P. Friedlingstein, P. Ciais, S. Sitch, and I. C. Prentice (2005). A dynamic global vegetation model for studies of the coupled atmosphere-biosphere system, *Global Biogeochem. Cycles*, **19**, GB1015.
- Gleeson T, Wagener T, Cuthbert M, Rahman S, Bierkens MFP, Döll P, Rosolem R, Zipper SC, Bresciani E, Ducharme A, Taylor R, Hill M, Wada Y, Lo MH, Luijendijk E, Maxwell R, Hartmann A, de Graaf I, Oshinlaja N, West C, S. Famiglietti JS, Kollet S, Condon L, Scanlon B, Kim H. Groundwater representation in continental to global hydrologic models (2019). A call for open and holistic evaluation, conceptualization and classification. *EarthArXiv*.
- Lawrence, D. M., et al. (2011). Parameterization improvements and functional and structural advances in Version 4 of the Community Land Model, *Journal of Advances in Modeling Earth Systems*, **3**(1), M03001.
- Lawrence, D. M., Fisher, R. A., Koven, C. D., Oleson, K. W., Swenson, S. C., Bonan, G., et al. (2019). The Community Land Model version 5: Description of new features, benchmarking, and impact of forcing uncertainty. *Journal of Advances in Modeling Earth Systems*, **11**, 4245-4287, <https://doi.org/10.1029/2018MS001583>
- Lo, M.-H., and J. S. Famiglietti (2011). Precipitation response to land subsurface hydrologic processes in atmospheric general circulation model simulations. *J. Geophys. Res. Atmos.*, **116**, D05107.
- Martens, B., Miralles, D. G., Lievens, H., Schalie, R. van der, Jeu, R. A. M. de, Fernández-Prieto, D., Beck, H. E., Dorigo, W. A. and Verhoest, N. E. C. (2017). GLEAM v3: satellite-based land evaporation and root-zone soil moisture, *Geosci. Model Dev.*, **10**(5), 1903–1925, doi:<https://doi.org/10.5194/gmd-10-1903-2017>.
- Maxwell, R. M., Chow, F. K., Kollet, S. J. (2007). The groundwater–land-surface–atmosphere connection: Soil moisture effects on the atmospheric boundary layer in fully-coupled simulations, *Advances in Water Resources*, **30**, 2447-2466.
- Moon, H., Gudmundsson, L., & Seneviratne, S. I. (2018). Drought persistence errors in global climate models. *Journal of Geophysical Research: Atmospheres*, **123**, 3483–3496. <https://doi.org/10.1002/2017JD027577>
- Niu, G. Y., Yang, Z. L., Dickinson, R. E., Gulden, L. E. & Su, H. Development of a simple groundwater model for use in climate models and evaluation with Gravity Recovery and Climate Experiment data. *Journal of Geophysical Research: Atmospheres* **112** (2007).
- O'Neill, B. C., Tebaldi, C., van Vuuren, D. P., Eyring, V., Friedlingstein, P., Hurtt, G., Knutti, R., Kriegler, E., Lamarque, J.-F., Lowe, J., Meehl, G. A., Moss, R., Riahi, K., and Sanderson, B. M.: The Scenario Model Intercomparison Project (ScenarioMIP) for CMIP6, *Geosci. Model Dev.*, **9**, 3461-3482, <https://doi.org/10.5194/gmd-9-3461-2016>, 2016.
- Padrón RS, Gudmundsson L, Ducharme A, Lawrence DM, Mao J, Peano D, Krinner G, Kim H, Seneviratne SI (2020). Observed changes in dry season water availability attributed to human-induced climate change. In revision for *Nature Geoscience*.
- Rodell, M., Beaudoin, H. K., L'Ecuyer, T. S., Olson, W. S., Famiglietti, J. S., Houser, P. R., Adler, R., Bosilovich, M. G., Clayson, C. A., Chambers, D., Clark, E., Fetzer, E. J., Gao, X., Gu, G., Hilburn, K., Huffman, G. J., Lettenmaier, D. P., Liu, W. T., Robertson, F. R., Schlosser, C. A., Sheffield, J. and Wood, E. F. (2015). The Observed State of the Water Cycle in the Early Twenty-First Century, *J. Clim.*, **28**(21), 8289–8318, doi:10.1175/JCLI-D-14-00555.1.
- Seneviratne, Corti, Davin, Hirschi, Jaeger, Lehner, Orlowsky, Teuling (2010). Investigating soil moisture-climate interactions in a changing climate: A review, *Earth-Science Reviews*, **99**, 125-161.
- Swenson, S. C., and D. M. Lawrence (2015), A GRACE-based assessment of interannual groundwater dynamics in the Community Land Model, *Water Resour. Res.*, **51**, 8817–8833, doi:10.1002/2015WR017582.

- Taylor, K.E., R.J. Stouffer, and G.A. Meehl, 2012: An Overview of CMIP5 and the Experiment Design. *Bull. Amer. Meteor. Soc.*, 93, 485–498, doi:10.1175/BAMS-D-11-00094.1
- Teuling, A. J., Van Loon, A. F., Seneviratne, S. I., Lehner, I., Aubinet, M., Heinesch, B., Bernhofer, C., Grünwald, T., Prasse, H., and Spank, U. (2013), Evapotranspiration amplifies European summer drought, *Geophys. Res. Lett.*, 40, 2071– 2075, doi:10.1002/grl.50495.
- Tootchi, A (2019). Development of a global wetland map and application to describe hillslope hydrology in the ORCHIDEE land surface model, PhD thesis, Sorbonne Université, Paris ([PDF](#)).
- Tootchi, A., Jost, A., and Ducharne, A. (2019). Multi-source global wetland maps combining surface water imagery and groundwater constraints, *Earth Syst. Sci. Data*, **11**, 189–220, doi:10.5194/essd-11-189-2019, 2019.
- Vergnes, J.-P., and B. Decharme (2012), A simple groundwater scheme in the TRIP river routing model: global off-line evaluation against GRACE terrestrial water storage estimates and observed river discharges, *Hydrol. Earth Syst. Sci.*, 16(10), 3889–3908, doi:10.5194/hess-16-3889-2012.
- Vergnes, J.-P., B. Decharme, and F. Habets (2014). Introduction of groundwater capillary rises using subgrid spatial variability of topography into the ISBA land surface model, *J. Geophys. Res. Atmos.*, **119**, 11,065–11,086, doi:10.1002/2014JD021573.
- Voldoire, A., Saint-Martin, D., Sénési, S., Decharme, B., Alias, A., Chevallier, M., et al. (2019). Evaluation of CMIP6 DECK experiments with CNRM-CM6-1. *Journal of Advances in Modeling Earth Systems*, **11**, 2177– 2213. <https://doi.org/10.1029/2019MS001683>
- Wang, F., Ducharne, A., Cheruy, F., Lo, M.-H., and Grandpeix, J.-L. (2018). Impact of a shallow groundwater table on the global water cycle in the IPSL land-atmosphere coupled model, *Climate Dynamics*, 50, 3505–3522, doi:10.1007/s00382-017-3820-9
- Wilks, D.S. (2016). “THE STIPPLING SHOWS STATISTICALLY SIGNIFICANT GRID POINTS” - How Research Results are Routinely Overstated and Overinterpreted, and What to Do about It, *BAMS*, 97, 2263–2273, <https://doi.org/10.1175/BAMS-D-15-00267.1>
- Zelinka, M. D., Myers, T. A., McCoy, D. T., Po-Chedley, S., Caldwell, P. M., Ceppi, P., et al. (2020). Causes of higher climate sensitivity in CMIP6 models. *Geophysical Research Letters*, 47, e2019GL085782. <https://doi.org/10.1029/2019GL085782>

F.5 CLIMATE CHANGE IMPACT ON GROUNDWATER (D3.3)

Wu WY, Lo MH, Wada Y, Famiglietti JSi, Reager JT, Yeh PJF, Ducharne A, Yang ZL. Divergent effects of climate change on future groundwater availability in key mid-latitude aquifers. Submitted to Nature Communications in March 2018, in revision.

Abstract

Groundwater provides critical freshwater supply, particularly in dry regions, where surface water availability is relatively limited. Climate change impacts on groundwater storage could affect the availability and sustainability of freshwater. Here, we used a fully-coupled climate model to investigate changes in groundwater storage due to climate-driven effects over seven critical aquifers that have been identified as significantly distressed. Results indicated that from 2006 to 2100, the projected future trends under business-as-usual scenario (RCP8.5) in groundwater storage changes for the United States Central Valley and Southern Plains aquifers are 1.8 and -23.3 mm equivalent water height per decade. The Middle East, northwestern India, North China Plain, Guarani aquifers and Canning basin exhibit the trends of -15.2, 7.4, 10.0, 54.3 and 3.6 mm equivalent water height per decade, respectively. Furthermore, the changes in groundwater do not necessarily reflect the long-term trends in precipitation; instead, they may result from changes in transpiration, enhancement of evaporation, and reduction in snowmelt, which collectively lead to divergent responses of groundwater across different aquifers. While two of these aquifers are projected to become more stressed with climate change, our results also suggest the potential for enhanced future groundwater use in some of the current most overstressed aquifers.

Introduction

Groundwater, the vast water reserve beneath Earth's surface¹, is an essential resource for humans and ecosystems. Globally, more than one-third of the water used originates from underground². In the mid-latitude, arid, and semiarid regions where lack sufficient surface water supply from rivers and reservoirs, groundwater is critical for sustaining global ecology and meeting societal needs of drinking water and food production. The demand for groundwater is rapidly increasing with population growth, while climate change is imposing additional stress on water resources³ and raising the possibility of severe drought⁴⁻⁶. Therefore, examining how groundwater storage may change in response to both climate-driven and anthropogenic impacts is crucial.

Climate change influences groundwater systems in several ways^{1,7}. In terms of the hydrologic cycle, climate change can affect the amounts of soil infiltration, deeper percolation, and hence groundwater recharge. In addition, rising temperature increases evaporative demand over land⁸, which limits the amount of water to replenish groundwater. By contrast, the anthropogenic impacts on groundwater resources are mainly due to groundwater pumping, irrigation and land use changes⁹.

Most estimates of large-scale groundwater storage change rely on numerical models^{10,11}. Previous studies²⁻²² have utilized the output data of General Circulation Models (GCMs) to drive the offline simulations of land hydrologic models and estimate the changes in global and regional groundwater availability. However, the offline model simulations involve various uncertainties, such as that from the downscaling of atmospheric forcing data of GCMs, or from the use of multiple GCMs data as well as under various emission scenarios. The identification and quantification of these sources of uncertainties are in general difficult¹⁶. The offline hydrologic simulation is a one-way approach which cannot capture important feedbacks when expanding from pure hydrology to a more holistic Earth system perspective. Moreover, previous studies^{23,24} have shown the feedback mechanisms of groundwater on the atmosphere, emphasizing the advantages of considering the groundwater dynamics in the coupled climate modeling studies^{23,24}.

In this paper, rather than using an offline model simulation, we use the climate model simulation data from the Community Earth System Model Large Ensemble Project (CESM-LE)²⁵. The CESM is a fully coupled climate model, including the land, atmosphere, ice, and ocean components. CESM-LE, designed for simulating climate change with the

internal climate variability²⁵, has been continuously developed²⁶, evaluated²⁷, and broadly used for investigating the dynamics of terrestrial water cycle components²⁸ such as snowpack^{27,29,30}, soil moisture³¹, snowmelt runoff³², and water availability³³. The approach of a large ensemble (an ensemble of 30 members will be used in this study) can provide uncertainties within the same physical model. The model simulation period is designed to be more than 2,000 years, necessary for the purpose of assessing the decadal-to-centennial trends in the long-memory groundwater storage process.

A physically-based groundwater parameterization is embedded in the version 4.0 of the Community Land Model (CLM4.0)³⁴⁻³⁶. In this study, CLM4.0 is first validated against the total water storage (TWS) data from the Gravity Recovery and Climate Experiment (GRACE) (see Supplementary Fig. 1). By simulating the water table depth, groundwater discharge and recharge, and the interactions with the overlying soil, the groundwater parameterization in CLM4.0 can simulate the physical storage changes in the unconfined aquifer³⁴, which is an essential part in a major component of terrestrial TWS^{37,38}. Owing to its coupling nature with the atmospheric and ocean models, the CESM is a more suitable tool for simulating the multiple interactions and feedbacks of groundwater among the hydrologic cycle in an Earth system framework^{23,39,40}.

For the estimation of future climate-driven groundwater changes, we used the simulation data of CESM-LE since 2006 with the identical forcing to that used in CMIP5 and under the strongest RCP 8.5 (Representative Concentration Pathway) emission scenario. Without considering the anthropogenic effects of water usage, such as groundwater pumping, dam construction and water management, the CESM simulations in this study only account for the natural processes that act on the water budget of the aquifers, which allows us to directly estimate and evaluate the only climate-driven changes in groundwater storage.

Results

Our results, aggregated from an ensemble of CESM simulations, demonstrate that the changes in groundwater do not necessarily only reflect the long-term trends in precipitation. Instead, they may result from changes in transpiration, enhancement of evaporation, and reduction in snowmelt. Under warming, the amount of future spring snowmelt, a major water resource at seasonal snow-cover regions, decreases. In addition, future evapotranspiration (the sum of evaporation and transpiration) increases because of larger atmospheric water demand under global warming. Vegetation dynamics are complicated to interpret because changes in transpiration vary by region with changes of phenology, stomatal conductance, CO₂ fertilization, and root water uptake⁴¹. These three hydrological feedbacks are the main mechanisms for the climate-driven effect (Fig. 1), and they interact, enhance, or compete with each other, causing different results globally (Fig. 2). Overall, changes in groundwater recharge are dominant by rainfall over monsoon and humid regions. The distribution of regions dominated by snow depends on latitude and elevation. Over dry regions, changes in evapotranspiration are a more dominant factor to groundwater recharge.

We analyze these simulations to assess the future climate-driven evolution for seven of the world's largest mid-latitude aquifers (Fig. 3), selected based on their importance to regional water supplies and food production. These aquifers have been identified as having experienced severe groundwater depletion during the past decade^{2,42-47}, mostly because of high water demand for irrigation or other water usages (Supplementary Fig. S2a). Therefore, it is essential to understand the mechanisms between climate factors and groundwater and how climate factors control the availability of groundwater under future warming.

The Central Valley of California accounts for one-sixth of the irrigated land in the United States⁴⁶. During drought periods, groundwater withdrawal increases to compensate for reductions in available surface water. Recent groundwater depletion is heavily influenced by human activities (Supplementary Fig. S2). The results from the CESM-LE indicate that basin-wide groundwater storage in this region has no significant long-term trend in the future, warmer climate, if anthropogenic groundwater pumping is excluded. The lack of a clear long-term trend is the consequence of several competing effects. In particular, less snowfall but more rainfall increases groundwater storage in winter—the season in which groundwater is replenished (Supplementary Fig. S3). However, a reduction in snowmelt

reduces groundwater recharge in early spring. Secondarily, greater evaporation caused by higher temperatures leads to increasing upward water movement from the water table⁴⁸, driven by the capillary rise, in order to satisfy the increasing atmospheric moisture demand as dictated by the Clausius-Clapeyron Equation. These changes in the seasonality of groundwater recharge and in the spatial redistribution of water in the soil column may become challenging for water management in the coming decades, despite the slightly positive climate-driven trend of groundwater storage.

The Southern Plains located in the central United States is another major agricultural region^{49,50}; however, it has little groundwater recharge because of a lack of precipitation. Studies have shown that the risk of future summer drought might become more serious in this region⁴⁹, consistent with our groundwater simulation results. The CESM-LE simulations demonstrate that groundwater declines significantly at a rate of 23.3 ± 11.4 mm per decade in the future through a climate-driven effect. Under a future warming climate, both decreases in infiltration (due to increased evaporation, Table 1) and spring snowmelt (due to decreased snow depth, Supplementary Fig. S4) can reduce groundwater recharge, leading to the deeper water table and reduced groundwater storage.

The central-north Middle East (Turkey, Syria, Iraq, and Iran), including the Tigris and Euphrates River Basins, falls under both transboundary and international water management rules⁴⁷. Groundwater storage here is strongly correlated with human usage, and in particular periods with drought³¹. Our results demonstrate that a combination of several complex factors contributes to a decline in future groundwater recharge. Most importantly, groundwater recharge exhibits a strong seasonal cycle with the largest values in March following snowmelt and infiltration (Supplementary Fig. S5). However, the amplitude of the seasonal cycle for groundwater recharge decreases significantly by the end of this century. The decline in snowfall over the Iranian and Anatolia plateaus reduces spring snowmelt, and hence reduces surface runoff, infiltration, and groundwater recharge. Long-term evaporation increases in the Middle East as the subsurface water replenishes the surface soil by the capillary rise to meet the demands of greater potential evapotranspiration from July to September (Supplementary Fig. S5). Besides, vegetation grows more rapidly owing to CO₂ fertilization and higher temperatures in spring. This contributes to the increased transpiration during the growing season, potentially reducing the water percolating into groundwater recharge. Consequently, a continuous decline in groundwater storage with the rate of -15.2 ± 3.4 mm/dec in the Middle East occurs under global warming.

Northwestern India, an aquifer beneath the upstream region of Indus River and Ganges River, is the basin that has been experienced in the most severe declines in groundwater storage⁴⁵ (Fig. 5). We estimate increasing groundwater resources under warming when only climate-driven factors are considered. Results suggest that long-term groundwater trends are associated with rainfall, snowmelt, and evapotranspiration (60%, 21%, and 19% respectively). Increases in precipitation overwhelm negative feedbacks of increasing evapotranspiration and declining snowmelt (Table 1). This suggests that, without considering pumping, changing climate may lead to greater groundwater sustainability in these two regions, which currently experience rapid rates of groundwater depletion to support irrigated agriculture⁴⁵.

Similarly, but without the contribution of snowmelt, the North China Plain⁴³, the significant increases in precipitation overwhelm the increasing evapotranspiration. More precipitation increases infiltration and groundwater recharge (Table 1). More groundwater recharge leads to a shallower water table depth in the North China Plain.

Our results show that increasing of groundwater resources over the Guarani aquifer in South America, and the Canning basin in northwest Australia. The annual rainfall is larger than 900 mm over these two basins, while less than 900 mm over other five basins maintained above. Rainfall is the dominant factor over these non-snow-covered and relatively humid regions. Evapotranspiration is a secondary factor. Increasing P-ET (precipitation minus evapotranspiration) leads to increases in infiltration and therefore groundwater storage in the model simulations.

The results shown in Fig. 2, 3, and Table 1 are based on the ensemble mean. To assess the uncertainties of internal climate variability, we further analyzed the uncertainties

through its 30 ensemble members. Results show that the amount of groundwater storage changes varies among ensemble members. (Fig. 4). The ensemble consensus on the sign of changes (+ or -) is all more than sixty-six percent, indicating the robustness of the ensemble mean. For example, all simulations agree on declines in groundwater over Southern Plains and the Middle East. Sixty-seven percent (20 members) agree on increases in groundwater over Central Valley. Eighty-three percent (25 members) agree on increases in groundwater over northwestern India. Ninety-seven percent (29 members) agree on increases in groundwater over the North China Plain. All simulations agree on increases over Guarani. Eighty-seven percent (26 members) agree on increases in groundwater over Canning Basin.

Our studied basins are chosen based on the severe declines in groundwater storage during the past decade². The reductions in groundwater storage are mainly due to the combined impacts of over-pumping and climate effects; however, the contribution of anthropogenic pumping could easily far exceed the natural replenishment⁵¹. Though quantifying groundwater trends with and without pumping is difficult, we provide a comparison based available datasets. The estimated trends of anthropogenic, climate-driven, and total (sum of anthropogenic and climate-driven) groundwater storage based on independent datasets are shown in Fig. 5. The period of present trends is from 2003 to 2014. In Central Valley and Northwestern India, recent groundwater depletion is dominated by the anthropogenic pumping. Over Southern plains and Middle East, recent groundwater loss is associated with both climate-driven effect (less natural recharge) and anthropogenic pumping (Fig. 5). Noteworthy, results show that groundwater declines significantly in the future by climate-driven with the rate of -23.3 mm/dec, which exceed both current climate-driven rate of -10.5 mm/dec and current anthropogenic rate of -19.1 mm/dec over Southern Plains. The climate-driven effect is associated with the long-term drought while the anthropogenic effect is the pumping to support irrigated agriculture over Southern Plains⁵². Generally, it should be aware that the negative trend in the last decade (blue bars in Fig. 5) far exceeds the trend that model-simulated climate effect for the future (red bars). Hence, with consideration of the negative contribution of anthropogenic pumping and climate-driven replenishment, the groundwater storage might still diminish globally.

Discussion

We explored the potential changes in groundwater storage caused by global warming, for the first time using simulations from a fully-coupled climate model (land + atmosphere + ocean + sea ice components with an unconfined aquifer module), which allows a physically mechanistic water budget analysis. The approach of CESM-LE assessed the uncertainties of internal climate variability²⁵, and the regional groundwater storage trends.

While our explanations of fundamental mechanisms followed a one-way approach, the results shown here considered all known feedbacks in the coupled system. For example, over Southern Plains, decreases in soil moisture influence the moisture supply for evapotranspiration, and the increases in rainfall are the result of both regional and atmospheric circulation changes.

A key finding is that future changes in groundwater storage are not only strongly governed by the projected changes in precipitation but also modulated by other hydrological processes (e.g., evaporation, transpiration, snowmelt, and plant growth). It is noteworthy that some of the mechanisms affecting groundwater recharge in this study are already occurring at present. For instance, changes in timing and the magnitude of spring snowmelt have been reported in observational datasets^{53,54} and likely influences the groundwater recharge⁵⁵.

In addition, our results show that the spatial heterogeneity in groundwater storage changes exists in the basins (Supplementary Fig.10), particularly in northwestern India and Central Valley, where the topography is complex. Therefore, our projection reveals that mountainous regions experience a decline in groundwater storage, with less replenishment from seasonal snowmelt, which is consistent with the previous literature addressing the hydrological impacts of climate change in mountainous areas^{53,56}. It also reveals that representation of complex terrain in GCM could be improved, such as that

downscaling to the finer resolution⁵⁷ and explicitly simulating lateral flow⁵⁸⁻⁶⁰ are suggested.

As the first one to address the impacts of climate change on groundwater in a full Earth system model, this study is an important step toward better understanding the future changes of this vital but limited resource. A better understanding of future socioeconomic development would be necessary to estimate the future rates of groundwater pumping because the effects of human interventions could easily exceed the effects of natural groundwater recharge in irrigated and urbanized regions¹⁷. In addition, other factors such as changes in soil properties⁶¹ might also affect the infiltration rate and groundwater changes.

Precipitation has been known as a dominant factor in hydrological simulations. However, it is challenging to correctly simulate its patterns and variability^{62,63}. Thus, our results may remain model-dependent even though internal climate variability is considered. Similar studies using other fully-coupled models or different scenarios can be done to better assess the impact of global warming on the natural supplies of groundwater.

Importantly, our results highlight the projected increase in future groundwater stress in the Southern Plains and Middle East regions, but also imply the possibility for future sustainable groundwater use for the regions with increasing groundwater storage, i.e. in the Central Valley, northwestern India, and the North China Plain, where rates of groundwater depletion are currently among the highest in the world². In these regions, increasing recharge and changes in groundwater management strategies could allow for slowed rates of depletion or even aquifer recovery. California's Sustainable Groundwater Management Act is an example of one such ongoing effort.

Methods

In this study, regional changes in groundwater were calculated for seven aquifers that were characterized by rapid rates of depletion using observations from the GRACE mission^{2,52,64}. We used monthly data from simulations of the Community Earth System Model Large Ensemble (CESM-LE)²⁵. CESM-LE experiments were performed with a fully-coupled land–ocean–atmosphere configuration of the CESM, including the Community Land Model (version 4; CLM4)²⁶, Community Atmosphere Model version 5⁶⁵, Parallel Ocean Program (version 2)⁶⁶, and Los Alamos Sea Ice Model (version 4)⁶⁷. CLM4 is a global land model established by the Land Model Working Group at the National Center for Atmospheric Research^{35,36}. Many processes are well-parameterized in CLM4 including hydrology, energy, biogeochemistry, and biogeophysics. In this study, we focused on the hydrological processes, containing an unconfined aquifer model, and a simple TOPMODEL-based runoff parameterization⁶⁸. Changes in groundwater storage result from groundwater recharge and baseflow. Groundwater recharge is represented as the combination of drainage by gravity and capillary rise; a positive value represents water inflows into groundwater storage from the upper soil layers. All the fluxes (such as precipitation, snowmelt, evapotranspiration, and runoff) could eventually affect groundwater recharge through the water cycle. In addition, groundwater discharge (baseflow) drains water from the groundwater aquifer.

Thirty different simulations, simulated from the CESM but differing in their initial atmospheric condition (air temperature in the order of 10^{-14} K) in 1920, are available for understanding the spread of projections. CESM-LE includes transient land cover changes but no soil texture changes. All 30 sets of simulations were created for the same case, with the same external forcing, the same horizontal resolution of 0.9-degree latitude by 1.25-degree longitude, and the same model; that is, we considered the same physical mechanisms. The ensemble mean of 30 ensemble members was considered in this study. To diagnose the long-term trend, the linear trend from 2006 to 2100 was calculated from the annual averaged groundwater storage (Fig.1a). The shading in the figures denotes +/- the single standard-deviation range among 30 ensemble members (Fig.1 and Supplementary Fig.S3–9). The anomalies in Fig.1b are calculated by removing the temporal average of the first decade (2006–2015). Human activities, such as groundwater pumping for irrigation and other uses, were not simulated in the CESM. Consequently, the changes in groundwater storage could be fully attributed to global warming, natural variability, and model internal variability.

However, human activity, such as pumping, and water management all affect changes in groundwater as well. For comparison climate-driven effect (major part of this study) and the anthropogenic effect briefly, we used the groundwater abstraction data from previous global studies^{21,22} (Fig.5). This data considered industrial, irrigation, agricultural and domestic water demand in historical period. For estimating “true” and total (climate-driven and anthropogenic) groundwater storage anomalies, we used the total water storage from GRACE and removed the changes in canopy water, snow, and soil moisture from NASA Global Land Data Assimilation System (GLDAS)⁶⁹. (See Supplementary for more details about the datasets).

In Fig. 2, the impact of climate-driven factors on groundwater recharge are calculated via the regression approach^{70,71}. First, we calculate the linear multiple regression coefficients.

$$y = a_1x_1 + a_2x_2 + a_3x_3 + b, \quad (1)$$

where y is the standardized groundwater recharge, and x_i are standardized annual rainfall, snowmelt, and evapotranspiration respectively across 85 years for each grid or area-averaged in each basin after applying an 11-year running mean. Only regions with significant regression at 90% confidence level are shown in Fig.2.

Then, the contribution of climate-driven factors (rainfall, snowmelt, evapotranspiration) to changes in groundwater recharge is based on the comparison of standardized coefficients as follows:

$$\text{Contribution}_i = \frac{|a_i|}{\sum_{i=1}^3 |a_i|} \quad (2)$$

Contribution of each factor (range from 0 to 1) is calculated based on the ratio of its absolute value of standardized coefficient to the summation of absolute values of standardized coefficient. These three variable of the assigned to RGB for triplet color display in Fig. 2.

Acknowledgments

We acknowledge the CESM Large Ensemble Community Project and supercomputing resources provided by NSF/CISL/Yellowstone. GRACE land data are available at <http://grace.jpl.nasa.gov>, supported by the NASA MEaSUREs Program. The GLDAS data used in this study were acquired as part of the mission of NASA's Earth Science Division and archived and distributed by the Goddard Earth Sciences (GES) Data and Information Services Center (DISC). This study was supported by MOST 104-2923-M-002-002-MY4 to the National Taiwan University; by the IGEM project “Impact of Groundwater in Earth system Models”, co-funded by the French Agence Nationale de la Recherche (ANR Grant no. ANR-14-CE01-0018-01) and the Taiwanese Ministry of Science and Technology; by the NASA GRACE Science Team; and by the Research and Technology Development program of the NASA Jet Propulsion Laboratory at the California Institute of Technology, under contract with NASA.

References

- 1 Taylor, R. G. *et al.* Ground water and climate change. *Nature Clim. Change* **3**, 322-329 (2013).
- 2 Famiglietti, J. S. The global groundwater crisis. *Nature Climate Change* **4**, 945, doi:10.1038/nclimate2425 (2014).
- 3 Wu, W.-Y., Lan, C.-W., Lo, M.-H., Reager, J. T. & Famiglietti, J. S. Increases in the annual range of soil water storage at northern middle and high latitudes under global warming. *Geophysical Research Letters* **42**, 3903-3910, doi:10.1002/2015GL064110 (2015).
- 4 Dai, A. Increasing drought under global warming in observations and models. *Nature Climate Change* **3**, 52 (2012).
- 5 Trenberth, K. E. *et al.* Global warming and changes in drought. *Nature Climate Change* **4**, 17, doi:10.1038/nclimate2067 (2013).
- 6 Marvel, K. *et al.* Twentieth-century hydroclimate changes consistent with human influence. *Nature* **569**, 59-65, doi:10.1038/s41586-019-1149-8 (2019).

- 7 Cuthbert, M. O. *et al.* Observed controls on resilience of groundwater to climate variability in sub-Saharan Africa. *Nature* **572**, 230-234, doi:10.1038/s41586-019-1441-7 (2019).
- 8 Berg, A. *et al.* Land-atmosphere feedbacks amplify aridity increase over land under global warming. *Nature Climate Change* **6**, 869, doi:10.1038/nclimate3029 (2016).
- 9 Lo, M.-H. & Famiglietti, J. S. Irrigation in California's Central Valley strengthens the southwestern U.S. water cycle. *Geophysical Research Letters* **40**, 301-306, doi:10.1002/grl.50108 (2013).
- 10 Fan, Y., Li, H. & Miguez-Macho, G. Global Patterns of Groundwater Table Depth. *Science* **339**, 940-943, doi:10.1126/science.1229881 (2013).
- 11 IPCC. *Climate Change 2013: The Physical Science Basis. Contribution of Working Group I to the Fifth Assessment Report of the Intergovernmental Panel on Climate Change.* (Cambridge University Press, 2013).
- 12 Allen, D. M., Cannon, A. J., Toews, M. W. & Scibek, J. Variability in simulated recharge using different GCMs. *Water Resources Research* **46**, n/a-n/a, doi:10.1029/2009WR008932 (2010).
- 13 Crosbie, R. S. *et al.* An assessment of the climate change impacts on groundwater recharge at a continental scale using a probabilistic approach with an ensemble of GCMs. *Climatic Change* **117**, 41-53, doi:10.1007/s10584-012-0558-6 (2013).
- 14 Crosbie, R. S. *et al.* Potential climate change effects on groundwater recharge in the High Plains Aquifer, USA. *Water Resources Research* **49**, 3936-3951, doi:10.1002/wrcr.20292 (2013).
- 15 Felix, T. P., Petra, D., Stephanie, E. & Martina, F. Impact of climate change on renewable groundwater resources: assessing the benefits of avoided greenhouse gas emissions using selected CMIP5 climate projections. *Environmental Research Letters* **8**, 024023 (2013).
- 16 Habets, F. *et al.* Impact of climate change on the hydrogeology of two basins in northern France. *Climatic Change* **121**, 771-785, doi:10.1007/s10584-013-0934-x (2013).
- 17 Haddeland, I. *et al.* Global water resources affected by human interventions and climate change. *Proceedings of the National Academy of Sciences* **111**, 3251-3256, doi:10.1073/pnas.1222475110 (2014).
- 18 McCallum, J. L., Crosbie, R. S., Walker, G. R. & Dawes, W. R. Impacts of climate change on groundwater in Australia: a sensitivity analysis of recharge. *Hydrogeology Journal* **18**, 1625-1638, doi:10.1007/s10040-010-0624-y (2010).
- 19 Prudhomme, C. *et al.* Hydrological droughts in the 21st century, hotspots and uncertainties from a global multimodel ensemble experiment. *Proceedings of the National Academy of Sciences* **111**, 3262-3267, doi:10.1073/pnas.1222473110 (2014).
- 20 Schewe, J. *et al.* Multimodel assessment of water scarcity under climate change. *Proceedings of the National Academy of Sciences* **111**, 3245-3250, doi:10.1073/pnas.1222460110 (2014).
- 21 Wada, Y., van Beek, L. P. H. & Bierkens, M. F. P. Nonsustainable groundwater sustaining irrigation: A global assessment. *Water Resources Research* **48**, n/a-n/a, doi:10.1029/2011WR010562 (2012).
- 22 Wada, Y. *et al.* Global depletion of groundwater resources. *Geophysical Research Letters* **37**, n/a-n/a, doi:10.1029/2010GL044571 (2010).
- 23 Lo, M.-H. & Famiglietti, J. S. Precipitation response to land subsurface hydrologic processes in atmospheric general circulation model simulations. *Journal of Geophysical Research: Atmospheres* **116**, n/a-n/a, doi:10.1029/2010JD015134 (2011).
- 24 Maxwell, R. M. & Kollet, S. J. Interdependence of groundwater dynamics and land-energy feedbacks under climate change. *Nature Geoscience* **1**, 665, doi:10.1038/ngeo315 (2008).
- 25 Kay, J. E. *et al.* The Community Earth System Model (CESM) Large Ensemble Project: A Community Resource for Studying Climate Change in the Presence of Internal Climate Variability. *Bulletin of the American Meteorological Society* **96**, 1333-1349, doi:10.1175/bams-d-13-00255.1 (2015).
- 26 Lawrence, D. M. *et al.* Parameterization improvements and functional and structural advances in Version 4 of the Community Land Model. *Journal of*

- Advances in Modeling Earth Systems **3**, n/a-n/a, doi:10.1029/2011MS00045 (2011).
- 27 Toure, A. M. et al. Evaluation of the Snow Simulations from the Community Land Model, Version 4 (CLM4). *Journal of Hydrometeorology* **17**, 153-170, doi:10.1175/jhm-d-14-0165.1 (2016).
- 28 Zeng, Z. et al. Impact of Earth Greening on the Terrestrial Water Cycle. *Journal of Climate* **31**, 2633-2650, doi:10.1175/jcli-d-17-0236.1 (2018).
- 29 Fyfe, J. C. et al. Large near-term projected snowpack loss over the western United States. *Nature Communications* **8**, 14996, doi:10.1038/ncomms14996 (2017).
- 30 Mudryk, L., Kushner, P., Derksen, C. & Thackeray, C. Snow cover response to temperature in observational and climate model ensembles. *Geophysical Research Letters* **44**, 919-926 (2017).
- 31 Cheng, S., Huang, J., Ji, F. & Lin, L. Uncertainties of soil moisture in historical simulations and future projections. *Journal of Geophysical Research: Atmospheres* **122**, 2239-2253, doi:10.1002/2016jd025871 (2017).
- 32 Mankin, J. S., Viviroli, D., Singh, D., Hoekstra, A. Y. & Diffenbaugh, N. S. The potential for snow to supply human water demand in the present and future. *Environmental Research Letters* **10**, 114016, doi:10.1088/1748-9326/10/11/114016 (2015).
- 33 Ferguson, C. R., Pan, M. & Oki, T. The Effect of Global Warming on Future Water Availability: CMIP5 Synthesis. *Water Resources Research* **54**, 7791-7819, doi:10.1029/2018wr022792 (2018).
- 34 Niu, G. Y., Yang, Z. L., Dickinson, R. E., Gulden, L. E. & Su, H. Development of a simple groundwater model for use in climate models and evaluation with Gravity Recovery and Climate Experiment data. *Journal of Geophysical Research: Atmospheres* **112** (2007).
- 35 Oleson, K. et al. Improvements to the Community Land Model and their impact on the hydrological cycle. *Journal of Geophysical Research: Biogeosciences* **113** (2008).
- 36 Oleson, K. W. et al. Technical description of version 4.0 of the Community Land Model (CLM). (2010).
- 37 Gulden, L. E. et al. Improving land-surface model hydrology: Is an explicit aquifer model better than a deeper soil profile? *Geophysical Research Letters* **34**, doi:10.1029/2007gl029804 (2007).
- 38 Cai, X. et al. Assessment of simulated water balance from Noah, Noah-MP, CLM, and VIC over CONUS using the NLDAS test bed. *Journal of Geophysical Research: Atmospheres* **119**, 13,751-13,770, doi:10.1002/2014jd022113 (2014).
- 39 Lin, Y.-H., Lo, M.-H. & Chou, C. Potential negative effects of groundwater dynamics on dry season convection in the Amazon River basin. *Climate Dynamics* **46**, 1001-1013, doi:10.1007/s00382-015-2628-8 (2016).
- 40 Wada, Y. et al. Fate of water pumped from underground and contributions to sea-level rise. *Nature Climate Change* **6**, 777, doi:10.1038/nclimate3001 (2016).
- 41 Richardson, A. D. et al. Climate change, phenology, and phenological control of vegetation feedbacks to the climate system. *Agricultural and Forest Meteorology* **169**, 156-173, doi:<https://doi.org/10.1016/j.agrformet.2012.09.012> (2013).
- 42 Famiglietti, J. S. et al. Satellites measure recent rates of groundwater depletion in California's Central Valley. *Geophysical Research Letters* **38**, n/a-n/a, doi:10.1029/2010GL046442 (2011).
- 43 Feng, W. et al. Evaluation of groundwater depletion in North China using the Gravity Recovery and Climate Experiment (GRACE) data and ground-based measurements. *Water Resources Research* **49**, 2110-2118, doi:10.1002/wrcr.20192 (2013).
- 44 Richey, A. S. et al. Quantifying renewable groundwater stress with GRACE. *Water Resources Research* **51**, 5217-5238, doi:10.1002/2015WR017349 (2015).
- 45 Rodell, M., Velicogna, I. & Famiglietti, J. S. Satellite-based estimates of groundwater depletion in India. *Nature* **460**, 999, doi:10.1038/nature08238 (2009).
- 46 Scanlon, B. R. et al. Groundwater depletion and sustainability of irrigation in the US High Plains and Central Valley. *Proceedings of the National Academy of Sciences* **109**, 9320-9325, doi:10.1073/pnas.1200311109 (2012).
- 47 Voss, K. A. et al. Groundwater depletion in the Middle East from GRACE with

- implications for transboundary water management in the Tigris-Euphrates-Western Iran region. *Water Resources Research* **49**, 904-914, doi:10.1002/wrcr.20078 (2013).
- 48 Yeh, P. J.-F. & Famiglietti, J. S. Regional Groundwater Evapotranspiration in Illinois. *Journal of Hydrometeorology* **10**, 464-478, doi:10.1175/2008jhm1018.1 (2009).
- 49 Cook, B. I., Ault, T. R. & Smerdon, J. E. Unprecedented 21st century drought risk in the American Southwest and Central Plains. *Science Advances* **1**, doi:10.1126/sciadv.1400082 (2015).
- 50 Steward, D. R. et al. Tapping unsustainable groundwater stores for agricultural production in the High Plains Aquifer of Kansas, projections to 2110. *Proceedings of the National Academy of Sciences* **110**, E3477-E3486, doi:10.1073/pnas.1220351110 (2013).
- 51 Gleeson, T., Wada, Y., Bierkens, M. F. P. & van Beek, L. P. H. Water balance of global aquifers revealed by groundwater footprint. *Nature* **488**, 197, doi:10.1038/nature11295 (2012).
- 52 Rodell, M. et al. Emerging trends in global freshwater availability. *Nature* **557**, 651-659, doi:10.1038/s41586-018-0123-1 (2018).
- 53 Barnett, T. P., Adam, J. C. & Lettenmaier, D. P. Potential impacts of a warming climate on water availability in snow-dominated regions. *Nature* **438**, 303, doi:10.1038/nature04141 (2005).
- 54 Cayan, D. R., Kammerdiener, S. A., Dettinger, M. D., Caprio, J. M. & Peterson, D. H. Changes in the Onset of Spring in the Western United States. *Bulletin of the American Meteorological Society* **82**, 399-416, doi:10.1175/1520-0477(2001)082<0399:citos>2.3.co;2 (2001).
- 55 Earman, S., Campbell, A. R., Phillips, F. M. & Newman, B. D. Isotopic exchange between snow and atmospheric water vapor: Estimation of the snowmelt component of groundwater recharge in the southwestern United States. *Journal of Geophysical Research: Atmospheres* **111**, n/a-n/a, doi:10.1029/2005JD006470 (2006).
- 56 Immerzeel, W. W., van Beek, L. P. H. & Bierkens, M. F. P. Climate Change Will Affect the Asian Water Towers. *Science* **328**, 1382-1385, doi:10.1126/science.1183188 (2010).
- 57 Rhoades, A. M., Ullrich, P. A. & Zarzycki, C. M. Projecting 21st century snowpack trends in western USA mountains using variable-resolution CESM. *Climate Dynamics* **50**, 261-288, doi:10.1007/s00382-017-3606-0 (2018).
- 58 Maxwell, R., Condon, L. & Kollet, S. A high-resolution simulation of groundwater and surface water over most of the continental US with the integrated hydrologic model ParFlow v3. *Geoscientific Model Development* **8**, 923 (2015).
- 59 Maxwell, R. M. et al. Surface-subsurface model intercomparison: A first set of benchmark results to diagnose integrated hydrology and feedbacks. *Water resources research* **50**, 1531-1549 (2014).
- 60 Fan, Y., Miguez-Macho, G., Weaver, C. P., Walko, R. & Robock, A. Incorporating water table dynamics in climate modeling: 1. Water table observations and equilibrium water table simulations. *Journal of Geophysical Research: Atmospheres* **112** (2007).
- 61 Hirmas, D. R. et al. Climate-induced changes in continental-scale soil macroporosity may intensify water cycle. *Nature* **561**, 100-103, doi:10.1038/s41586-018-0463-x (2018).
- 62 Trenberth, K. E. Changes in precipitation with climate change. *Climate Research* **47**, 123-138 (2011).
- 63 Shepherd, T. G. Atmospheric circulation as a source of uncertainty in climate change projections. *Nature Geoscience* **7**, 703, doi:10.1038/ngeo2253 (2014).
- 64 Tapley, B. D. et al. Contributions of GRACE to understanding climate change. *Nature Climate Change* **9**, 358-369, doi:10.1038/s41558-019-0456-2 (2019).
- 65 Neale, R. B. et al. Description of the NCAR community atmosphere model (CAM 5.0). *NCAR Tech. Note NCAR/TN-486+ STR* **1**, 1-12 (2010).
- 66 Danabasoglu, G. et al. The CCSM4 Ocean Component. *Journal of Climate* **25**, 1361-1389, doi:10.1175/jcli-d-11-00091.1 (2012).
- 67 Hunke, E. C., Lipscomb, W. H., Turner, A. K., Jeffery, N. & Elliott, S. CICE: the Los Alamos Sea Ice Model Documentation and Software User's Manual Version 4.1 LA-CC-06-012. *T-3 Fluid Dynamics Group, Los Alamos National Laboratory* **675**

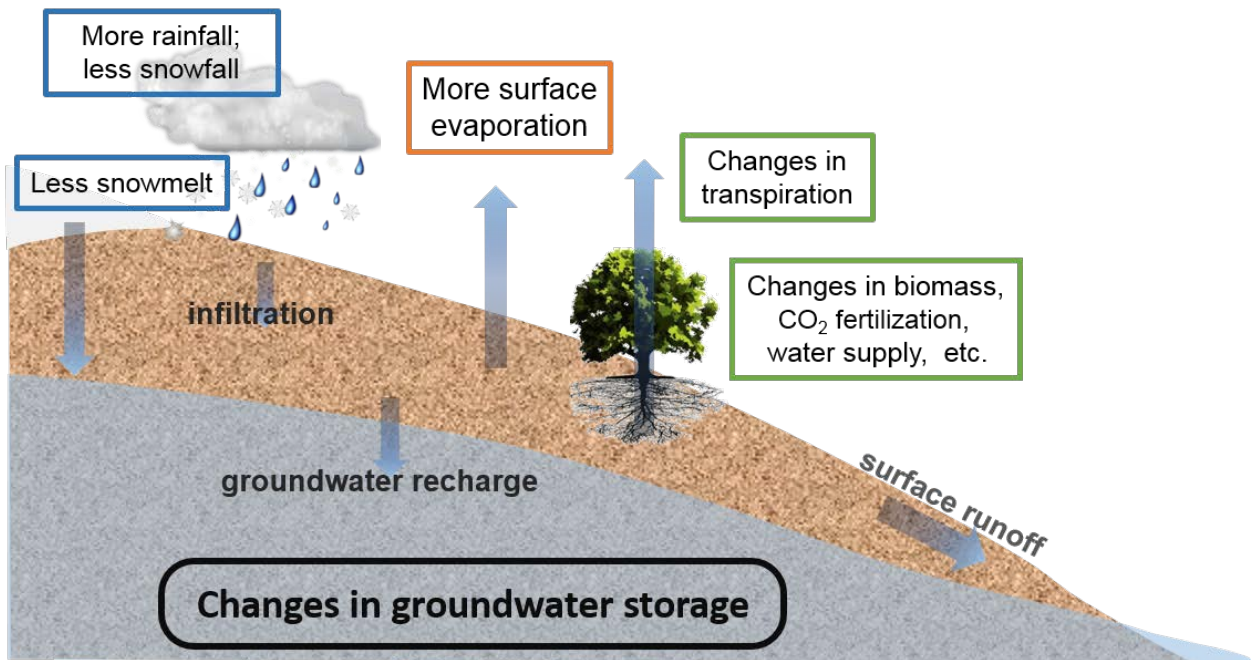
- (2010).
- 68 Niu, G. Y., Yang, Z. L., Dickinson, R. E. & Gulden, L. E. A simple TOPMODEL-based runoff parameterization (SIMTOP) for use in global climate models. *Journal of Geophysical Research: Atmospheres* **110** (2005).
- 69 Rodell, M. et al. The Global Land Data Assimilation System. *Bulletin of the American Meteorological Society* **85**, 381-394, doi:10.1175/bams-85-3-381 (2004).
- 70 Feng, Q., Ma, H., Jiang, X., Wang, X. & Cao, S. What Has Caused Desertification in China? *Scientific Reports* **5**, 15998, doi:10.1038/srep15998 (2015).
- 71 Nemani, R. R. et al. Climate-Driven Increases in Global Terrestrial Net Primary Production from 1982 to 1999. *Science* **300**, 1560-1563, doi:10.1126/science.1082750 (2003).

Table 1. Trend of water fluxes in the seven aquifers from 2006 to 2100 under RCP8.5

Variable	Unit	1	2	3	4	5	6	7
		Central Valley	Southern Plains	Middle East	North western India	North China Plain	Guarani	Canning Basin
Total Precipitation	mm/y r/dec	10.6	0.7*	-0.1*	6.3	22.8	10.0	9.1
Rainfall	mm/y r/dec	22.2	5.0	4.3	8.6	26.4	10.0	9.1
Snowfall	mm/y r/dec	-11.6	-4.3	-4.4	-2.3	-3.6	-0.1	0.0
Evaporation	mm/y r/dec	4.0	3.9	1.5	4.0	6.4	5.8	6.2
Snowmelt	mm/y r/dec	-13.3	-4.6	-5.6	-3.2	-3.8	-0.1	0.0
Infiltration	mm/y r/dec	4.5	-2.3	-0.7	1.0*	12.4	1.5	1.2*
Transpiration	mm/y r/dec	-1.1	-2.2	0.1*	-1.5	8.8	0.6*	-2.3
Groundwater Recharge	mm/y r/dec	5.5	-0.2*	-0.6	2.0	3.7	0.7	3.3
Groundwater storage	mm/dec	1.8*	-23.3	-15.2	7.4	10.0	54.3	3.6

* Asterisk denotes trends are not significant at p<0.05.

(a)



(b)

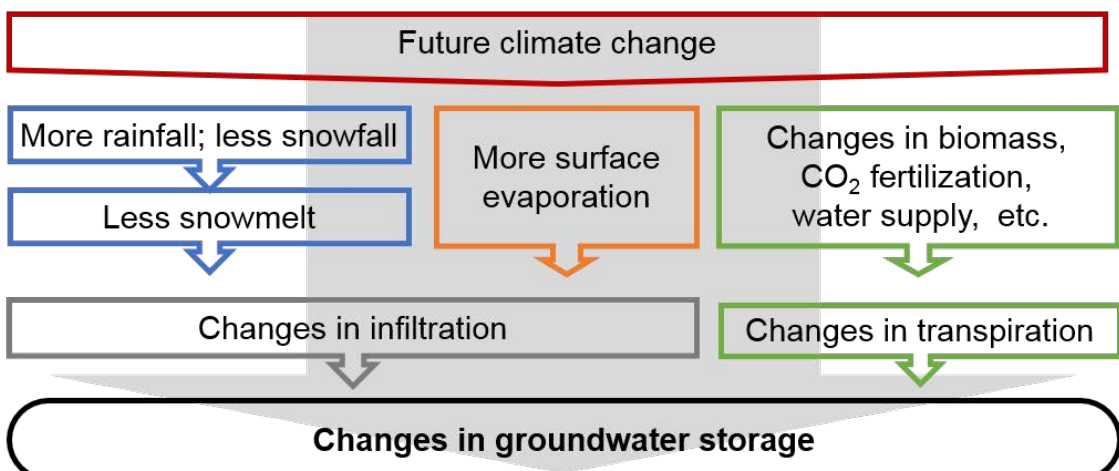


Fig. 1: **a**, Schematic of land hydrological processes and **b**, controlling factors affecting divergent groundwater responses.

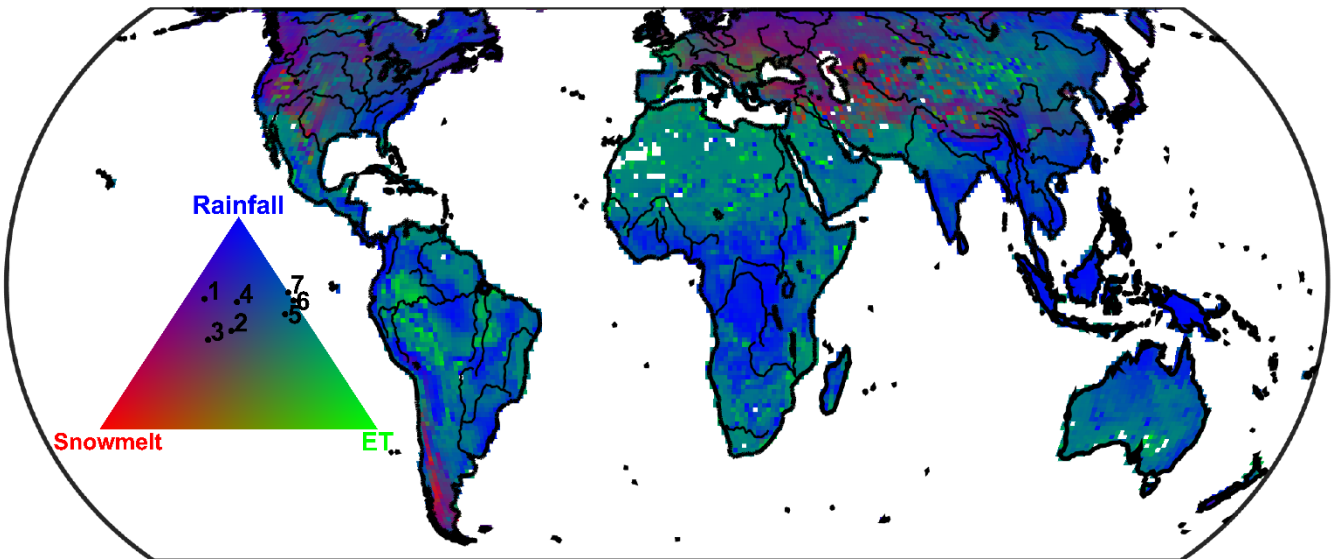


Fig. 2 Contribution of three climate-driven factors to groundwater recharge derived from statistics of CESM-LE outputs. Results are from 2006 to 2100, the projected future trends under business-as-usual scenario (RCP8.5). Each point represents three coefficients based on rainfall (blue), snowmelt (red), and evapotranspiration (green). Basin-averaged results are labeled on the colorbar with numbers of locations shown in Fig. 3.

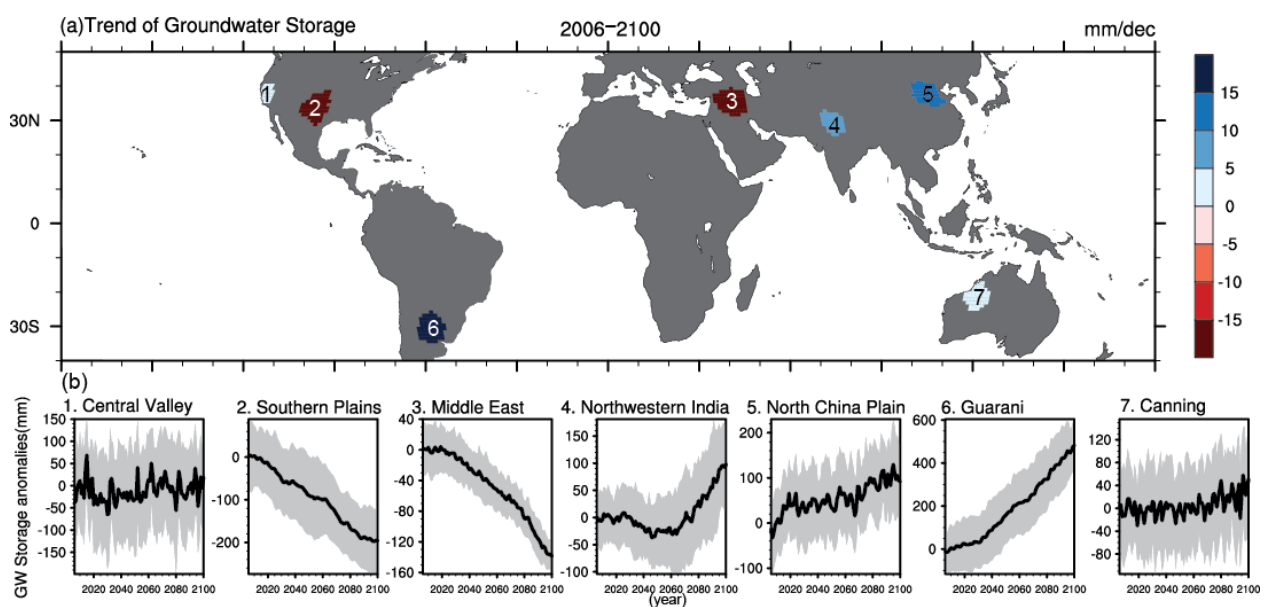


Fig. 3: Projection of climate-driven groundwater storage under RCP8.5 **a**, Trend of climate-driven groundwater storage in the studied basins for the future (2006–2100) **b**, Time series of climate-driven groundwater storage anomalies relative to present; shaded areas represent +/- the ensemble standard deviation.

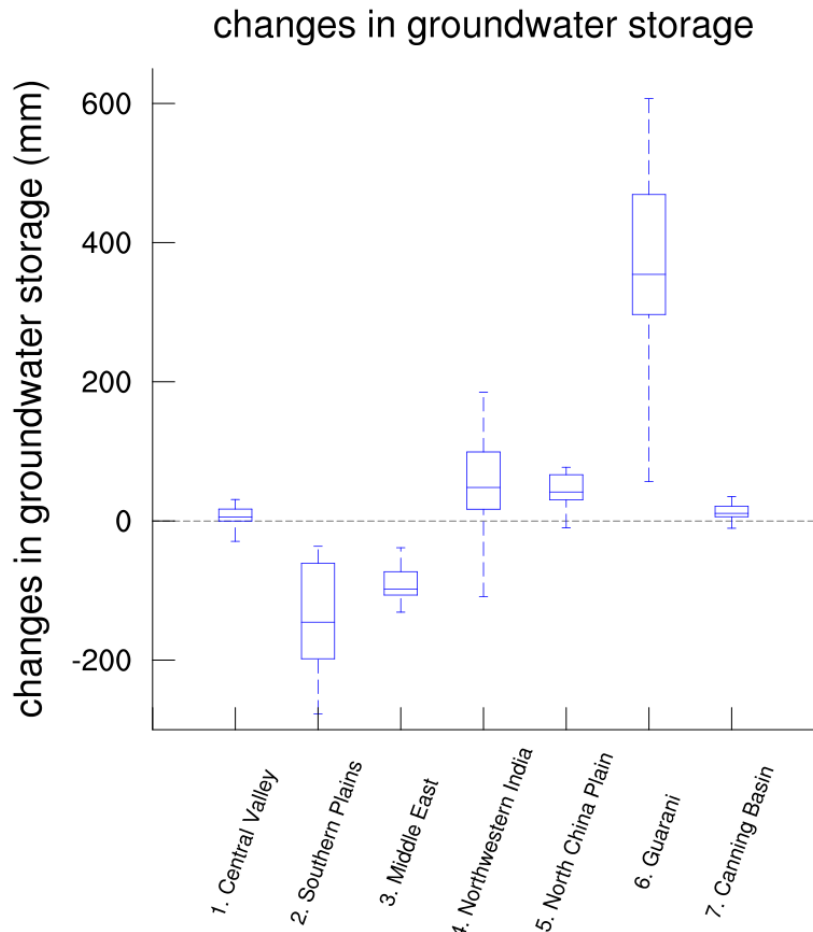


Fig 4 Statistics for 30 ensemble members (min, 25th percentile, median, 75th percentile, max) in each basin. Changes in groundwater in each individual ensemble member between 2071–2100 and 2006–2035

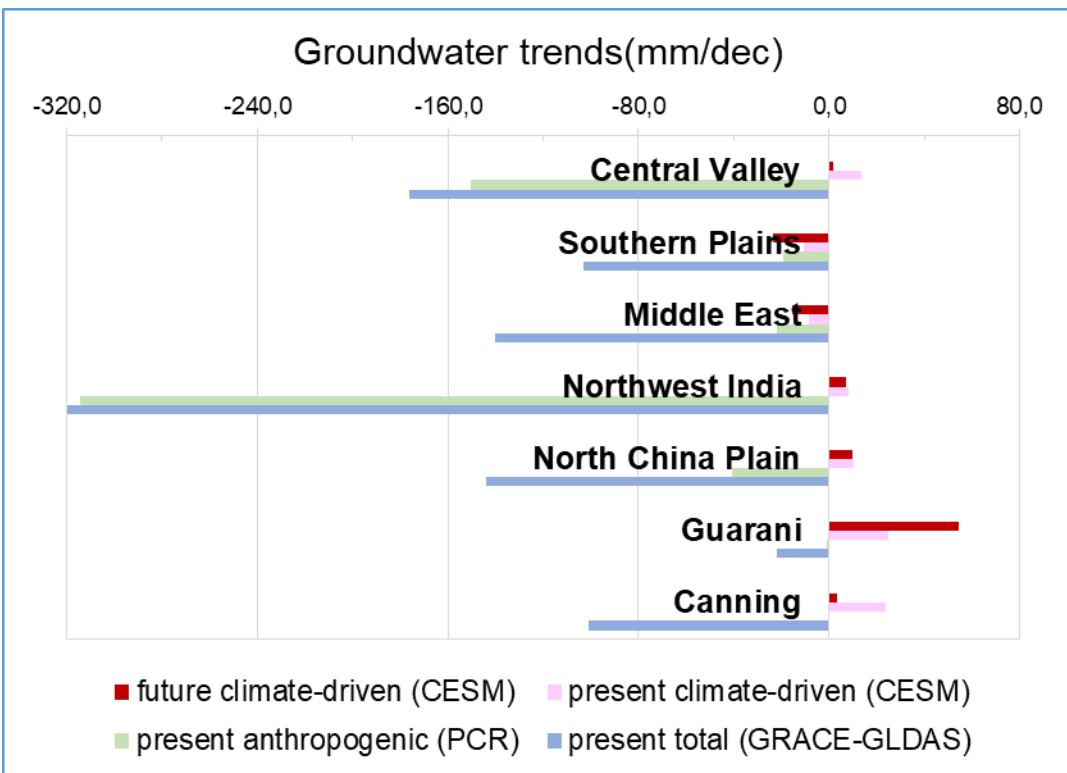


Fig 5. Trend of groundwater storage: future climate-driven groundwater trend is estimated from CESM-LE for 2006–2100; present climate-driven groundwater is estimated from CESM-LE for 2003–2014; present anthropogenic groundwater is estimated from groundwater depletion from Wada (2010)^{19,20} for 2003–2014; Present total groundwater is estimated from GRACE and GLDAS for 2003–2014

